SEISMOLOGICAL SOCIETY OF AMERICA 93rd ANNUAL MEETING

March 16–18, 1998 (Monday–Wednesday)
University Memorial Center, University of Colorado
Boulder, Colorado, USA
For Current Information:
Via WWW: http://geohazards.cr.usgs.gov/ssa98
Email: ssa98@ght.cr.usgs.gov

Important Dates	
Abstract Submission Deadline:	January 9, 1998
Abstract Withdrawal Deadline:	January 31, 1998
Program/Abstracts on WWW:	February 14, 1998
Preregistration Deadline:	February 21, 1998

MEETING CHAIRS

Kaye M. Shedlock
USGS
MS 966
Box 25046
Denver, CO 80225
TEL: 303-273-8571
FAX: 303-273-8600
Email: shedlock@gldvxa.cr.usgs.gov

Anne F. Sheehan
CU/CIRES
Campus Box 216
University of Colorado
Boulder, CO 80309
TEL: 303-492-4597
FAX: 303-492-1149
Email: afs@mantle.colorado.edu

EXHIBITS

Address inquiries to K. Shedlock.

REGISTRATION

Registration information is published in this issue of SRL. Registration will take place Sunday March 15 from 4:00-7:30 PM and Monday through Wednesday in the lobby area outside the Glenn Miller Lounge and Ballroom.

Special Meeting Events

Sunday March 15
5:00–7:00 PM: Icebreaker in Glenn Miller Lounge

Monday March 16
12:00 noon–2:30 PM: SSA Annual Luncheon in Glenn Miller Ballroom. The SSA Medal will be presented to Lynn R. Sykes. The President's Invited Address will be given by David P. Hill, "Science, Geologic Hazards, and the Public in a Large Restless Caldera."

Wednesday March 18
1:30–5:00 PM: CNSS "off-year" meeting in the Forum Room. For more information, please contact Steve Malone (steve@geophys.washington.edu).

PROGRAM

Program Committee (Geoff Abers, Jon Ake, Tom Boyd, Tony Crone, Dennis Mileti, John Rundle, Scott Smithson, and Gabriel Toro) can be reached via e-mail: ssatcomm@ght.cr.usgs.gov

Lodging—SSA '98

Holiday Inn
800 28th Street
Boulder, CO 80303-2299
Tel: (303) 443-3322; Fax: (303) 443-0397

Cut-off date is February 15, 1998, for special rates of
Single: $75/night + tax
Double: $80/night + tax
Triple: $85/night + tax
Quad: $90/night + tax

College Inn
1729 Athens Street
Boulder, CO 80302
Tel: (303) 444-2676; Fax: (303) 444-1706

Operated by the University of Colorado; on the campus. Accomodations are the level between a residence hall and hotel (private baths, no bar, etc.). Room packages include the nights of Sunday, March 15, through Wednesday, March 18 (check out the morning of the 19th), with breakfast provided the mornings of March 16–18.

Single: $269.84 per person
Double: $161.732 per person

Nearby Attractions

Colorado skiing (www.skicolorado.org), Rocky Mountain National Park, Dinosaur Ridge National Natural Landmark, Denver (www.diveindenver.com), Golden (including the Coors Brewery and Colorado School of Mines), Celestial Seasonings Headquarters, and many more.

Child Care

Please see http://geohazards.cr.usgs.gov/ssa98.

TRAVEL ARRANGEMENTS

Get there for less! Call our official travel agency, Conventions in America, at 1-800-929-4242 and ask for Group #515. You will receive 5%–10% off the lowest applicable fares on *United Airlines*, or the lowest available fare on any carrier. Travel between March 13–21, 1998. All attendees booking through CIA will receive free flight insurance and be entered into their quarterly drawing for domestic travel for two! *Alamo Rent A Car* is also offering special rates starting as low as $32/day or $150/week, with unlimited free mileage and bonus frequent flyer miles.

Call Conventions in America, 1-800-929-4242, ask for Group #515. Outside 800 area, call 619-453-3686, fax: 619-453-7976. Also see http://www.scitravel.com.
Reservation hours: M–F 6:30 AM–5:00 PM Pacific time (24-hour emergency number).
Internet: flycia@scitravel.com.
If you call direct:
United 1-800-521-4041, ask for Tour Code #514QM
Alamo 1-800-732-3232, ID# 469840GR.

93nd Annual Meeting of the Seismological Society of America
University of Colorado at Boulder ❖ March 16–18, 1998

Full payment must accompany registration
For multiple registrations, please duplicate this form

☐ Dr. ☐ Ms. ☐ Mrs. ☐ Mr.

First Name: ____________ Middle Initial: ______ Last Name: ____________

Preference for Name Tag: ____________

Affiliation: ____________

Mailing Address: ____________

City, State, ZIP code: ____________

Business Phone: ____________ Fax: ____________

Home Phone: ____________ E-mail: ____________

SSA ID Number (Required for Member Registration): ____________

Registration Fees

	Pre-registration until March 1	One-day registration	Registration after March 1	
SSA Member	$90	$60	$120	______
Non-member (registration only)	150	70	180	______
Non-member (with SSA membership*)	190		220	______
Student member	40	30	60	______
Student non-member	60	40	80	______
Student non-member (with SSA membership*)	70		90	______

* SSA Membership includes 6 issues of *Seismological Research Letters* and 6 issues of the *Bulletin of the Seismological Society of America*

Annual Luncheon, March 16: ________ Tickets @ $25 _____

Total Amount Enclosed: ________

Enclosed is my:

☐ Check payable to University of Colorado (note SSA98 on memo line).

☐ Charge $______ to my ☐ Mastercard ☐ Visa ☐ American Express

Card Number: ____________ Name on card: ____________ Expiration Date: ________

Authorized Signature: ____________

Mail Registration form to:

University of Colorado
Office of Conference Services
Campus Box 454
500 30th Street
Boulder, CO 80309

Credit-card registrations may be faxed to: 303-492-5959. Payment to be made in U.S. dollars only.

Overview of Technical Program

Oral Sessions

	Forum Room	Meeting Room 235
Monday 8:30 AM–11:45 AM	Seismic Hazards from the Rocky Mountain Region to the Great Basin: Results from Seismology and Paleoseismology	Theory and Simulations of the Earthquake Source
Monday 2:00 PM–4:45 PM	GPS and Seismology	North American Lithosphere and Asthenosphere
Tuesday 8:30 AM–Noon	Developments in Ground Motion and Ground Failure for Engineering Applications	The Tenth Anniversary of the Predicted Parkfield Earthquake Structure and Deformation in Subduction Zones
Tuesday 1:30 PM–5:00 PM	Developments in Ground Motion and Ground Failure for Engineering Applications	Explosion and Impact Event Analyses and Monitoring
Wednesday 8:30 AM–11:45 AM	The U.S. National Seismic System	Eastern Hemisphere Structure and Faulting
Wednesday 1:30 PM–5:00 PM	The U.S. National Seismic System (CNSS Meeting)	California Seismicity and Structure

Poster Sessions—Glenn Miller Lounge

Tuesday 8:30 AM–5:00 PM	Shallow High-Resolution Seismology for Environmental and Seismic Hazard Studies A1–A8
	GPS and Seismology B1–B3
	North American Lithosphere and Asthenosphere C1–C2
	Seismic Hazards from the Rocky Mountain Region to the Great Basin: Results from Seismology and Paleoseismology D1–D4
	California Seismicity and Structure E1–E3
	Seismic Methods F1–F7
	Seismic Systems and Instrumentation G1–G5
Wednesday 8:30 AM–5:00 PM	Seismic Hazard Assessments H1–H17
	Intraplate Seismotectonics I1–I11
	Explosion and Impact Event Analyses and Monitoring J1–J7

SSA-98
Program for the 93rd Annual Meeting
University Memorial Center
University of Colorado, Boulder—March 16–18, 1998

Presenter is indicated in **bold**

Monday AM, March 16, 1998—Forum Room
Seismic Hazards from the Rocky Mountain Region to the Great Basin: Results from Seismology and Paleoseismology
Presiding: Tony Crone, *USGS*
and **Joan Gomberg**, *USGS*

08:30 Paleoseismic data and seismic-hazard mapping in the intermountain west—Contributions and limitations. **Crone, A.J.**

08:45 On the use of surface rupture lengths to determine paleoseismic event magnitudes. **Zollweg, J.E.**

09:00 Preliminary results, paleoseismicity and seismic hazard investigation of the Hurricane Fault, Southwestern Utah and Northwestern Arizona. **Lund, W.R.**, Stenner, H.D., and Pearthree, P.A.

09:15 Progress report on the paleoseismicity of the Pajarito Fault, New Mexico: Results of the 1997 trenching campaign. **McCalpin, J.P.**

09:30 Subsurface fault delineation in central New Mexico using three temporally and spatially related earthquake swarms. **Balch, R.S.**, Sanford, A.R., Jaksha, L.H., Hartse, H.E., and House, L.S.

09:45 Seismic hazards of the Rio Grande Rift/GreatPplains transition zone in west Texas and southern New Mexico from seismological studies. **Doser, D.I.**

10:00 BREAK

10:15 Slow, gravity-driven lithospheric extension in the western United States. Unruh, J.R., **Jones, C.H.**, and Sonder, L.J.

10:30 Implications of GPS deformation measurements on earthquake hazard assessment of the Wasatch Fault Zone. Smith, R.B., **Meertens, C.M.**, and Martinez, L.J.

10:45 Do new geodetic data indicate higher seismic hazard in the Salt Lake City—Ogden region, Utah? **Pechmann, J.**

11:00 New probabilistic seismic hazard estimates for Salt Lake City, Utah. **Wong, I.G.**, Bott, J.D.J., Olig, S.S., and Becker, A.M.

11:15 SEA98, an updated predictive relation for earthquake ground motions in extensional tectonic regimes. **Spudich, P.**, Joyner, W.B., Boore, D.M., Lindh, A.G., and Margaris, V.N.

11:30 The importance of random seismicity in seismic hazard evaluations within the Intermountain West, and engineering consequences. **Ake, J.**, LaForge, R., and Vetter, U.

Monday AM, March 16, 1998—Room 235
Theory and Simulations of the Earthquake Source
Presiding: John Rundle, *Univ. of Colorado*
and **Nick Beeler**, *USGS*

08:30 Dynamic Modeling Of Thrust and Normal Faults: Differences In Near-Source Ground Motion. **Oglesby, D.O.**, Archuleta, R.J., and Nielsen, S.B.

08:45 Beginning of earthquakes modeled with the Griffith fracture criterion. **Sato,T.**, and Kanamori, H.

09:00 Nucleation, growth, and arrest of earthquakes: Models and implications for general earthquake models. **Rundle, J.B.**, Gross, S., and Klein, W.

09:15 Dynamic simulation of spontaneous rupture with heterogeneous stress drop. **Andrews, D.J.**, and Boatwright, J.

09:30 What underlies the Gutenberg-Richter law? **Scholz, C.H.**, and Spyropoulos, C.

09:45 On coseismic changes of slip direction: The effect of low initial shear stress on 3-D dynamic simulation of spontaneous rupture. **Guatteri, M.**, and Spudich, P.

10:00 BREAK

10:30 Can rate-and-state friction explain how the 1911 Morgan Hill, CA, earthquake broke through the 1906 stress shadow? **Harris, R.A.**, and Simpson, R.W.

10:45 High-frequency radiation from an extended fault: implications of choice of the subevent slip history. **Tumarkin, A.G.**

11:00 Repeating earthquakes and the long-term evolution of seismicity on the San Andreas fault near Bear Valley, California. **Ellsworth, W.L.**, Cole, A.T., Dietz, L.D., and Dodge, D.A.

11:15 Apparent stress, seismic efficiency, and friction. **McGarr, A.**

Monday PM, March 16, 1998—Forum Room
GPS and Seismology
Presiding: Paul Segall, *Stanford*

2:00 Complementarity of GPS and seismological data for tectonic studies. **Stein, S.**, and Dixon, T.

2:15 Imaging slow seismic sources using GPS. **Segall, P.**, Cervelli, P., Murray, M.H., Owen, S., and Burgmann, R.

2:30 GPS as a tool for assessing hazard from crustal earthquakes in the Pacific Northwest. **Rogers, G.C.**, and Dragert, H.

2:45 Resolution of the interseismic subsurface slip distribution along the Hayward fault, California from GPS and SAR interferometry data. **Burgmann, R.**, Sukhatme, J., and Fielding, E.

3:00 BREAK

3:30 Modeling postseismic deformation in southern California after the 1992 Landers earthquake. **Bock, Y.**, Williams, S., and Prawirodirdjo, L.

3:45 Real-time earthquake geodesy. **Murray, M.H.**, Dreger, D.S., Neuhauser, D.S., Baxter, D.R., Gee, L.S., and Romanowicz, B.

4:00 GPS measurements of interseismic, coseismic, and postseismic slip along a terrane suture, the Ramu-Markham Fault in Papua New Guinea. **Stevens, C.**, Silver, E.A., McCaffrey, R., Tregoning, P., Little, R., Jackson, R., English, P., and Loratung, W.

4:15 Periodic strain across the east African rift using continuous GPS. **Bendick, R.**, Bilham, R., and Braun, J.

4:30 Integrated networks for GPS geodesy, seismology and atmospheric science. **Meertens, C.M.**, C. Rocken, T. Vanhove, R. Ware, Smith, R.B., and Benz, H.

Monday PM, March 16, 1998—Room 235
North American Lithosphere and Asthenosphere
Presiding: Ken Dueker, *Univ. of Colorado*
and **Joydeep Bhattacharyya**, *Yale*

2:00 An overview of crustal structure in the Rocky Mountain Region. **Keller, G.R.**, Snelson, C.M., Miller, K., Sheehan, A., Dueker, K., Levander, A., and Henstock, T.J.

2:15 Teleseismic receiver function imaging of upper mantle structure below the Colorado Plateau. **Gilbert, H. J.**,Sheehan, A. F., and Dueker, K. G.

2:30 Implications of transition zone discontinuities beneath the western U.S. **Dueker, K.G.** and Sheehan, A.F.

2:45 Attenuation structure near the Coso geothermal region. **Bhattacharyya, J.**, and Lees, J.

3:00 BREAK

3:30 Seismic anatomy of a geothermal field in three-dimensions: Poisson's ratio, porosity, attenuation, anisotropy and stress. **Lees, J.M.**

3:45 Crustal structure along the Pacific North America plate boundary derived from three-dimensional V_p and V_p/V_s velocity models for southern California. **Hauksson, E.**

4:00 Characterization of the crust by topography, gravity, and thickness for predicting waveguide efficiency. **Baker, G. E.**, and Mclaughlin, K.L.

Tuesday AM, March 17, 1998—Forum Room
Developments in Ground Motion and Ground Failure for Engineering Applications
Presiding: Jamison Steidl, *UCSB*

08:30 Modeling of non-linear soil response from earthquakes in Los Angeles. **Jones, E.M.**, and Olsen, K.B.

08:45 Stochastic finite-fault modeling of ground motions from the 1994 Northridge, California earthquake: Widespread nonlinear response at soil sites. **Beresnev, I.A.**, Atkinson, G.M., Johnson, P.A., and Field, E.H.

09:00 Direct observation of nonlinear soil response in acceleration time histories. **Archuleta, R.**

09:15 Nonlinear site response: From laboratory modeling to field data modeling. **Bonilla, L.F.**, Lavallee, D. and Archuleta, R.J.

09:30 Response spectral scaling for various damping ratios compatible with updated rock and soil response spectral attenuation relationships for 5% damping. **Sadigh, K.**, Makdisi, F.I., Egan, J.A., and Rosidi, D.

09:45 Updated response spectral attenuation relationships for vertical motions from shallow crustal earthquakes. **Sadigh, K.**, Rosidi, D., Powers, M.S., Egan, J.A., and Makdisi, F.I.

10:00 BREAK

10:30 Evaluation of empirical attenuation relations for southern California. **Anderson, J.G.**, Lee, Y., Ni, S.D., Zeng, Y., and Abrahamson, N.

10:45 Site response for probabilistic seismic hazard analysis in southern California. **Steidl, J.H.**

11:00 Probabilistic seismic hazard in southern California: 3-D basin effects. **Olsen, K.B.** and Archuleta, R.J.

11:15 Probabilistic seismic hazard analysis of southern California. Mahdyiar, M., and **Abrahamson, N.**

11:30 A new probabilistic earthquake hazard model for California: comparison with recent USGS hazard maps. **Schneider, J.F.**, Mendez, A.J., Zeghal, M., Li, Y., and Wu, L.

11:45 A method for producing probabilistic seismic landslide hazard maps for southern California. **Jibson, R.W.**, and Harp, E.L.

Tuesday AM, March 17, 1998—Room 235
The Tenth Anniversary of the Predicted Parkfield Earthquake
Presiding: Robert Wesson, *USGS*

08:30 Hydrology and/or tectonics: Results from the Parkfield water-level monitoring network. **Roeloffs, E.**

08:50 Possible increase in fault slip rate at Parkfield in 1993 as inferred from deformation measurements from 1986 to 1997. **Langbein, J.**, Gwyther, R.L., and Gladwin, M.T.

09:10 The Parkfield experiment: A new view of fault-zone process. **Nadeau, R.M.**, and McEvilly, T.V.

09:30 Parkfield earthquake: Not likely this year. **Jackson, D.D.** and Kagan, Y.Y.

09:50 Short-term exciting, long-term correcting models for earthquake occurrence times. **Schoenberg, F.R.**, and Bolt, B.A.

Tuesday AM, March 17, 1998—Room 235
Structure and Deformation in Subduction Zones
Presiding: Geoff Abers, *Univ. of Kansas*
and **Susan Schwartz,** *UCSC*

10:30 A global survey of slab structures and internal processes using a combined data base of high-resolution earthquake hypocenters, tomographic images and focal mechanism data. **Engdahl, E.R.**, Van Der Hilst, R.D., Kirby, S.H., and Ekstrom, G.

10:45 Upper mantle S-velocity structure of South America from portable and permanent seismic stations. **Van Der Lee, S.**, James, D.E., and Silver, P.G.

11:00 Shallow mantle structure and evolution of the Andean subduction zone at 20° South. **Myers, S.C.**, Beck, S., Zandt, G., and Wallace, T.

11:15 Termination of subduction and the deformation of South Island, New Zealand. **Wu, F.T.**, and Klosko, E.

11:30 Observing dispersion of regional body waves in subducted slabs: A signal from subducted crust? **Abers, G.A.**

Tuesday PM, March 17, 1998—Forum Room
Developments in Ground Motion and Ground Failure for Engineering Applications
Presiding: Andres Mendez, *Impact Forecasting*

1:30 Inversion of source parameters and site effects from strong motion records using genetic algorithm approach—Aftershocks of the 1995 Kobe earthquake. **Moya, C.A.**, and Irikura, K.

1:45 Effects of randomization of source parameters for estimating strong ground motion with empirical Green's functions. Liu, P-C and **Archuleta, R.J.**

2:00 Correlation of rise time with the style-of-faulting factor in strong ground motions. **Somerville, P.G.** and Sato, T.

2:15 Broadband simulation of ground motions in the Santa Monica area for the Northridge earthquake: Effects of shallow basin-edge structure. **Graves, R.W.** and Pitarka, A.

2:30 Strong ground motion from surface waves generated at the edge of deep sedimentary basins. **Joyner, W.B.**

2:45 Near-field peak ground motion scaling for rock versus real rock: how do PHA and PHV scale with increasing rock foundation S-wave velocity? **O'Connell, D.R.H.**

3:00 BREAK

3:15 Disaggregation of seismic hazard. **Bazzurro, P.,** and Cornell, C.A.

3:30 A deterministic-stochastic approach to strong motion synthesis for hazard assessment. **Mendez, A.J.**

3:45 "Parametric-historic" procedure for probabilistic seismic hazard analysis. **Kijko, A.**, and Graham, G.

4:00 Past and future seismicity modelling by spatial smoothing. **Lapajne, J.K.**, Zabukovec, B., and Zupancic, P.

4:15 Probabilistic seismic hazard maps of Alaska. **Wesson, R.L.**, Frankel, A.D., Mueller, C.S., Harmsen, S.C., and Lahr, J.C.

4:30 Peak ground motions from the second major 16 December 1811 New Madrid earthquake. **Johnston, A.C.**

4:45 Ground motion models in the eastern and central United States from National Seismographic Network data. **Saikia, C.K.**, Somerville, P.G., Thio, H.K., and Pitarka, A.

Tuesday PM, March 17, 1998—Room 235
Explosion and Impact Event Analyses and Monitoring
Presiding: Chris Young, *Sandia National Laboratory*

1:30 An explanation for degassing explosions at Karymsky Volcano, Kamchatka, Russia. **Johnson, J.B.** and Lees, J.M.

1:45 Characteristics of seismic signals from the collapse of underground cavities. **Walter, W.R.**, and Mayeda, K.

2:00 Representing short-period regional P/S discriminants for CTBT monitoring in the Middle East. **Rodgers, A.**, Walter, W., and Lay, T.

2:15 Calibration of International Data Center (IDC) magnitudes for event screening using the M_s/m_b criterion. **Murphy, J.R.** and Barker, B.W.

2:30 A procedure for estimation of source and propagation amplitude corrections for regional seismic discriminants. **Taylor, S.R.**, and Hartse, H.E.

2:45 Nonstationary Bayesian Kriging: Application of spatial travel-time corrections to improve seismic location. **Schultz, C.A.**, Myers, S.C., Ruppert, S.D., Hipp, J., and Young, C.J.

3:00 BREAK

3:30 Testing the DOE model for improving seismic event locations using Kriged traveltime corrections. **Young, C.J.**, Hipp, J.R., Shepherd, E., and Moore, S.G., Schultz, C.A., and Myers, S.C.

3:45 Maximum spectral energy timing method for epicenter determination and location errors reduction. Part II: P-waves. **Yacoub, N.K.**

4:00 Recent developments in SAC2000. **Dodge, D.**, Firpo, M., and Goldstein, P.

4:15 In search of a robust 3 component bearing estimator. **Claassen, J.P.**

Tuesday, 8:30 AM–5:00 PM
Glenn Miller Ballroom
Posters
Shallow High-Resolution Seismology for Environmental and Seismic Hazard Studies

---

A1 High-resolution seismic imaging of strata buried by basalt flows, Bellemont, Arizona. **Rymer, M.J.**, Catchings, R.D., and Goldman, M.R.

A2 Correlation of 1- to 10-Hz earthquake resonances with surface measurements of P- and S-wave reflections and refractions in the upper 70 M. **Williams, R.A.**, Stephenson, W.J., Odum, J.K., Meremonte, M.E., Cranswick, E., and Frankel, A.D.

A3 Use of combined seismic reflection and refraction high-resolution imaging for environmental, water resource, and earthquake hazards investigations. **Catchings, R.D.**, Rymer, M.J., and Goldman, M.R.

A4 High-resolution seismic imaging of quaternary faulting across the Commerce geophysical lineament, southeast Missouri. **Stephenson, W.J.**, Odum, J.K., Williams, R.A., Pratt, T.L., Harrison, R., and Hoffman, D.

A5 Seismic surface wave tomography for near-surface structures. **Long, L.T.**, Kocaoglu, A.H., and Doll, W.E.

A6 Rapid 3d refraction traveltime tomography with a variable grid. **Zhang, J.**

A7 Hydrostratigraphic characterization using shallow seismic reflection profiling, northwestern Monterey County, California. **Underwood, D.H.**, Silver, E.A., Lewis, S.D., and Fisher, A.T.

A8 Soil properties and bedrock fracture distributions from shallow seismic observations. **Alexander, S.S.**, Falkenstern, D.M., Gebbie, T.J. and Zeisloft, M.

Tuesday, 8:30 AM–5:00 PM
Glenn Miller Ballroom
Posters
GPS and Seismology

B1 Integration of the Northern Basin and Range (NBAR) and Wasatch front GPS networks for crustal deformation in and around the southern intermountain seismic belt. Bennett, R.A. and Davis, J.L., **Meertens, C.M.**, and Smith, R.B., and Wernicke, B.P.

B2 Institutional collaborations for joint seismic and GPS measurements. **Perin, B.J.**, Meertens, C.M., Neuhauser, D.S., Baxter, D.R., Murray, M.H., and Butler, R.

B3 A technique for measuring the timing accuracy on GPS-based seismic waveform recorders. **Kromer, R.P.**, and McDonald, T.S.

Tuesday, 8:30 AM–5:00 PM
Glenn Miller Ballroom
Posters
North American Lithosphere and Asthenosphere

C1 Receiver function studies from digital broadband data recorded at El Paso, Texas. **Kilbride, F.E.A.**, and Doser, D.I.

C2 New maps of North American crustal structure. **Chulick, G.S.**, and Mooney, W.D.

Tuesday, 8:30 AM–5:00 PM
Glenn Miller Ballroom
Posters
Seismic Hazards from the Rocky Mountain Region to the Great Basin: Results from Seismology and Paleoseismology

D1 Surficial geologic mapping and paleoseismic investigations on the West Cache fault zone, Cache County, Utah. **Black, B.D.**, and Solomon, B.J.

D2 Some sensitivity studies of probabilistic seismic hazard estimates for New Mexico. **Lin, K.W.,** Sanford, A.R., and Tsai, I.C.

D3 Stress interaction and its application to the earthquake hazard analyses of the Wasatch fault, Utah. **Chang, W.L.**, and Smith, R.B.

D4 Microearthquake field study of the front range of Colorado. **Sheehan, A.F.**, Hughes, N. D., and Jones, C. H.

Tuesday, 8:30 AM–5:00 PM
Glenn Miller Ballroom
Posters
California Seismicity and Structure

E1 3D subsurface data of the Ventura Basin: Testing the reliability of 2D models to infer deep fault structure in the western Transverse Ranges. **Nicholson, C.**, Valentine, D., Kamerling, M.J. and Hopps, T.E.

E2 Late Quaternary growth of the San Joaquin Hills anticline—a new source of blind thrust earthquakes in the Los Angeles basin. **Mueller, K.J.**, Grant, L.B., and Gath, E.

E3 Seismicity of the southern Sierra Nevada from two portable experiments. **Edwards, J.**, and Jones, C.H.

Tuesday, 8:30 AM–5:00 PM
Glenn Miller Ballroom
Posters
Seismic Methods

F1 A 3-D mantle model from free-oscillation data. **Resovsky, J.S.**, and Ritzwoller, M.H.

F2 Modeling wave propagation through heterogeneous media using the extended local Rytov Fourier method: Effects of random heterogeneity on regional waveforms. **Fehler, M.C.**, and Huang, L-J.

F3 Spectral inversion of regional waves from earthquakes in presence of random and model errors. **Xie, J.**

F4 High frequency ground motion scaling from regional array data in central Italy and Germany. **Malagnini, L.**, Maceira, M., Herrmann, R., and Koch, K.

F5 Applying waveform correlation event detection and location at regional and local scales. **Aster, R.C.**, Withers, M.M., and Young, C.J.

F6 An automatic method for determination of Lg arrival times using wavelet transforms. **Tibuleac, I.M.**, and Herrin, E.

F7 Automatic phase repicking for improved hypocenter locations in large data sets. **Rowe, C.A.** Aster, R.C., Fehler, M.C., Phillips, W.S. and Alde, D.M.

Tuesday, 8:30 AM–5:00 PM
Glenn Miller Ballroom
Posters
Seismic Systems and Instrumentation

G1 Earthworm collaborative development report. **Dietz, L.**, Kohler, W., Luetgert, J., Pitt, M., Bittenbinder A., Bogaert, B., Ketchum, D., Lombard, P., Johnson, C.E., Chavez, D., Kragness, D., Moon, B. and Rohay, A.

G2 A dial-up system for rapid retrieval of remote digital strong-motion and event-triggered seismic data. **Wood, C.**, Viksne, A., and Copeland, D.

G3 Performance of modern broadband seismic instrumentation. **Uhrhammer, R.A.**

G4 Self-noise spectra and shake table tests of the Wilcoxon 731-4A and the Kinemetrics FBA-23DH accelerometers. **Rodgers, P.W.**, Swain, S.T., and Steidl, J.H.

G5 Response, calibration, and noise of the homemade hardware store broadband leaf-spring vertical seismometer. **Morrisey, S.T.**

Wednesday AM, March 18, 1998—Forum Room
The U.S. National Seismic System
Presiding: Steve Malone, *Univ. of WA*
and **Harley Benz**, *USGS*

08:30 The Council of the National Seismic System—The first five years. **Malone, S.D.**

08:45 ORB: A new real-time data exchange and seismic processing system. **Harvey, D.J.**, Quinlan, D.M., Vernon, F.L., and Hansen, R.

09:00 CREST and the U.S. National Seismograph Network. **Oppenheimer, D.**, Dietz, L., Kohler, W., Bittenbinder, A., Bogaert, B., Buland, R., Benz, H., Weaver, C., Malone, S., Hansen, R., and Okubo, P.

09:15 SCSN/TriNet: Modern, multi-functional real-time seismic network. **Hauksson, E.**, Clayton, R., Hafner, K., Heaton, T., Hutton, K., Kanamori, H., Maechling, P., Jones, L., Given, D., Mori, J., and Wald, D.

09:30 The Canadian National Seismic Network In western Canada. **Baldwin, R.E.**, Beverley, K.I., and Rogers, G.C.

09:45 Invited

The NEIC role in the NSS. **Buland, R.**, and Benz, H.M.

10:00 BREAK

10:30 The New Madrid and Southern Appalachian Cooperative Seismic Networks: Outlook 1998. **Withers, M.M.**, Johnston, A.C., Herrmann, R.B., Haug, E.J., Powell, C.A., Chapman, M.C., and Snoke, A.J.

10:45 Seismic monitoring and cooperation in the Puerto Rico region. **Von Hillebrandt-Andrade, C.**, Huerfano, V. and Lugo, J.

11:00 The CNSS composite catalog. **Gee, L.**, Malone, S., Neuhauser, D., Oppenheimer, D. Buland, R., and members of the CNSS

11:15 Useful products for electrical utilities from integrated regional seismic networks. **Savage, W.U.**, Abrahamson, N.A., McLaren, M.K.

11:30 Recent earthquake web pages for California and Nevada at http://quake.usgs.gov/recenteqs/. **Simpson, R.W.**, Ellsworth, W.L., Michael, A.J., and Oppenheimer, D.H.

Wednesday AM, March 18, 1998—Room 235
Eastern Hemisphere Structure and Faulting
Presiding: Laura Jones, *Los Alamos National Laboratory*

08:30 Slip parameters for the Rann of Kachchh, India, 16 June 1819 earthquake quantified from contemporary accounts. **Bilham, R.**

08:45 Seismicity of northern Thailand: Past, present and future. **Bott, J.D.**, Wong, I.G., Prachuab, S., and Wechbunthung, B.

09:00 Historical and recent seismicity of southwestern China. **Dober, M.C.**, Van Dusen, S.R., and Doser, D.I.

09:15 Predictions of the 1997 strong earthquakes in Jiashi, Xinjiang, China. Zhang, G., Zhu, L., **Song, X.**, Li, Z., Yang, M., Su, N., and Chen, X.

09:30 High resolution surface-wave dispersion studies in China. **Jones, L.E.**, and Patton, H.J.

09:45 Path effects on regional phases in China. **Phillips, W.S.**, Randall, G.E., Hartse, H.E. and Taylor, S.R.

10:00 BREAK

10:30 2-D image of seismic attenuation of the mantle from the deep seismic sounding profile "QUARTZ", Russia. **Morozov, I.B.**, Morozova, E.A., and Smithson, S.B.

10:45 Pn velocity structure from South Western Europe to Western Asia. **McNamara, D.E.**, Schultz, C., and Hansen, R.A.

11:00 Surface wave continental tomography. **Levshin, A.L.**, Ritzwoller, M.H., and Vdovin O.Y.

11:15 The propagation of seismic waves in North African and Mediterranean lithosphere. **Dial, P.**, Doser, D.I., Keller, G.R.

Wednesday PM, March 18, 1998—Forum Room
Council of the National Seismic System (CNSS) Meeting—1:30 PM to 5:00 PM
Presiding: Steve Malone, *Univ. of Washington* and **Harley Benz**, *USGS*

Wednesday PM, March 18, 1998—Room 235
California Seismicity and Structure
Presiding: Edward Field, *USC*

01:30 Earthquake deficits, seismic moment deficits, and $M \geq 6$ seismicity in southern California since 1903. **Hanks, T.C.**, and Stein, R.S.

01:45 An integrated seismic-hazard source model for southern California: No deficit or $M > 8$ earthquakes required. **Field, E.H.**, Jackson, D.D. and Dolan, J.F.

02:00 A correlation between crustal thickness and cut-off depth of earthquakes in southern California. **Zhao, D.**, Teng, T., and Kanamori, H.

02:15 Aftershocks from rate and state dependent friction. **Gross, S.J.**

02:30 Does the California generic "aftershock" model also represent foreshock-mainshock occurrence? **Reasenberg, P.A.**

02:45 Moment tensor solutions of 1997-1998 Long Valley earthquake swarm. **Pasyanos, M.E.**, Tkalcic, H., Dreger, D., and Hill, D.S.

13:00 Imaging attenuation structure and source properties at the Coso geothermal field. **Hough, S.E.**, Lees, J., and Monastero, F.

Wednesday, 8:30 AM–5:00 PM
Glenn Miller Ballroom
Posters
Seismic Hazard Assessment

H1 Average annual losses for earthquakes in the continental United States. **Nishenko, S.P.**, Jamieson,G., and Lawson, R.S.

H2 New developments in the UCSB strong motion database. **Lindley, G.**, Tumarkin, A., and Archuleta, R.

H3 Site characterization and site response effects at the Tarzana, California, CSMIP stations. **Graizer, V.M.**, and Shakal, A.F.

H4 Controls on ground failure in alluvium: Lessons from the 1994 Northridge, California, earthquake. **Ponti, D.J.**, Craven, A.E., Tinsley, J.C. III, and Holzer, T.L.

H5 Estimates of ground accelerations at Point Reyes, California during the 1906 San Francisco earthquake. **Anooshehpoor, A.**, Heaton, T.H., Shi, B., and Brune, J.N.

H6 Precarious rock constraints on ground motion from great earthquakes along the San Andreas Fault, California. **Brune, J.N.**

H7 Non-ergodic probabilistic seismic hazard analysis. **Anderson, J.G.**, and Brune, J.N.

H8 Which potential earthquakes dominate seismic hazard in the U.S.? A regional comparison. **Harmsen, S.C.** and Frankel, A.

H9 Stress drops in extensional regimes. **Becker, A.M.**, and Abrahamson, N.

H10 Probabilistic seismic hazard and ground motions in Alaska. **Wells, D.L.**, Rosidi, D., and Youngs, R.R.

H11 Non-characteristic behavior and complex recurrence of large subduction zone earthquakes. **Schwartz, S.Y.**

H12 The relationship of seismicity in the Prince William Sound region (1964-1996) to the asperities of the 1964 great Alaskan earthquake. **Velasquez, M.**, Doser, D.I., and Veilleux, A.M.

H13 Variability of local tsunami runup relative to M_w. **Geist, E.L.**

H14 Investigation of regional and site attenuation characteristics in the Bursa city, northwestern Anatolia, using the acceleration records of micro-earthquakes. **Akinci, A.**, and Eyidogan, H.

H15 An energy-based motion parameter for probabilistic determination of scenario earthquakes. **Chapman M.C.**

H16 Geologic hazards evaluation of the U.S. Military Academy, West Point, New York. **Rosidi, D.**, Wells, D.L., and Egan, J.A.

H17 Probabilistic ground motion hazard analysis for the state of Oklahoma. **Laforge, R.**

Wednesday, 8:30 AM–5:00 PM
Glenn Miller Ballroom
Posters
Intraplate Seismotectonics

I1 Determination of *RMS Lg* values and seismic energy for regional earthquakes in the northeastern United States. **Shi, J.**, Kim, W.Y., and Richards, P.G.

I2 Paleoseismicity: Seismicity evidence for past large earthquakes. **Ebel, J. E.**, Bonjer, K.-P. and Oncescu, M. C.

I3 Seismograms recorded by New England PEPP Stations. **Kafka, A.L.**, Honkonen, A., Ruszczyk, E., Strother, P.K., and Cochrane, L.

I4 Focal mechanism and source parameters of the 1997 November 6, Quebec Earthquake. **Kim, W.Y.**

I5 Source studies of seismic events in North America using broadband data recorded by the United States and Canadian National Networks. **Thio, H.K.**, and Saikia, C.K.

I6 A noteworthy earthquake in an unlikely place. **Gomberg, J.**, Wolf, L., Raymond, D., Raymond, R., Barnes, A., Carver, D., Bice, T., Cranswick, E., Meremonte, M., Frankel, A., Overturf, D., Hopper, M., Rhea, S., and Eckhoff, O.

I7 Aftershock investigation of the October 24, 1997, earthquake near Atmore, Alabama., **Carver, D.**, Bice, T., Cranswick, E., Meremonte, M., Gomberg, J., Frankel, A., Rhea, S., and Overturf, D.

I8 Analysis of local and regional seismograms of the 1997 southern Alabama earthquake sequence: Source parameters, site response, and crustal propagation. **Frankel, A.**, Carver, D., Cranswick, E., Meremonte, M., Gomberg, J., Bice, T., Rhea, S., and Overturf, D.

I9 Faulting parameters of the October 24, 1997 southern Alabama earthquake. **Chang, T.M.**, Ammon, C.J., and Herrmann, R.B.

I10 Three dimensional P-wave velocity structure for the New Madrid seismic zone. Vlahovic, G., **Powell, C.**, and Chiu J.-M.

I11 Applications of modern, GIS-based, seismotectonic maps. **Wheeler, R.L.**, Rhea, S., and Diehl, S.F.

Wednesday, 8:30 AM–5:00 PM
Glenn Miller Ballroom
Posters
Explosion and Impact Event Analyses and Monitoring

J1 Monitoring mine explosions in the conterminous U.S. **Dewey, J.**

J2 The seismic signal strength of chemical explosions and magnitude distributions of mine blasting activity in different regions. Khalturin, V.I., Rautian, T.G., and **Richards, P.G.**

J3 The 16 August 1997 Novaya Zemlya seismic event as viewed from GSN stations KEV and KBS. **Hartse, H.E.**

J4 Regional recordings of the 1997 Kazakhstan depth of burial experiment. **Myers, S.C.**, Walter, W., Mayeda, K., and Glenn, L.

J5 Analysis of seismograms from the atmospheric impact of the El Paso Bolide (October 9, 1997). **Doser, D.I.**, Chael, E.P., and Baker, M.R.

J6 A comparison of seismic signals from several Bolide events. **Chael, E.P.**

J7 Modelling of oceanic and on-land propagation of (T-) waves from an underwater explosion. **Piserchia, P.-F.**, Rodrigues, D., Virieux, J., Gaffet, S.

SSA-98
93rd Annual Meeting
Meeting Abstracts
These abstracts are listed in the order they appear in the program.

Monday AM, March 16, 1998—Forum Room
Seismic Hazards from the Rocky Mountain Region to the Great Basin: Results from Seismology and Paleoseismology
Presiding: Tony Crone, *USGS*
and **Joan Gomberg,** *USGS*

PALEOSEISMIC DATA AND SEISMIC-HAZARD MAPPING IN THE INTERMOUNTAIN WEST—CONTRIBUTIONS AND LIMITATIONS

CRONE, A.J., U.S. Geological Survey, MS 966, Box 25046, Denver, CO 80225, crone@gldvxa.cr.usgs.gov

Seismic-hazard maps in the Intermountain West can be further improved by greater use of paleoseismic data. Pre-1996 versions of the USGS's National Seismic Hazard Maps (NSHM) relied heavily on historical seismicity to quantify the hazard even though the recurrence time of large earthquakes on many faults is typically 10-100 times longer than the region's ~200-yr. historical record. Thus, historical seismicity incompletely identifies seismic sources that are used to assess the seismic hazard. Paleoseismic data collected during the past two decades better defines the hazard by characterizing fault behavior over geologically significant time intervals. Paleoseismic studies improve hazard assessments by providing data on : 1) the location of potential sources (Quaternary faults) including those that are currently aseismic, 2) an estimate of paleoearthquake magnitude, 3) the time since the last major event on a fault, and 4) frequency or recurrence time of surface-rupturing earthquakes. With appropriate attenuation relations, this information can be used to calculate probabilistic ground motions in areas of little or no historical seismicity.

An adverse aspect of using geological data is that they add a variety of uncertainties to the hazard maps, . These uncertainties include those related to measuring specific geological parameters such as earthquake time, amount of offset, and rupture length. Surficial processes (erosion and deposition) create gaps in the geological record that may leave paleoseismic histories incomplete. Moderate-magnitude ($M \leq 6$) events may not cause enough deformation to be recorded in the geologic record, but such events are often damaging. Furthermore, intrinsic uncertainties in the faulting process exist including the inherent variability of the process, variations in displacement amounts between individual events, variation in recurrence times between successive events, and the likelihood that short-term slip rates ($<10^4$ yrs) can differ greatly from long-term ($>10^5$ yrs) rates.

At a July 1997, USGS-sponsored workshop, geoscientists discussed issues related to using geological data in the NSHM. One result of the workshop was a simple 4-category system to broadly defined confidence levels of geological data used in the maps. In the coming months, the USGS will work with geoscientists and State Geological Surveys in the Intermountain West and with the Western States Seismic Policy Council to define a review and revision process for paleoseismic data used in future versions of the NSHM.

ON THE USE OF SURFACE RUPTURE LENGTHS TO DETERMINE PALEOSEISMIC EVENT MAGNITUDES

Zollweg, J. E. (Sponsor: Anthony Crone), Department of Geosciences, Boise State University, Boise, ID 83725, zollweg@sisyphus.idbsu.edu.

Rupture lengths estimated from mapping of prehistoric fault traces are commonly used to derive magnitudes for paleoseismic events from historic length versus magnitude data. Such a practice makes three implicit assumptions: first, that the rupture lengths obtained for the prehistoric events are the same as what would have been mapped had the earthquakes occurred historically; second, that erosion has negligible influence upon rupture length estimates; and third, that historic surface rupture length is the best estimator of paleoseismic event magnitude. All three assumptions are somewhat questionable, possibly leading to significant underestimates of paleoseismic event magnitudes. Surface ruptures of large historic events often consist of multiple or discontinuous traces and do not always closely follow the trace of the "master" fault in the vicinity. Failure to recognize all the strands that ruptured in a single event may lead to an underestimate of the proper rupture length to be used. Erosion of small-displacement scarps will eventually make them unrecognizable, implying that the rupture length mapped for a paleoseismic event may become smaller as a function of the elapsed time since the event. Finally, historic rupture length versus magnitude relations are commonly determined from a mixture of mapped surface rupture lengths and lengths determined from instrumental epicenters of aftershocks, and aftershocks nearly always occur beyond the ends of the mapped ruptures.

If fault displacement data are available for a paleoseismic event, it may be possible to determine whether the surface rupture length has been underestimated by the aspect ratio between displacement and length *D/L*. While historic displacement versus magnitude data typically display a larger standard deviation than rupture length versus magnitude data, the displacement data alone are often probably better predictors of magnitudes of paleoseismic events than are the rupture length estimates.

Preliminary Results, Paleoseismicity and Seismic Hazard Investigation of the Hurricane Fault, Southwestern Utah and Northwestern Arizona.

LUND, W.R., Utah Geological Survey, SUU Box 9053, Cedar City, UT 84720, lund@suu.edu; STENNER, H.D., Dept. of Geology, Arizona State University, Tempe, AZ 85283, heidi.stenner@asu.edu; PEARTHREE, P.A., Arizona Geological Survey, 416 West Congress, Tucson, AZ 85701.

The Utah Geological Survey and the Arizona Geological Survey are conducting a cooperative research project to evaluate the potential for large, damaging earthquakes on the Hurricane fault, an active normal-slip fault that extends for 250 km from Cedar City, Utah to south of the Grand Canyon in Arizona. Goals of the study include: 1) estimating fault slip rates over a variety of geologic time periods, 2) assessing how much of the fault has ruptured in individual large prehistoric earthquakes, and 3) estimating the size and timing of those earthquakes. Our study is focused on areas along the fault where Quaternary basalt flows or unconsolidated alluvium are displaced. We have submitted samples from several faulted basalt flows in southern Utah and from near the Grand Canyon in Arizona for Ar/Ar dating, which should provide fault slip-rate estimates for the mid- and late Quaternary and possibly for all of Quaternary time. Investigation of sites in Utah and Arizona with faulted alluvium provides evidence for recurrent late Quaternary movement and probable Holocene faulting. At the northern end of the fault near Cedar City, a late Quaternary alluvial surface (possible Bull Lake age, 80–120 kyr) at Shurtz Creek is displaced about 12 m and a probable early to mid-Holocene alluvial fan at Murie Creek is displaced 3 m. At Cottonwood Canyon in Arizona, late Quaternary alluvial surfaces are displaced about 5 and 20 m, repectively. A trench across a scarp formed on probable early to mid-Holocene alluvium revealed about 60 cm of displacement. At Whitmore Canyon near the Colorado River, late Quaternary alluvial surfaces record recurrent fault movement, older surfaces are displaced 5 to 7 m and younger surfaces are displaced about 1.5 to 3 m. With further work, we hope to better define the the length of the young ruptures, integrate this information with long-term slip-rate data, evaluate rupture segmentation, and paleoearthquake magnitudes on the fault.

Progress Report on the Paleoseismicity of the Pajarito Fault, New Mexico: Results of the 1997 Trenching Campaign

MCCALPIN, J.P., GEO-HAZ Consulting, Inc., P.O. Box 1377, Estes Park, CO 80517, mccalpin@geohaz.com

The Pajarito fault is the western boundary fault of the Rio Grande rift at the latitude of Santa Fe, New Mexico. Although historically quiescent, fault movement in the past 1.2 Ma has displaced the Pajarito Plateau (Bandelier Tuff) vertically 100–125 m, for a long-term slip rate of ca. 0.1 mm/yr. The Pajarito fault is the major source of seismic hazard to Los Alamos National Laboratory and has been trenched in two recent campaigns to characterize Mmax, recurrence, and slip rate. No Quaternary geomorphic surfaces younger than 1.2 Ma are displaced by the main fault trace, so work has concentrated on scarps in bedrock. Geologic mapping of the scarp at 1:1200 scale in 1996 revealed that the scarp is composed of several structural styles: 1) single, high-angle fault (20% of length), 2) scarp disturbed by slumping (30%), and 3) articulated monocline (50%). In 1997 a transect of 7 trenches was dug in an articulated monocline section, across the 50 m-high main scarp, the crestal tension fissure, 2 synthetic and 2 antithetic scarps.

Trenches across the 2 synthetic scarps showed tuff bedrock at the surface throughout, highly shattered fault zones, and no colluvial wedges. Antithetic scarps 0.5–1 m high were 75% buried by alluvium coming from upslope, and contained evidence for multiple Quaternary faulting and one early Holocene faulting event. The main scarp was fronted by a minor fault zone with only 3–4 m total displacement. The largest deformation was in the crestal tension fissure, an 8 m-deep filled fissure formed by westward toppling of the monoclinal slab of tuff. Three of the 7 trenches showed evidence for an early Holocene event, but the penultimate event was at least 50–60 ka and probably 100 ka. TL and ^{14}C dates are pending. The unusual structure of this bedrock fault zone required development of new trenching strategies and interpretive models.

SUBSURFACE FAULT DELINEATION IN CENTRAL NEW MEXICO USING THREE TEMPORALLY AND SPATIALLY RELATED EARTHQUAKE SWARMS

Balch, R. S., Sanford, A. R., and Jaksha, L. H., Geophysical Research Center, New Mexico Tech, Socorro, NM 87801, balch@baervan.nmt.edu; Hartse, H. E., and House, L. S., Los Alamos National Laboratory, MS D-443, Los Alamos, NM 87545, hans@geophysics.lanl.gov.

Three spatially and temporally-related earthquake swarms occurred along a 16 km linear trend in the central Rio Grande rift of New Mexico. The Arroyo Del Coyote (ADC) swarm (16 August 1985 to 8 May 1986) occurred near the center of the linear trend and had a M_d=4.0 main shock. The northernmost Puertecito de Bowling Green (PBG) swarm (17-20 September 1985) had three events with M_d=2.73, 2.52 and 2.57. The southernmost Loma de Las Canas (LDC) swarm (16 April to 23 May 1986) had a main shock of M_d=3.1. The swarms were recorded within a permanent, telemetered network of 11 stations, supplemented with three to six temporary stations. We used direct P and S phases for locating events, and when observed, we included reflected phases P_zP, S_zP, and S_zS from the mid-crustal Socorro Magma Body to reduce errors of focal depth estimates. A total of 840 events were recorded and we computed 309 high quality hypocenter locations (x, y, and z errors $\leq$ 0.5 km) and a 154-event subset of focal mechanisms. In cross-section the swarms occupy a slab-like volume 2.5-km thick, dipping 10° north, and ranging in depth between 6.0 and 9.5 km. The central ADC swarm was dominated by two types of focal mechanisms: Thirty-one Type 1 events had strike-slip solutions with an average T-axis orientation of 248° ± 10° and 22 Type 2 events had strike-slip solutions with an average T-axis orientation of 214° ± 9°. For both types T-axis plunge was nearly horizontal. Type 1 events were most common prior to and during the PBG swarm to the north, while Type 2 events were more common from 27 August 1985 to the onset of the LDC swarm to south. The PBG swarm had focal mechanisms that are similar (T-axis orientation 237° ± 5°) to the ADC Type 1 events, and the LDC swarm had mechanisms that are similar (T-axis orientation 220° ± 8°) to the ADC Type 2 events. Spatially, the PBG events appear to be aligned with the Type 1 ADC events and the LDC events appear to be aligned with the Type 2 ADC events. These swarms probably represent activity on a single left-lateral strike-slip fault that has a sharp bend at the location of the ADC swarm. The spatial separation of the Type 1 and 2 mechanisms narrowly constrains the location of the bend in the fault. The proposed fault has no surface expression though its trend mimics structural grain in exposed rock 2 km to the east. If the whole fault were to rupture at once, a M_d=6.5 earthquake could result without breaking the surface.

Seismic Hazards of the Rio Grande Rift/Great Plains Transition Zone in West Texas and Southern New Mexico from Seismological Studies

DOSER, D.I., Dept. Geol. Sciences, Univ. Texas at El Paso, El Paso, TX 79968, doser@geo.utep.edu

The Rio Grande Rift/Great Plains Transition zone in west Texas and southern New Mexico has no current evidence for Holocene faulting, and until this decade the limited seismicity of the region had been commonly thought to be related to oil field activity in the Permian Basin. The occurrence of two moderate earthquakes in 1992 (Rattlesnake Canyon, NM, mbLG=5.0) and 1995 (Alpine, TX, Mw=5.7) within this region, as well as more detailed studies of Permian Basin seismicity, indicate that much of the regional seismicity is tectonically related. Focal mechanisms of earthquakes in the rift and transition zone indicate normal-oblique faulting at shallow (< 20 km depths). The direction of extension, however, changes across the region, with NNE oriented extension in the Permian Basin (including Rattlesnake Canyon), E-W oriented extension in the Alpine region and NW oriented extension associated with the 1931 Valentine, Texas, (Mw=6.3) mainshock, located within the Rio Grande Rift ~120 km west of the Alpine event. Results of regional waveform modeling, first motion, aftershock relocation and isoseismal studies for events of the transition zone and rift will be presented to characterize the differences and similarities in earthquake behavior and site response of these tectonic regions.

Slow, Gravity-Driven Lithospheric Extension in the Western United States

UNRUH, J.R. (Wm. Lettis & Assoc., Walnut Creek, CA 94596; unruh@lettis com), JONES, C.H. (Dept. Geol. Sci., Univ. of Colorado, Boulder, CO 80309-0399; cjones@mantle.colorado.edu), and SONDER, L.J. (Dept. of Earth Sciences, Dartmouth College, Hanover, NH 03755; leslie.j.sonder@dartmouth.edu) (Sponsor: William R. Lettis)

The very low slip rates exhibited by many faults in the western U.S., as well as the limited duration of seismological and geodetic observations, are problematic for evaluating regional deformation rates and associated seismic hazards. Using an approach that combines estimates of the buoyancy force available to drive deformation with estimates of average lithospheric strength (Jones et al. 1996), we compare predicted strain rates in the Sierra Nevada and southern Rocky Mountains with the best geologic estimates of late Cenozoic strain rates. Based on preliminary analyses, the buoyancy force available to drive extensional deformation in the northern Sierra Nevada is sufficient to produce average extension rates of 10e−18 /s to 10e−17 /s, given estimates of average viscosity of the Sierran lithosphere. Total dip-slip displacement of late Miocene volcanic flows along a 70 km NE-SW transect across the northern Sierra Nevada (Page et al. 1995) suggests an average integrated late Cenozoic extensional strain rate of about 10e−17 /s, consistent at the order-of-magnitude level with predicted rates. A similar analysis of the southern Front Range, central Colorado, indicates that normal faults with long recurrence intervals for surface-rupturing events also may be accommodating slow, gravity-driven spreading of the southern Rockies lithosphere. These preliminary results suggest that: (1) large areas of the western U.S. are subject to intrinsic buoyancy forces that are capable of driving active deformation; and (2) variations in rates of seismic and surface-faulting activity in the western U.S. east of the Pacific/North American plate boundary reflect variations in the effective viscosity of the lithosphere, in addition to variations in the magnitude of the horizontal deviatoric tensile stress available to drive deformation.

Implications of GPS Deformation Measurements on Earthquake Hazard Assessment of the Wasatch Fault Zone

SMITH, R.B., MEERTENS, C.M., and MARTINEZ, L.J., Department of Geology and Geophysics, University of Utah, Salt Lake City, Utah, 84112, USA, chuckm@unavco.ucar.edu, rbsmith@mines.utah.edu.

Repeated GPS surveys and comparisons with older geodetic data from the Wasatch fault zone show relatively rapid crustal extension at a rate of 0.05 ± 0.02 microstrain/yr, corresponding to a 2.7 ± 1.3 (1 sigma) mm/yr rate of horizontal displacement across a 55-km wide area. This rate is two to three times larger than the average Late Quaternary fault slip rate on the Wasatch fault. It is also tens of times larger than the displacement rates inferred from the cumulative seismic moments which are small due to the absence of significant historical earthquakes. The U.S. Geological Survey has recently compiled a series of National Earthquake Hazard Maps in terms of the estimated annual exceedance rates of peak ground acceleration (PGA) using just the fault slip rates and historical earthquake rates [Frankel, et al., 1996]. The PGA values for a 10% probability of exceedance in 50 years for the Wasatch fault zone are as large as 0.2 to 0.25 g. The observed GPS deformation rates, if indicative of loading of the Wasatch fault zone, significantly raise the PGA to 0.3 to 0.35 g. These new findings demonstrate the importance of GPS deformation measurements in earthquake hazard assessment.

DO NEW GEODETIC DATA INDICATE HIGHER SEISMIC HAZARD IN THE SALT LAKE CITY – OGDEN REGION, UTAH?

PECHMANN, J. C., University of Utah, Department of Geology and Geophysics, 135 S 1460 E Rm 705, Salt Lake City, UT 84112-0111; pechmann@seis.utah.edu

Geodetic observations from 1962-1994 for a region surrounding the Wasatch fault near Salt Lake City and Ogden, Utah, show an unexpectedly high ENE-WSW extensional strain rate of 51±18 (2σ) nanostrains/yr (Martinez et al., 1995, EOS 76, no. 46, F361). This strain rate corresponds to an extension rate of 3.6±1.3 mm/yr across the ~70 km width of the study region. I examine the question of whether or not probabilistic seismic hazard analyses (PSHAs) for this region, which are based on geological and seismological data only, should be revised to account for these new geodetic data.

Assuming normal faulting on planes dipping 45° ENE or WSW and applying Kostrov's equation, the observed strain rate translates into an expected seismic moment rate of $2.1 \pm 0.8 \times 10^{24}$ dyne-cm/yr within the ~70 by 100 km area of the geodetic network. Slip rates and lengths of active faults in this area, plus a recurrence relation for background earthquakes of $M \leq 6.5$, give a long-term seismic moment rate of $0.76^{+.34}_{-.30} \times 10^{24}$ dyne-cm/yr. This rate is the maximum moment rate attributable to strain accumulation and release on known seismic sources in the area, because the strain accumulation zones for at least some of the faults probably extend beyond the area boundaries. Thus, the geological/seismological moment rate estimate is lower than the geodetic estimate by a factor of three or more.

If the geodetically-measured deformation rate is ascribed entirely to long-term strain accumulation on faults, then it is very difficult to use this rate in a PSHA without contradicting other data which are more directly related to earthquake occurrence. Given the tectonic setting, it is unlikely that there are any buried faults with slip rates high enough to explain the excess deformation rate. Alternative explanations for the high geodetic deformation rate measurement include (1) a short-term strain transient, (2) aseismic deformation, and (3) measurement error. Although (1) could be interpreted to suggest higher seismic hazard, higher-than-average strain rates have primarily been observed after large earthquakes when the hazard is presumably much lower. Regarding (3), it is worth noting that the 95% confidence limits (2σ) on the geodetic strain rate are large enough to account for more than half of the apparent moment rate discrepancy. Considering all these uncertainties, it appears premature to revise seismic hazard estimates for this region upward by using the geodetic strain rate in PSHAs.

NEW PROBABILISTIC SEISMIC HAZARD ESTIMATES FOR SALT LAKE CITY, UTAH

WONG, I.G., BOTT, J.D.J., and OLIG, S.S., Woodward-Clyde Federal Services, 500 12th Street, Oakland, CA 94607; BECKER, A.M., WCFS, Salt Lake City, UT 84047

As a prelude to a recently USGS-funded microzonation mapping project for ground shaking, we have performed a probabilistic seismic hazard analysis of selected sites in the Salt Lake City metropolitan area. We have incorporated the most up-to-date information on five late-Quaternary faults within 100 km of the city (Wasatch, East Great Salt Lake, Oquirrh, West Valley, and Stansbury) and a background earthquake areal zone with a maximum magnitude of M_w 6½ ± ¼. The fault characterization, which included fault geometry, rupture segmentation, maximum earthquakes, recurrence model, and recurrence intervals/slip rates, was based primarily on the extensive paleoseismic investigations that have been performed in the region. The characteristic earthquake model was generally adopted for each of the faults. The recurrence of the background earthquake was based on the historical earthquake record which dates from 1900 to 1994. Three California-based empirical attenuation relationships and the Spudich *et al.* (1997) relationship, which was developed for extensional tectonic regimes like the Salt Lake Valley, were used in the probabilistic analysis.

Based on our analysis, the probabilistic peak horizontal accelerations at stiff and deep soil sites range from about 0.30 to 0.40 g and 0.60 to 0.80 g for return periods of 500 and 2,500 years, respectively. The dominant contributor to the ground shaking hazard in Salt Lake City is the Wasatch fault with its relatively short recurrence intervals of 1400 to 7,000 years and maximum earthquakes of M_w 6¾ to 7¼ for the various segments. Because the hazard is dominated by the nearby Wasatch fault, the rate of ground motion attenuation was not a critical factor. However, if stress drops of extensional earthquakes are smaller than those of California events (Becker and Abrahamson [this volume]) as implied by the Spudich *et al.* (1997) relationship, this factor can be crucial in lowering the computed level of ground shaking hazard by 20% or more both in the Salt Lake Valley and elsewhere in the Basin and Range Province.

SEA98, an Updated Predictive Relation for Earthquake Ground Motions in Extensional Tectonic Regimes

SPUDICH, P., JOYNER, W.B., BOORE, D.M., LINDH, A.G., U.S. Geological Survey, Menlo Park, CA 94025 USA, spudich@samoa.wr.usgs.gov, joyner@samoa.wr.usgs.gov, boore@samoa.wr.usgs.gov, lindh@andreas.wr.usgs.gov, MARGARIS, V.N., Inst Eng Seismol and Eq Eng, Thessaloniki, Greece, margaris@quake.itsak.gr

We present SEA98, an update to the predictive relation SEA96 (Spudich et al., SRL, 1997) for horizontal peak ground acceleration and 5%-damped pseudo-velocity response spectrum. SEA98 differs from SEA96 because about 20% more records were used and because a one-step regression was used to obtain the magnitude and distance dependence. SEA98 is based on data from extensional regime earthquakes having moment magnitude M > 5.0 recorded at distances less than 105 km. SEA98 may be used in the 5.0–7.7 magnitude range and the 0–70 km distance range for extensional regime earthquakes.

Our data set consisted of earthquakes in Europe, the Middle East, New Zealand, and Central America if either their focal mechanisms, neotectonic stress indicators, or geologic setting indicated extensional regime classification, and western United States events associated with active tectonic extension, such as those in the Basin and Range province, the Yellowstone hot spot, the Salton trough, and in volcanically or geothermally active areas like Long Valley, California.

Recording sites were classified into two geologic catagories, 'rock' and 'soil,' following the classification scheme of Joyner and Boore (1981). We used the source-receiver distance metric of Joyner and Boore (1981, 1988), the shortest distance from the receiver to the vertical projection onto the Earth's surface of the fault rupture area. To determine this area, we first estimated the extent of the slipped region on the fault from ground motion inversions, geodetic inversions, aftershock distributions, or from a moment - rupture area relation (Wells and Coppersmith, 1994). The boundary of the rupture area was then taken to be a rectangular box enclosing this slipped region on the fault plane.

Because our extensional regime data set had no events larger than M=7.2, we adopted the magnitude dependence determined from a larger data set by Boore et al. (1993, 1994) and used our extensional regime data set to constrain the constant term and the distance and site dependent terms. The constant term would roughly account for possible systematic stress drop differences between extensional and other tectonic regimes.

The Importance of Random Seismicity in Seismic Hazard Evaluations within the Intermountain West, and Engineering Consequences

AKE, J., LAFORGE, R., VETTER, U., U.S. Bureau of Reclamation, Seismotectonics and Geophysics Group, PO 25007, MS D-8330, Denver, CO 80225, jake@seismo.usbr.gov

The evaluation of seismic hazards for critical structures can be very different depending on the tectonic characteristics of the region in question. For example, in much of southern and western California, the seismic hazard is dominated by faults whose maximum magnitudes occur at intervals of less than 1000 years. However, within the Rocky Mountain-intermountain region, with very few exceptions (i.e. within ~15 km of a few faults with moderate slip rates) the hazard for annual frequencies of exceedence of engineering interest is dominated by the occurrence of background or random earthquakes. When attempting to evaluate seismic hazard probabilistically under these circumstances, the uncertainty in parameters and models become very important.

This situation becomes especially critical when engineering evaluations are conducted using time series in a risk-based framework. For cases where the site of interest is near a significant fault with appreciable slip-rate (the engineer's nightmare), the assessment of the hazard is dominated by ground motions arising on that fault. This makes selection of time histories relatively straightforward (the seismologist's blessing). However, in cases where the hazard is dominated by background earthquakes, the absolute hazard level may be somewhat lower (engineering nirvana) but the assignment of representative time series becomes much more problematical (seismological purgatory). Multiple attribute analysis (response spectra, Fourier spectra, peak velocity, intensity, energy) may help reduce the inherent nonuniqueness in these cases and aid in selection of a finite number of time histories for use in failure-based engineering analyses.

Monday AM, March 16, 1998—Room 235
Theory and Simulations of the Earthquake Source
Presiding: John Rundle, *Univ. of Colorado* and **Nick Beeler**, *USGS*

Dynamic Modeling of Thrust and Normal Faults: Differences in Near-Source Ground Motion

OGLESBY, D.O., ARCHULETA, R.J., Institute for Crustal Studies and Dept. of Geological Sciences, UC Santa Barbara, Santa Barbara, CA 93106, oglesby@quake.crustal.ucsb.edu, ralph@quake.crustal.ucsb.edu; NIELSEN, S.B., Institute for Crustal Studies and Materials Research Laboratory, UC Santa Barbara, Santa Barbara, CA 93106, snielsen@quake.crustal.ucsb.edu

We have previously shown (Oglesby et al. 1998, under review) that the rupture and slip processes of a dip-slip fault are greatly affected by the asymmetric geometry of the fault and free surface. Two effects of this broken symmetry are: 1) The hanging wall moves more than the footwall; 2) The interaction of the stress field with the free surface leads to a time-dependent normal stress on the fault that in turn leads to a time-dependent frictional stress. This time-dependent frictional stress causes a thrust fault to produce much larger ground motion than a normal fault with identical initial stress magnitude. Our previous work dealt only with faults that intersected the free surface; here we investigate the dependence of the foregoing effects on the depth of a buried fault. Both the hanging wall/footwall effect and the effect of time-dependent normal stress decrease rapidly with increasing burial of the fault. Differences between thrust and normal faulting become negligible at burial depths greater than approximately 2 km. Considering only dynamic effects, our results suggest that the style of faulting affects the ground motion only if the fault penetrates or nearly penetrates the free surface. However, this conclusion ignores other differences, such as the mean stress field, which may cause differences between thrust and normal fault motions. We also investigate the effect of time-dependent normal stress on faults that intersect the free surface by comparing simulations which include/exclude this time-dependence. While the difference between hanging wall and footwall motions persists, the difference between thrust and normal faulting disappears when the time-dependence of normal stress is ignored. The implication is that dynamic earthquake simulations on dipping faults that intersect the free surface must include the time dependence of normal stress.

Beginning of Earthquakes Modeled with the Griffith Fracture Criterion

SATO,T., Dept. of Earth and Environmental Sciences, Hirosaki Univ., Hirosaki 036, Japan, tamao@cc.hirosaki-u.ac.jp; KANAMORI, H., Seismological Laboratory, California Institute of Technology, Pasadina, CA91125, hiroo@gps.caltech.edu

We present a source model for the beginning of earthquakes based on the Griffith fracture criterion. The initial state we choose for this model is a critical state of pre-existing circular fault, which is on the verge of instability. After the onset of instability, the fault grows with a progressively increasing rupture speed, satisfying the condition of fracture energy balance at the crack tip. We investigate the difference in rupture growth patterns in two classes of models which are considered to represent end-member cases. In the first model (Spontaneous Model), faults with small initial dimensions grow in the medium with small surface energy, and those with large initial dimensions, in large surface energy. The time taken for the rupture speed to reach its limitting velocity is proportional to the initial fault length. The synthetic velocity seismogram at far-field shows a weak initial phase of which duration scales with the initial fault length. In the second model (Trigger Model), we envisage that pre-existing faults in the crust with various length are locked by some obstacle at their ends (e.g. fault segmentation, strong asperity etc). This situation is modeled with a local increase in the surface energy near the ends of faults. In this model, once an earthquake is triggered, the rupture speed attains its limitting velocity almost instantaneously. The synthetic velocity seismogram at far-field shows an abrupt, linear increase in amplitude without the weak initial phase that appears in the Spontaneous Model. These two end-member models indicate that the variability in the observed seismic initiation phase may represent a variation of strength (surface energy) and local stress distributions surrounding the pre-existing faults.

NUCLEATION, GROWTH AND ARREST OF EARTHQUAKES: MODELS AND IMPLICATIONS FOR GENERAL EARTHQUAKE MODELS

RUNDLE, J.B., GROSS, S., Colorado Center for Chaos & Complexity, & CIRES, CB 216, University of Colorado, Boulder, CO, 80309, USA, rundle@fractal.colorado.edu; KLEIN, W., Dept. of Physics, Boston University, Boston, MA 02215, USA, klein@buphyc.bu.edu

In geometrically realistic simulations of earthquake fault systems proposed some years ago (1988), in which earthquakes driven via plate motion occur in a layered viscoelastic model of Southern California, a variety of phenomenology characteristic of real earthquakes was observed. At that time, quantitative tests of the models and simulations were hampered due to the lack of adequate data, as well as understanding of the basic statistical mechanics of the system. In this talk we summarize the results of recent research that provides unifying themes for understanding the physics of earthquake occurrence, including nucleation, growth, and arrest. We describe recent understanding of the physics of how earthquakes nucleate in a statistically rough stress field, the implications for the Gutenberg-Richter relation, and the construction of the growth-and-breakout curve that describes whether and how earthquakes arrest. For individual faults and relatively isolated fault systems, these models are characterized by a process of "punctuated equilibrium" that is consistent with the idea of Intermittent Criticality proposed by Sammis and coworkers. In particular, we focus on observational consequences of these models that can in principle provide methods for testing the various models and simulations, a focus that is consistent with that of new ideas for General Earthquake Models. We note that many of the codes described in this talk that are used for the simulations are available on our anonymous ftp site: (/fractal/users/ftp/pub/Viscocodes) for public use.

Dynamic Simulation of Spontaneous Rupture with Heterogeneous Stress Drop

ANDREWS, D.J., and BOATWRIGHT, J., U.S. Geological Survey, MS 977, Menlo Park, CA 94025, jandrews@moorea.wr.usgs.gov

We model a dynamic earthquake source using a randomly generated function for initial stress on a 2D planar fault. The spatial spectrum of stress is chosen to have equal power in equal logarithmic intervals of wavenumber. The resulting slip distribution has a degree of irregularity resembling that observed in actual earthquakes. The calculation is done with a new 3D finite difference code that uses spatial differencing equivalent to rectangular-box finite elements. The fault is a plane of split nodes that move dynamically under the action of fault traction and stress in adjoining elements. Fault traction is determined from a friction law, which in this work is simply a drop to kinetic friction after the static friction is reached. The stress drop is spread out in time sufficiently to reduce numerical noise. Calculated slip velocity has concentrations in space and time that resemble subevents. Rupture speed is variable. In future work we plan to use models with such verisimilitude to investigate practical ground motion questions, such as directivity.

What Underlies the Gutenberg-Richter Law?

SCHOLZ, C.H., Lamont-Doherty Earth Observatory, Columbia Univ., Palisades, NY, 10964, scholz@ldeo.columbia.edu; SPYROPOULOS,C., Dept. Appl. Physics, Columbia Univ., New York, NY, 10027, cspyro@appmath.columbia.edu.

Earthquakes, when measured in a linear scale like moment, obey a ubiquitous power-law size distribution known as the Gutenberg-Richter law. When sampled over sufficiently large temporal and spacial ranges, the exponent B in this distribution takes on two universal values, 2/3 for small earthquakes and 1 for large earthquakes, where 'small' and 'large' earthquakes refer to their dimensions relative to the seismogenic width.

It has more recently become known that faults and fault segments also obey power-law size distributions. Can it be that the Gutenberg-Richter law derives from these underlying fault and fault segment size distributions? Formally, this appears to be true. When one takes the observed relation between large and small earthquakes for the seismic cycle and integrates this over a fault population, the full Guterberg-Richter law is obtained, with the correct two universal exponents. The problem then reduces to explaining the size distribution of faults. A numerical model of the growth of a population of cracks in a brittle layer overlying a ductile substrate shows that the power-law size distribution develops spontaneously through the stress interactions between cracks. In this model, in which the layer properties are uniform with low random disorder and in which only a local fracture criterion is prescribed, these stress interactions propagate to all length scales to produce the observed fractal nature of the population as a whole.

On Coseismic Changes of Slip Direction: The Effect of Low Initial Shear Stress on 3-D Dynamic Simulation of Spontaneous Rupture

GUATTERI, M., Dept. of Geophysics, Stanford Univ., Stanford, CA 94306-2215, patti@pangea.stanford.edu; SPUDICH, P., U.S.Geological Survey, 345 Middlefield Rd, MS 977, Menlo Park, CA 94025, spudich@samoa.wr.usgs.gov

We investigate the dynamics of rupture at low stress level. We show that one main difference between the dynamics of high and low stress events is the amount of coseismic temporal rake rotation occurring at given points on the fault. Curved striations on exposed fault surfaces and earthquake dislocation models derived from ground motion inversion indicate that the slip direction can change with time at a point on the fault during rupture. We use a 3-D B.I. method to model temporal rake variations during dynamic rupture propagation assuming a slip-weakening friction law and isotropic friction. The points at which the slip rotates most are characterized by an initial shear stress direction substantially deviating from the average stress direction. We show that for a given value of stress drop the level of initial shear stress determines the amount of rotation in slip direction. We infer that seismic events that show evidence of temporal rake rotations are characterized by a low initial shear stress level with spatially variable direction on the fault and an almost complete stress drop.

The initial rake is in general collinear with the initial stress at the hypocentral zone, supporting the assumptions made in stress tensor inversion from first motion analysis. At other points on the fault, especially away from the hypocenter, the initial slip rake may not be collinear with the initial shear stress, contradicting the usual assumption of structural geology. On the other hand, the later part of slip in our models is systematically more aligned with the average stress direction than the early slip. Our modeling suggests that the length of the straight part of curved striations could give an upper bound of the slip-weakening distance over the fault plane, and the direction of the late part of slip should have more weight in the estimate of initial stress direction.

CAN RATE-AND-STATE FRICTION EXPLAIN HOW THE 1911 MORGAN HILL, CA EARTHQUAKE BROKE THROUGH THE 1906 STRESS SHADOW?

HARRIS, R.A., and R.W. SIMPSON, U.S. Geological Survey, Mail Stop 977, 345 Middlefield Road, Menlo Park, CA 94025, harris@usgs.gov; simpson@gold.wr.usgs.gov

The great 1906 San Francisco, California earthquake silenced many nearby faults in central California for decades, producing an apparent quiescence, at least for large earthquakes. Calculations of static stress-changes, using elastic-dislocation theory, show that the spatial and temporal pattern of this post-1906 quiescence is generally quite consistent with Coulomb failure models.

There is, however, at least one exception to the 1906 Coulomb-failure stress-shadow model. A large M=6.5 earthquake in 1911 appears to have occurred at a relaxed site on the Calaveras fault. It has been suggested that this earthquake was an earlier version of the 1984 Morgan Hill earthquake. We examined the possibility that another friction formulation, that of rate-and-state friction, as expressed by Dieterich [JGR, 1994] could explain this apparently anomalous earthquake. Rate-and-state friction laws predict that there is not a simple failure threshold (as in CF), but that time-to-failure is a complex function of prior state history as well as the current state of the system. The result is that rate-and-state friction can allow earthquakes to 'break-through' a Coulomb-failure stress-shadow, if the affected fault was already close to failure before the stress-changes occurred. We applied Dieterich's [1994] rate-and-state time-to-failure equations to the 1911-case, using the previously calculated stress-changes, and plausible ranges of values for the numerous rate-and-state variables. We find that rate-and-state friction is consistent with the location and timing of the 1911 earthquake, if the earthquake had been close to failure already, in 1906. This does not imply that rate-and-state friction is the only explanation for this anomalous event, only that rate-and-state does offer a possible explanation.

High-Frequency Radiation From an Extended Fault: Implications of Choice of the Subevent Slip History

TUMARKIN, A.G., Institute for Crustal Studies, University of California, Santa Barbara, CA 93106-1100.

We are studying the problem of how to choose the functional form of the subfault slip history in a kinematic modeling of a seismic rupture. This is especially important for predicting high-frequency radiation (and, consequently, the damage potential of an earthquake), as the low frequencies are well constrained by the total seismic moment.

One of the fundamental principles of simulating a continuous medium is that the results of the discretization procedure should tend to a finite limit as the cell's size decreases to zero. Irikura (1983) and Joyner and Boore (1986) were first to notice a major problem with using earthquake-like source-time functions to represent the rupture of a discrete cell. Simple physical and formal scaling considerations provide valuable insight on the acceptable slip-rate subfault histories. They allow us to reject a w-squared subevent in the form of the Brune's pulse in a general case, and to substantiate the use of the Boatwright's asperity subevent model (Boatwright, 1988; Tumarkin and Archuleta, 1994, 1997).

We show the examples of simulating past earthquakes with different choices of subevents. The increase of high-frequency radiation with a decreased subfault size is apparent in the w-squared slip-rate case (Tumarkin et al., 1994; Beresnev and Atkinson, 1998), while the use of the asperity model produces stable high-frequency levels.

Repeating Earthquakes and the Long-Term Evolution of Seismicity on the San Andreas Fault Near Bear Valley, California

ELLSWORTH, W.L., COLE, A.T., DIETZ, L.D., U.S. Geological Survey, MS-977, Menlo Park, CA 94025, ellswrth@andreas.wr.usgs.gov; DODGE, D.A., Lawrence Livermore National Laboratory, L-206, Livermore, CA 94550.

Seismicity along the creeping segment of the San Andreas fault in central California is characterized by a dense concentration of earthquakes on a narrow, steeply-dipping zone that defines the seismic expression of the fault. Within the fault zone, the earthquakes group in spatial clusters that have approximately maintained their shape through many cycles of main shock/aftershock activity for at least the last 25 years. Although we can recognize the presence of the clusters using catalog locations, we can say little about their structure and temporal organization because the uncertainty in travel time-based locations is many times greater than the source dimensions of the events themselves. We report on a high resolution study of the seismicity, M 1.0 - 4.1, within a small region (approximately 3 km long and 2 km high) containing a well-established repeating M 4.1 ± 0.1 earthquake. This moderate earthquake has occurred 7 times between 1934 and 1995 at an average interval of 10.1 ± 2.6 years, most recently in 1987 and 1995. Our objective is to determine if nearby microearthquake activity also repeats, tiles the fault plane with time, or has a random spatial and temporal structure. We use both frequency-domain and time-domain cross correlation methods to compute high precision locations for all earthquakes on the fault occurring between 1984 and 1995 using the seismograms from the USGS Northern California Seismic Network. The resulting locations have uncertainties comparable to or smaller than the source dimensions of the events. The new locations are not only much more highly clustered than the catalog locations, but naturally form families of repeating earthquakes. Thus, it appears that spatial organization of seismicity is strongly controlled by local properties of the fault, and is comparatively insensitive to the temporal evolution of the stress field.

APPARENT STRESS, SEISMIC EFFICIENCY AND FRICTION

McGarr, A., U.S. Geological Survey, 345 Middlefield Road, MS-977, Menlo Park, CA 94025, mcgarr@usgs.gov.

Apparent stress τ_a is defined as $\tau_a = \eta \bar{\tau}$, where $\bar{\tau}$ is the shear stress loading the fault plane to cause slip and η, the seismic efficiency, is defined as E_s/E, where E_s is the energy radiated seismically and E is the total energy released by the earthquake. Over nearly 18 orders of magnitude in seismic moment, apparent stresses, measured for various types of earthquakes, show no systematic dependence on moment or magnitude. For these events, which include mining-induced tremors, earthquakes triggered at a depth of about 9 km in the German KTB hole, and natural tectonic earthquakes, the apparent stresses τ_a exhibit upper bounds defined by $\tau_a/\bar{\tau} \leq 0.06$. Thus, seismic efficiency η is less than 0.06, or so. The behavior of τ_a and η can be expressed in terms of two simple aspects of stick-slip friction events observed in the laboratory. During such an event, the loading stress drops from its initial value τ_1 to its final value τ_2. At the same time the frictional resisting stress diminishes abruptly from τ_1 to $\bar{\tau}_r$, about which it fluctuates closely for most of the slip event. In the laboratory one observes a median value $\tau_1/\bar{\tau}_r = 1.18$ which yields a seismic efficiency in the range 0 to 0.08, depending on the fault-slip overshoot $(\bar{\tau}_r-\tau_2)/(\tau_1-\tau_2)$, which can vary from 0 to ½. Overshoots observed in the laboratory are distributed about a median value of 0.27, which yields $\eta = 0.05$. Accordingly, bounds on seismic efficiency observed for induced, triggered, and natural earthquakes in a variety of tectonic settings, with a broad range of ambient stress states and pore pressures, and on any scale can be understood in terms of the two stick-slip friction parameters, $\tau_1/\bar{\tau}_r$ and overshoot, which can both be measured in the laboratory. To the extent that these results have general applicability, then measurements of apparent stress for suites of earthquakes can be used to estimate absolute levels of $\bar{\tau}$ in seismic source zones.

Monday PM, March 16, 1998—Forum Room
GPS and Seismology
Presiding: Paul Segall, *Stanford*

Complementarity of GPS and Seismological Data for Tectonic Studies

STEIN, S., Department of Geological Sciences, Northwestern University, Evanston, IL 60208, seth@earth.nwu.edu; DIXON, T., Rosenstiel School for Marine and Atmospheric Sciences, University of Miami, Miami, FL 33149, tim@corsica.rsmas.miami.edu

For tectonic studies, GPS and other space-based geodetic data complement seismological data in several ways beyond study of individual earthquakes. First, by establishing that rates of plate motion over a few years are very similar to those predicted by global plate motion models which average over millions of years, they validate the use of such models for seismic slip and hazard analyses. For example, without space geodetic data, it would be unclear whether the discrepancy between the rate inferred geologically for the San Andreas and the higher rate predicted for Pacific-North America plate motion reflected deformation off the San Andreas or a change in plate motion in the past few million years. Second, because they directly measure the degree to which plate interiors act rigidly, they provide insight into processes responsible for intraplate seismicity. For example, GPS data suggest that strain rates near the New Madrid seismic zone exceed the platewide rates, and so may be largely post-seismic effects of the 1811–1812 earthquakes and hence underestimate their recurrence interval. Third, because GPS data measure motion rates in plate boundary zones, they directly constrain the fractions of seismic and aseismic deformation. For example, GPS data at the Peru subduction zone shows the rate at which slip accumulates on the locked boundary and should be released in future great earthquakes. This estimate avoids many difficulties in previous aseismic slip estimates due to the limited earthquake history, the variability of large earthquakes in space and time, and the possibility of slow or silent earthquakes or afterslip. Similarly, GPS data directly measure the rate of crustal shortening in the foreland thrust belt which is building the Andes, and show that this rate is much faster than inferred from seismic moments, presumably because most occurs aseismically.

Imaging Slow Seismic Sources Using GPS

SEGALL, P., CERVELLI, P., MURRAY, M.H., OWEN, S., Geopysics Department, Stanford University, Stanford, CA, 94305, segall@geo.stanford.edu, and BURGMANN, R., Department of Geology, U.C. Davis, Davis, CA 95616.

In this paper we review methods for estimating source geometry and slip distribution from surface measurements of strain and displacement. Simulated annealing, Random Cost, and other Monte Carlo methods provide reasonable strategies for finding the best fitting finite source fault geometry, while gradient and higher-order derivative methods may provide efficient means for bootstrapping confidence intervals in the estimated parameters.

Inverting for fault slip in space and time is a linear problem once the fault geometry is specified. Estimation has, however, been hampered by poor signal to noise in the data, contaminating non-tectonic motions near the instrument (benchmark wobble), and our lack of knowledge of the temporal character of aseismic motions. Recently, Segall and Matthews (1997, JGR) introduced a Network Inversion Filter (NIF) that yields estimates of quasi-static fault slip as a function of space and time using data from dense continuous geodetic networks. The NIF employs time domain (Kalman) filtering, and allows for non-parametric descriptions of slip velocity, local benchmark motion, and measurment error. A state-space model for the full geodetic network is adopted, so that all data from a given epoch are analyzed together, which allows the filter to distinguish between non-steady fault slip and local surficial effects.

We describe new methods for applying spatial smoothing at each iteration of the filter to model rapidly decaying phenomenon, such as post-seismic fault slip. A revised NIF that incorporates spatial smoothing at each iteration of the filter, will be described that allows one to correctly model space-time behavior of post-seismic slip. Examples will be shown, including post-seismic slip following the 1989 Loma Prieta earthquake.

GPS as a Tool for Assessing Hazard from Crustal Earthquakes in the Pacific Northwest

ROGERS, G.C. and DRAGERT, H., Geological Survey of Canada, Pacific Geoscience Centre, P.O. Box 6000, Sidney B.C. V8L 4B2 Canada, rogers@pgc.emr.ca

Interpreting crustal seismicity presents the greatest source of uncertainty in assessing seismic hazard in the densely populated Puget Sound/Georgia Strait lowland that straddles the Canada-United States border in the Pacific Northwest region of North America. There is a persistent concentration of small crustal earthquakes in the region that appears to be caused by compression parallel to the subduction margin and occurs in a relatively low stress environment. Paleoseismic evidence suggests large earthquakes have occurred in the vicinity of Seattle, Vancouver and Victoria in prehistoric time. However, the three largest (M>7) historic crustal earthquakes (1872, 1918, 1946) have occurred outside the present day concentration of seismicity. Different interpretations of the historical earthquake pattern can lead to different recurrence relations and thus imply different rates of crustal deformation. Direct crustal strain measurements using GPS receivers have the potential to clarify the crustal strain rate and thus lead to a more robust estimate of seismic hazard. A relatively sparse network of continuously operating GPS receivers with average station spacing of about 200km is currently in place and can be used to address this problem. A denser GPS network spanning this seismic region is desirable to measure margin-parallel strain accumulation and to resolve detailed spatial variations of crustal motions.

Resolution of the Interseismic Subsurface Slip Distribution Along the Hayward Fault, California from GPS and SAR Interferometry Data

BURGMANN, R., and SUKHATME, J., Dept. of Geology, University of California Davis, Davis, CA 95616, burgmann@geology.ucdavis.edu, FIELDING, E., JPL, Caltech, 4800 Oak Grove Drive, Pasadena, CA 91109

The Hayward fault in the eastern San Francisco Bay area is thought to be accumulating elastic strain since the 1868 M = 6.8 earthquake that ruptured a ~50-km stretch of the fault. However, aseismic surface creep (5–9 mm/yr) along the full length of the fault at rates approaching the long-term slip rate of ~10mm/yr makes estimates of the strain accumulation rate difficult. Previous analyses of historic trilateration data showed little evidence for strain accumulation along the Hayward fault. To better resolve the distribution of locked and creeping segments along the fault we combine surface creep measurements with historic trilateration and GPS data. These data are consistent with a locking depth of about 5 km, but cannot resolve significant slip variation along the fault.

Analysis of recent Interferometric Synthetic Aperture Radar (IFSAR) measurements reveal active deformation along the Hayward fault between 1992 and 1996. Assuming pure strike slip, 1992-to-1995 slip rates estimated from IFSAR range changes are consistent with creepmeter and alignment array measurements along much of the fault. However, along the southern Fremont segment IFSAR slip estimates of ~16 mm/yr are about twice of those measured in the field. This suggests a significant vertical slip component that may be caused by shallowing of the creeping portion of the fault at the southern tip. We are now trying to formally combine the traditional geodetic measurements with the IFSAR data to improve our resolution of the spatial distribution of currently locked portions of the Hayward fault at depth.

Modeling Postseismic Deformation in Southern California after the 1992 Landers Earthquake

BOCK, Y., WILLIAMS, S., and PRAWIRODIRDJO, L., Cecil H. and Ida M. Green Institute of Geophysics and Planetary Physics, Scripps Institution of Oceanography, 9500 Gilman Drive, La Jolla, CA 92037-0225, ybock@ucsd.edu.

Time series analysis of daily positions estimated for continuous GPS sites in southern California after the 1992 Landers earthquake indicates significant postseismic deformation at 3 well-distributed sites within a radius of about 200 km from the epicentral region but no deformation at a 4th site more than 300 km away (Bock *et al., J. Geophys. Res.,* 102, pp. 18,035–18,055, 1997). The postseismic slip is in the same direction as the coseismic slip. Furthermore, our analysis of three years of continuous GPS data collected after the 1994 Northridge earthquake indicates that the horizontal velocities are now the same as their pre-Landers earthquake values for 3 of the 4 sites. The nature of the observed postseismic deformation indicates that not all the elastic-strain energy was released instantaneously (coseismically) by the Landers earthquake, rather a fraction of it stored in the crustal rocks and slowly released for at least several months after the event. We discuss one interpretation of these observations as deep aseismic afterslip on the main ruptured faults, an elastic rheology, and laboratory-derived constitutive laws for rock friction. Our observations, if systemic to large strike-slip earthquakes that rupture postseismically below the seismogenic layer, can partially explain the apparent deficit of moderate to large earthquakes in southern California attributed to the discrepancy between geologic and geodetic deformation rates and historical seismicity. That is, seismic moment estimates (including mainshocks and aftershocks) provide an underestimate of total elastic-energy release and crustal deformation.

Real-Time Earthquake Geodesy

MURRAY, M.H., DREGER, D.S., NEUHAUSER, D.S., BAXTER, D.R., GEE, L.S., ROMANOWICZ, B., Berkeley Seismological Laboratory, Univ. of California, Berkeley, CA 94720-4760, mmurray@seismo.berkeley.edu

Coseismic geodetic measurements provide useful constraints on earthquake faulting, including the location and extent of the rupture plane, unambiguous resolution of the nodal plane, and distribution of slip on the fault plane unbiased by rupture velocity assumptions. They can be combined with complementary seismic observations to improve estimates of fault slip and geometry, rupture propagation, strong-ground motion, and surface deformation. We are developing methods to combine GPS and broadband seismic observations in near real-time to provide earthquake notification information for hazard mitigation and emergency response activities. We are telemetering continuous real-time data from more than ten GPS sites in the northern California, most co-located with broadband seismic stations equipped with Quanterra dataloggers and continuous frame relay or radio telemetry circuits. We have developed methods to acquire continuous GPS data using the reliable real-time telemetry stream between the Quanterra datalogger and the central site, and to unpack the data for subsequent processing and archiving. Station positions, currently estimated hourly using fixed predicted orbits and one hour of GPS measurements, can reliably detect 5-cm horizontal and 15-cm vertical displacements. We are implementing Kalman filter techniques that will significantly improve the precision and processing speed. We use Monte Carlo-based optimization techniques to rapidly estimate finite-fault characteristics from the displacements. Simulations suggest that a M=7 earthquake on the Hayward fault earthquake would be reasonably well resolved by the current sparse BARD network in the San Francisco Bay area. Starting from a rapidly determined seismic location and moment tensor, a geodetically improved estimate of the fault geometry would be available within 12–15 minutes of the mainshock.

GPS Measurements of Interseismic, Coseismic, and Postseismic Slip Along a Terrane Suture, The Ramu-Markham Fault in Papua New Guinea

STEVENS, C., SILVER, E.A., University of California, Santa Cruz, CA 95064, cstevens@earthsci.ucsc.edu; MCCAFFREY, R., Rensselaer Polytechnic Institute, Troy, NY 12180; TREGONING, P., Australian National University, Canberra, Australia: LITTLE, R., JACKSON, R., University of Technology, Lae, Papua New Guinea; ENGLISH, P., LORATUNG, W., National Mapping Bureau, Port Moresby, Papua New Guinea

GPS measurements were made in the Markham Valley of Papua New Guinea (PNG) in August of 1993 to monitor strain accumulation in the zone of collision between the Finisterre terrane and the Australian plate. The predicted convergence rate derived from recent regional GPS measurements (Tregoning et al., submitted to JGR, 1997) is about 35 mm/yr. Comparison of the 1993 GPS to 1973 EDM measurements reveals a convergence rate of about 4 mm/yr across the Markham Valley. We infer the slip to be interseismic because no large earthquakes occurred in this 20 year period. We explain this low rate by the proximity of the sites to a locked fault. In October of 1993 four large (Mw = 6.3–6.8) thrust earthquakes occurred just north of our GPS network. Our remeasurement of the GPS sites in January 1994 indicates 20cm of coseismic slip across the Markham Valley. Waveform modeling of the earthquakes shows gently dipping (~15 degrees) thrust events with centroid depths of about 20 km. Together these data suggest that the Ramu-Markham fault is a low-angle mid-crustal detachment fault that steepens southward, connecting to a high-angle ramp fault near the Markham Valley. Sites were again measured with GPS in April 1997. Preliminary results reveal an average postseismic slip rate of about 35 mm/yr, which is close to the predicted plate rate and suggests aseismic fault creep. The GPS measurements have thus determined average rates of interseismic, coseismic, and postseismic slip on the Ramu-Markham fault, and supports other studies showing major postseismic creep as part of the earthquake cycle. Remeasuring these sites in mid–1998 will reveal whether the fault continues to creep or is now locked.

Periodic Strain Across the East African Rift Using Continuous GPS

BENDICK, R., BILHAM, R. CIRES & Dept of Geol.Sciences. University of Colorado at Boulder, CO 80309-0250, and BRAUN, J., UNAVCO, UCAR, Boulder

A pair of GPS receivers separated by 120 km on the flanks of the East African Rift in Ethiopia, measures a secular widening rate of ≈4 mm/year, and is being used simultaneously to search for amplification of the earth's strain tide, resulting from possible rheological weakness in the rift zone. Data are sampled every 30 s and averaged for 10 minutes to yield 3-D position estimates with point-to-point scatter of several cm. Spectral analysis of 3 months of continuous data obtained during Ethiopian monsoon conditions (an unfavorably heterogeneous wet troposphere) records strain tides close to the noise level (6 mm in horizontal components). Similar studies using continuous Japanese data are reported to provide 0.2 mm noise levels at diurnal and semidiurnal periods, presumably due to more uniform tropospheric conditions, whose noise contributions are better estimated during analysis. Current data from Ethiopia indicate a noise level of ≈1 mm for periodic displacements between 20 minutes (the current aliasing frequency) and 60 minutes, corresponding to a strain resolution of 10E–8. These amplitudes and frequencies are adequate to record the Earth's free oscillations in normal crustal materials. In that we seek the degree of amplification of signals across the rift, and corresponding attenuation of signals on the flanks of the rift, it is important that we know the far-field amplitude of these applied signals. We plan to do this in the future, by installing additional receivers in regions contiguous to the rift on the African and Somali blocks. The resulting array will measure the amplitude and phase of applied tidal and seismic strain signals, and their modification by the rift. Because both the Earth tide signal and the free oscillation signal contain volumetric and shear components, we envisage probing the bulk and shear modulii of the rift zone at various wavelengths, and hence to various depths.

Integrated Networks for GPS Geodesy, Seismology and Atmospheric Science

MEERTENS, C.M., C. ROCKEN, T. VANHOVE, and R. WARE, University NAVSTAR Consortium/University Corporation for Atmospheric Research, chuckm@ucar.edu; SMITH, R.B., Dept. of Geology and Geophysics, University of Utah, Salt Lake City, Utah, 84112, rbsmith@mines.utah.edu; BENZ, H., U. S. Geological Survey, Golden, CO, 80225, benz@gldage.cr.usgs.gov.

Co-location of GPS, seismological and meteorological instrumentation can significantly reduce infrastructure costs and provide data of broad scientific interest. GPS measurements provide precise geodetic coordinates and, over time, crustal displacement and strain rates. By making continuous observations at high-quality monuments, GPS geodesy is capable addressing a new class of large-scale geologic problems where the deformation rates are only a few mm/year or less. Some examples include hot spot-plate interaction, measurement of the earthquake deformation cycle, glacial rebound, and coastal subsidence. GPS signals also sense properties of the ionosphere and neutral atmosphere and can provide valuable data for meteorology, climate, and "space weather" research applications. A shared need for long-term observations helps to ensure the continuity needed to measure slower deformation rates and climatic changes. Near-real time GPS processing for meteorological parameters for weather applications, in the mean time, provides results of immediate interest and utility. An informal collaboration involving the Univ. of Utah, USGS, UNAVCO and NOAA demonstrates the potential of such an integrated network. At the Yellowstone caldera, a Univ. of Utah GPS receiver and a National Seismic System digital broadband seismic station continuously transmit data via VSAT to the USGS in Golden. These data, and data from the Univ. of Utah Wasatch fault GPS network, are sent hourly via internet to the UNAVCO/Boulder GPS data archives. The U. of Utah determines precise coordinates and velocities at daily and monthly intervals while hourly data from these sites, as well as NOAA GPS sites in the midcontinent, are processed for tropospheric water vapor estimates by UCAR and NOAA. This automated, integrated system takes full advantage of developed power, data collection and transmission systems, and provides, with no additional cost, a wealth of data to scientists from different fields.

Monday PM, March 16, 1998—Room 235
North American Lithosphere and Asthenosphere
Presiding: Ken Dueker, *Univ. of Colorado* and **Joydeep Bhattacharyya**, *Yale*

An Overview of Crustal Structure in the Rocky Mountain Region

KELLER, G. RANDY, SNELSON, C.M., MILLER, KATE, Department of Geological Sciences, University of Texas at El Paso, El Paso, TX 79968, keller@geo.utep.edu; SHEEHAN, ANNE, DUEKER, KEN, Department of Geological Sciences, CIRES, University of Colorado, Boulder, CO, 80309, afs@mantle.colorado.edu; LEVANDER, ALAN, HENSTOCK, T.J., Department of Geology and Geophysics, Rice University, Houston, TX, 77005, alan@geophysics.rice.edu.

In spite of much interest in the tectonic evolution of the Rocky Mountain region, our knowledge of its lithospheric structure is modest. From a physiographic point of view, the Rio Grande rift is an extensional feature which follows the crest of an uplift on which the Southern Rocky Mountains are located. Thus, these features share much in terms of their tectonic evolution. This evolution has effected the lithosphere pervasively, and the associated modification of the crust has been very complex. In the Rio Grande rift, distinct crustal thinning (at least 5 km relative to adjacent areas) can be documented from Albuquerque, New Mexico southward and widens southwards as does the physiographic expression of the rift. The thinnest crust documented to date (about 28 km) is found west of El Paso, Texas. In contrast with East Africa, the crustal thinning is gradual from the rift valley to the shoulders perhaps reflecting the thermal regime which existed prior to rifting. The thickest crust in the region (about 50 km) appears to be associated with both Southern Rockies in Colorado and the Great Plains in Colorado and New Mexico. This lack of correlation between topography and crustal thickness implies that the mantle is playing a major role in the attainment of isostatic balance in the area. The magmatic modification of the crust during rifting appears to have been minor. However, the modification due to the voluminous mid-Tertiary magmatism in the Datil-Mogollon volcanic field (southwestern New Mexico) and San Juan volcanic field (southwestern Colorado) is substantial (about 20% of the crust is

a batholith). In the northern Rocky Mountain region, relatively little is known about crustal structure in Wyoming. However, there is evidence of the crust thinning northward from Colorado. This thinning could be a relic of the rifting of the southern margin of the Wyoming craton. Further north, the DEEP PROBE project has revealed thick (about 50 km) crust beginning in central Wyoming and extending across Montana. The lowermost crust is also anomalously thick (about 20 km) and has a velocity of about 7.2 km/s. In the same region, a high velocity layer is observed in the mantle at a depth of about 120 km. This combination of features correlates with the Archean Wyoming craton suggesting that they might be Archean in age.

Teleseismic Receiver Function Imaging of Upper Mantle Structure Below the Colorado Plateau

GILBERT, H.J., SHEEHAN, A.F., and DUEKER, K.G., University of Colorado, Boulder, Colorado, 80309, hersh@mantle.colorado.edu

In this study we examine the mantle structure below the Eastern Basin and Range and Colorado Plateau in order to explore the link between the upper mantle, mantle transition zone, and surface tectonics. We use approximately 250 radial receiver functions measured from data collected in the 1994–1995 Colorado Plateau-Great Basin IRIS PASSCAL deployment across Utah and eastern Nevada. We study the mantle discontinuity structure by analyzing converted P to S (Pds) phases produced by mode conversions at velocity discontinuities.

A stack of all radial receiver functions shows depths for the 410 and 660 km discontinuities at approximately 428 and 676 km respectively migrated with the TNA shear wave velocity model (Grand and Helmberger, 1984) and a constant Vp/Vs ratio of 1.83. An average transition zone thickness of 248 km is found from a stack of all receiver functions from the study area. Imaging of the discontinuity topography is accomplished by constructing geographic bins of Pds conversion points. This process is analogous to common mid-point stacking in reflection seismology.

We examine different subsets of the array in order to search for the high velocity anomaly imaged by Van der Lee and Nolet (1997) which they interpreted as the Farrallon slab. We see 30 km of transition zone thickness variation. By combining our results with Snake River Plain, Rocky Mountain Front, and Green River PASSCAL data sets we have constructed an image of the topography of the 410 and 660 km discontinuity structure for a large portion of the western United States.

Implications of Transition Zone Discontinuities Beneath the Western U.S.

DUEKER, K.G. and A.F. SHEEHAN, University of Colorado at Boulder, Campus box 399, Boulder, Co 80302 ken@mantle.colorado.edu

The 410 and 660 km seismic discontinuities most likely manifest the pressure induced phase transformations of the olivine component of the mantle. In the past, mapping of topography on these discontinuities has lacked high spatial resolution because either long period SdS or PdP phases or single station Pds phases have been used. To improve spatial resolution of discontinuity topography, PASSCAL array data is used to construct common-mid point (CMP) stacks of receiver functions. This allows images of the spatial variation in discontinuity depths to be produced. In addition, the CMP stacks prove superior to single station stacks because the coherent signal generated noise present at any given station (e.g., basin reverberations, topographically scattered Rg) will stacked incoherently in a CMP gather. Mapping of the topography present on the 410 and 660 km discontinuities beneath Colorado, Utah, Idaho, and SE Wyoming from 3 separate PASSCAL deployments documents the occurrence of large short-wavelength topography. Our most robust observation is that 30–40 km of variation in the transition zone thickness exists. This is a very surprising result given that 40 km is the global peak to peak variation in transition zone thickness found by Flanagan and Shearer (in press). A second finding is that no anti-correlation of 410 and 660 topography exists as the thermally coherent transition zone model predicts. This suggests that the transition zone beneath the our study area is not thermally coherent and/or other mechanisms are modulating the discontinuity topography. To conclude, we compare our discontinuity topography against existing velocity models and review the range of mechanism which may modulate discontinuity topography such as variable water content, finite velocity discontinuity gradients and the effect of the aluminous mantle component mineral reactions.

Attenuation Structure Near the Coso Geothermal Region

BHATTACHARYYA, J., LEES, J., Yale University, New Haven, CT 06520, USA, joydeep@hess.geology.yale.edu

We present an analysis of seismic shear waveforms to constrain the attenuation structure near Coso geothermal area, located between the Sierras and the Garlock fault. Several laboratory studies indicate that seismic attenuation is sensitive to subsurface temperature variations. Though initial attenuation measurements using P waves provide important constraints, Q models can be considerably improved if S-waves are used since they are more strongly temperature dependent. These waveforms are isolated from the transverse component seismograms and a multiple taper algorithm is used to make robust t* measurements. Our primary dataset is the high quality recordings made at three-component borehole stations installed near the Coso geothermal field. With a dense path coverage, this dataset is ideal for high resolution attenuation tomography of a geothermal field.To correctly isolate a transversely polarized SH waveform, we need to properly orient horizontal component seismometers. We have analyzed directly arriving P-waveforms to detect, identify, and correctly obtain the incident angles at the station. This technique is based on principal component analysis and requires three-component seismic data for each station. The method examines the largest eigenvalue of the data sample covariance matrix as a function of time. Given the three orthogonal components, this technique allow us to identify the orientation of the "natural" coordinate system. Knowing the source and receiver locations, the proper orientation of the horizontal components (N-S and E-W or radial and transverse) can be obtained. A simple rotation operator can then be applied to the recorded seismograms. The rotated transverse component seismograms are then analyzed to model shear wave attenuation structure.

Seismic Anatomy of a Geothermal Field in Three-Dimensions: Poisson's Ratio, Porosity, Attenuation, Anisotropy and Stress

LEES, J.M., and H. WU, Department of Geology and Geophysics, Yale University, New Haven, CT, 06510, lees@love.geology.yale.edu

In this paper we present a summary of the full three-dimensional analyses so far investigated on the geothermal field at Coso, California. These include tomographic inversions for P and S-wave velocity, three-dimensional distribution of Poisson's ratio, estimates of porosity from Vp*Vs products, P-wave anisotropy, distributions of deviatoric stress and associated seismicity, and distributions of Q (attenuation) with the geothermal field. We found that heat sources in the geothermal field play a significant role in three-dimensional variations of seismic parameters. A new method of estimating three-dimensional P-wave anisotropy will be illustrated and used to estimate deviatoric stress in the geothermal field. Anisotropy results can be used to map out physical parameters such as crack density and resultant permeability. The average crack density estimates are then compared to crack density estimates from shear wave splitting measurements. By rectifying the difference between shear-wave splitting results and our estimates of crack density we can derive bounds for crack aspect ratio with the target volume. The combined models for velocity, attenuation and anisotropy provide a detailed three-dimensional structural model for the geothermal region.

Crustal Structure Along the Pacific North America Plate Boundary Derived From Three-Dimensional V_P and V_P/V_S Velocity Models for Southern California

HAUKSSON, E., Seismological Laboratory, California Institute of Technology, Pasadena CA 91125, hauksson@gps.caltech.edu

We use *P* and *S* arrival times from 12,000 earthquakes and explosions, recorded by the Southern California Seismic Network (SCSN), to invert for the three-dimensional V_P and V_P/V_S structure. To include long-wavelength features of the velocity structure, we invert for a model with a sparse grid (40 km, spacing of horizontal grid nodes), interpolate this model to a 15 km grid, and repeat the inversion. Layers of grid nodes are placed at depths of 1, 5.0, 6.0, 12, 15.5, 16.5, and 20 km. The data variance decreased significantly in the gradational inversion. The model is well resolved, except along the edges, to the southwest in the offshore region, and at depths greater than 25 km. The tomographic velocity model provides new insights into the crustal structure along the Pacific North America plate boundary in southern California. Average continental crustal velocities are observed within the North America Plate with V_P of 5.0 to 6.2 km/s extending down to depths of 25 km. A high V_P body at shallow depth beneath the Tehachapi Mountains is a notable exception. In contrast larger spatial variations in V_P of 3.0 to 7.4 km/s are observed within the Pacific plate, also manifested as major basins with V_P of 3.0 to 5.5 km/s and batholiths with V_P of

6.3 to 7.4 km/s. The larger heterogeneity of the crustal structure within the Pacific Plate reflects the transition from continent to ocean and the past tectonic processes, extending back more than 20 million years. For instance, at depth beneath the Ventura basin the high V_P/V_S and high V_P suggest the presence of ophiolitic assemblages or mid-Miocene volcanics. Beneath Imperial Valley the high V_P at relatively shallow depth is interpreted as reflecting thinned crust related to the ridge spreading processes. Similarly, the spatial distribution of the seismicity reflects shallower brittle to ductile transition within the North America plate and more complex three dimensional distribution within the Pacific plate.

Characterization of the Crust by Topography, Gravity, and Thickness for Predicting Waveguide Efficiency

BAKER, G.E., and MCLAUGHLIN, K.L., Maxwell Technologies, San Diego, CA, 92126, U.S.A., eli@maxwell.com, scatter@maxwell.com

We are developing a statistical model relating easily measurable geophysical properties to efficiency of crustally guided P- and S-wave propagation. The model will be used to make path corrections for the regional Lg/Pg amplitude ratio discriminant for nuclear discrimination. Preliminary analysis has involved cluster analysis of median elevation, short wavelength topographic roughness, long wavelength topographic gradient, median isostatic gravity residual and its horizontal gradient, and crustal thickness and its gradient, averaged over quarter degree grids in southern California. Regardless of the number of crustal types we allow, the types are clustered for the most part into seemingly reasonable contiguous areas (e.g. the Mojave block is largely one crustal type). The divisions however, are not all as one might simply draw on a map. The southern Sierra for example, is divided between 2 or 3 fairly contiguously arrayed types of crust, depending on the total number of crustal types allowed. The significance of the segmentations is unclear and must be evaluated with respect to some criteria based on the problem of interest. Our problem of interest is seismic propagation in the crustal waveguide. The next step therefore, which we will present results of, is to perform an analysis of variance for an exhaustive set of measures (to avoid reliance on pre-conceived biases) of the parameters, integrated along the paths over which we have measures of crustal phase amplitude changes, against these amplitude changes. This will test the dependence of the parameters and the significance of correlations observed.

Tuesday AM, March 17, 1998—Forum Room
Developments in Ground Motion and Ground Failure for Engineering Applications
Presiding: Jamison Steidl, *UCSB*

Modeling of Non-Linear Soil Response from Earthquakes in Los Angeles

JONES, E.M., Los Alamos National Laboratory, MS F659, Los Alamos, NM 87545, honais@vega.lanl.gov; OLSEN, K.B., Institute for Crustal Studies, UC Santa Barbara, Santa Barbara, CA 93106, kbolsen@crustal.ucsb.edu.

We have developed a hybrid finite-difference technique capable of modeling non-linear soil amplification from the 3-D finite-fault radiation pattern for earthquakes in arbitrary earth models. The method is applied to model non-linear effects in the soils of the Los Angeles basin (downtown Los Angeles, site TAH) from a hypothetical **M** 6.75 earthquake on the Elysian Park fault, and in the soils of the San Fernando Valley at the Van Norman Complex from the 1994 **M** 6.7 Northridge earthquake. 0–7 Hz source-time functions are computed by linear modeling below the sites of interest, and the strike-perpendicular component is propagated to the ground surface using either elastic/plastic or Masing Rule non-linear models. The elastic soil parameters are approximated from profiles in the 3-D velocity model by Magistrale and others. Because site-specific non-linear material parameters from the San Fernando Valley and downtown Los Angeles are currently unavailable, values are estimated from analyses of ground motions observed at the U.S. Nevada Test Site. Our synthetic strike-perpendicular Elysian Park source-time function with peak velocity of 65 cm/s at 10 km depth below TAH generated a surface peak velocity of 215 cm/s. At the Van Norman Complex, our Northridge source-time function with peak velocity of 35 cm/s at 5 km depth generated a surface peak velocity of 180 cm/s. Compared to linear simulations, both elastic/plastic and Masing Rule non-linear synthetics show similar reductions in spectral amplitude of up to a factor of two, in particular for frequencies above about 1.5 Hz. We find that the spectral content of the source-time function is critical for determining the frequency dependence of non-linear effects, which are strongest at the frequencies at which strain reversals occur.

Stochastic Finite-Fault Modeling of Ground Motions from the 1994 Northridge, California Earthquake: Widespread Nonlinear Response at Soil Sites

BERESNEV, I.A., ATKINSON, G.M., Department of Earth Sciences, Carleton University, 1125 Colonel By Drive, Ottawa, Ontario K1S 5B6, beresnev@ccs.carleton.ca, gma@ccs.carleton.ca; JOHNSON, P.A., EES-4, MS-D443, Los Alamos National Laboratory, Los Alamos, NM 87545, johnson@seismo5.lanl.gov; FIELD, E.H., Department of Earth Sciences, University of Southern California, Los Angeles, CA 90089-0740, field@usc.edu

On average, soil sites behaved nonlinearly during the M 6.7 1994 Northridge, California earthquake. This conclusion follows from an analysis that combines elements of two independent lines of investigation. First, we apply the stochastic finite-fault simulation method, calibrated with 28 rock-site recordings of the Northridge main shock, to the simulation of the input motions to the soil sites which recorded this event. The calibrated method has a near-zero average bias in reproducing ground motions at rock sites in the frequency range from 0.1 to 12.5.

The soil sites selected are those where there is co-location of strong-motion accelerographs and temporary instruments from the Northridge aftershock observation network. At these sites, weak-motion amplification functions based on numerous aftershock records have been empirically determined. These empirical weak-motion amplification factors can be applied to the simulated input rock motions, at each soil site, to determine the expected motions during the mainshock (i.e. neglecting nonlinearity). These expected motions can then be compared to the actual recordings during the mainshock.

We show that the recorded strong-motion spectra are significantly overestimated if weak-motion amplifications are used. The null hypothesis, stating that the inferred differences between weak-motion and strong-motion amplifications are statistically insignificant, is rejected with 95 % confidence in at least two frequency ranges, between 2 and 5 Hz, and 7 and 12.5 Hz, approximately. On average, the difference between weak-motion and strong-motion amplifications exceeds a factor of 1.5. These findings suggest a significant nonlinear response at soil stations in the Los Angeles urban area during the Northridge mainshock.

Direct Observation of Nonlinear Soil Response in Acceleration Time Histories

ARCHULETA, R.J., Institute for Crustal Studies and Dept. of Geological Sciences, University of California, Santa Barbara, CA 93106, ralph@crustal.ucsb.edu

Most studies that report nonlinear soil response during seismic shaking rely on inference such as an apparent shift of a fundamental frequency, contrast in spectral amplification between weak and strong motion or modeling based on standardized laboratory tests. There have been a few direct observations of nonlinear response in vertical arrays and in isolated recordings of acceleration time histories where there is an obvious disappearance of high frequency acceleration. In this study I present evidence that nonlinearity can be directly observed in acceleration time histories simply by noting a characteristic waveform associated with the strain rate of nonlinear soil response. When nonlinear behavior is present, the acceleration time history shows a particular waveform, generally repeating itself with opposite polarity. The waveform is similar to the solution of a periodically forced Van der Pol's equation, i.e., sharp cusps followed by gentle shoulders. Examples of such nonlinear accelerograms are: Bonds Corner, 1979 Imperial Valley, CA; Wildlife refuge surface accelerogram, 1987 Superstition Hills, CA; Kushiro Port station, 1993 Kushiro-Oki, Japan, Jensen Main building, 1994 Northridge and the Japan Railway station TKT, 1995 Hyogo-ken Nanbu, Japan, among others. While the signature of a nonlinear response is directly observable at some stations, it appears to be absent at many sites with similar levels of acceleration and similar local geology. Moreover, the nonlinearity does not eliminate high frequencies; in fact, the opposite occurs.

Nonlinear Site Response: From Laboratory Modeling to Field Data Modeling

BONILLA, L.F., LAVALLEE, D. and ARCHULETA, R.J., Institute for Crustal Studies, University of California, Santa Barbara, CA 93106, fabian@crustal.ucsb.edu

Nonlinear site response studies have mostly been approached by using equivalent-linear and simplified hysteresis models. Engineers have usually used a hyperbolic stress-strain relationship with hysteresis following the so-called masing rules to characterize the nonlinear rheology of the soils observed in the laboratory tests. Masing rules describe the stress-strain path at any given time. The complication with these rules is that it is difficult to obtain a functional formulation; if they are not correctly implemented, the maximum stress that the material resists can be exceeded. We have modeled laboratory tests on sands and clays by developing extended masing rules for the hysteresis that follow general hyperbolic stress-strain relationships. First, we found that the extended masing rules better describe the hysteresis of soils. Second, the shape factor, usually assumed to be two, can be greater or less than two. Third, the strain rate time history is necessary to fit the observed data and represents the anelastic attenuation of the medium. We developed a functional form for the extended masing rules and incorporated it into a finite difference code to propagate vertically incident SH-waves in a layered medium. The simulations show amplitude reduction as well as the shift of the fundamental frequency to lower frequencies as observed on vertical arrays. The synthetic accelerograms show the development of high frequency peaks later in the signals as observed in acceleration records; these peaks seem to be related to the contribution of the strain rate. These peaks also produce high amplitude pulses in the strain time history as product of large deformations of the medium. The latter result can be important in the generation of pore pressure pulses capable of initiating the material liquefaction.

RESPONSE SPECTRAL SCALING FOR VARIOUS DAMPING RATIOS COMPATIBLE WITH UPDATED ROCK AND SOIL RESPONS SPECTRAL ATTENUATION RELATIONSHIPS FOR 5-PERCENT DAMPING

Sadigh, K., Makdisi, F.I., Egan, J.A., Rosidi, D., Geomatrix Consultants, Inc. 100 Pine Street, 10th Floor, San Francisco, CA 94111, fmakdisi@geomatrix.com

Response spectral attenuation relationships commonly in use are typically developed for a damping ratio of 5-percent. Response spectral estimates for damping ratios other than 5-percent require the use of scaling relationships which are typically generalized in nature and do not account for the dependence of damping ratio scaling relationships on magnitude, distance, or local site conditions.

The objective of this paper is to summarize the results of the authors' research studies on response spectral scaling conducted over the past several years and to develop damping relationships to be used in conjunction with the authors' recently updated 5-percent damped spectral attenuation relationships for rock-site and soil-site conditions published in the January/February 1997 issue of the Seismological Research Letters. The 5-percent damped attenuation relationships were updated using an extensive data base (including data from the 1989 M7 Loma Prieta, the 1992 M7.3 Landers, the 1992 M6.4 Big Bear and the 1994 M6.7 Northridge earthquakes) for rock-site and deep-stiff-soil-site recordings obtained form shallow crustal earthquakes of magnitude 4.5 to 7.5.

The spectral scaling relationships for damping values other than 5-percent are presented in terms of ratios of response spectral values for 2-, 7-, and 10-percent damping to the corresponding values at 5-percent damping. The spectral ratios are provided for several periods in the range of 0.04 to 4 seconds for magnitudes in the range 4.5 to 8.5 and source-to-site distances up to 100 km. Separate scaling relationships are provided for rock-site and soil-site conditions.

UPDATED RESPONSE SPECTRAL ATTENUATUION RELATIONSHIPS FOR VERTICAL MOTIONS FROM SHALLOW CRUSTAL EARTHQUAKES

Sadigh, K., Rosidi, D., Powers, M.S., Egan, J.A., Makdisi, F.I., Geomatrix Consultants, Inc. 100 Pine Street, 10th Floor, San Francisco, CA 94111, fmakdisi@geomatrix.com

Attenuation relationships are presented for response spectral acceleration of vertical motions from shallow crustal earthquakes. These relationships are based on strong motion data predominately from California earthquakes. Relationships are presented for strike-slip and reverse-slip earthquakes, rock and stiff-deep soil site conditions, earthquakes of moment magnitude 4.5 to 8.5, and source-to-site distances up to 100 km.

The attenuation relationships presented herein update and refine our previous relationships and are compatible with those for horizontal motions published in the January/February 1997 issue of the Seismological Research Letters. The vertical relationships were updated using an extensive data base (including data from the 1989 M7 Loma Prieta, the 1992 M7.3 Landers, the 1992 M6.4 Big Bear and 1994 M6.7 Northridge earthquakes) for rock-site and deep-stiff-soil-site recordings obtained from shallow crustal earthquakes of magnitude 4.5 to 7.5.

The ratios of the vertical to the horizontal response spectral values for periods in the range of 0.03 to 4 seconds are computed and compared with our previous relationships as well as the vertical/horizontal relationships by other investigators. The vertical/horizontal spectral ratios are presented as a function of earthquake magnitude, style of faulting, source-to-site distance, and local soil conditions.

Evaluation of Empirical Attenuation Relations for Southern California

JOHN G. ANDERSON, YAJIE LEE, SHEAN-DER NI, YUEHUA ZENG, Seismological Laboratory, University of Nevada, Reno, Nevada 89557, NORM ABRAHAMSON, Pacific Gas and Electric Co., Geosciences Dept., P. O. Box 770000, Mail Code N4C, San Francisco, CA 94177.

As part of the Phase III project for the Southern California Earthquake Center, we evaluated six attenuation relations for their applicability to the method this project uses to calculated seismic hazard. Attenuation relations were tested for their ability to predict peak acceleration and spectral acceleration with 5% damping at periods of 0.3 sec, 1.0 sec, and 3.0 sec. Site conditions were taken from a geological map and classified as Quaternary, Tertiary, or Mesozoic. We found that Quaternary and Tertiary sites best matched the "soil" category of site conditions in many regressions, while the Mesozoic sites should be regarded as "rock." Attenuation relations were first tested to see if their functional forms were consistent with predictions of theoretical models for synthetic ground motions on rock (which predict saturation and a shape that depends on magnitude) and with theoretical models for site response including nonlinearity. They were also tested for agreement with the entire set of accelerograms in the SCEC database for southern California earthquakes. In this empirical test, uncertainties were separated into a source term and a residual term that includes site-to-site variations for individual earthquakes. Residuals from one of the regressions that worked well were tested for their correlation with depth to basement, coda amplification, low-frequency amplification from basin modeling, kappa, detailed site geology when available, and site response in aftershocks, as all of these have been proposed to improve regression results. Although weak correlations were found with some of these parameters, the generally poor correlation led us to plot residual vs. residual for stations that have recorded multiple earthquakes. When displayed this way, we expected that a strong positive correlation would be the result of repeatable site response at the stations. However, for the subset of available stations, the correlation is very poor, especially at high frequencies, indicating that the site response is relatively unimportant compared to source and path effects in its contribution to the total scatter.

Site Response for Probabilistic Seismic Hazard Analysis in Southern California

STEIDL, J.H., Institute for Crustal Studies, UCSB, Santa Barbara, CA 93110

Predicting ground shaking from future earthquakes is typically accomplished by using existing empirical attenuation relations for a specific soil type, and a regional earthquake source model. Specifically, an attenuation relation provides an estimated mean value and standard deviation for peak ground acceleration (PGA) or response spectral acceleration (RSA). The standard deviation represents the uncertainty in the predicted ground motion due to the scatter of real data about the estimated mean value. Reduction of the uncertainty in the ground motion predictions, that is, greater ability to predict the variation in level of shaking and damage patterns of a large earthquake, is an important objective of engineering seismology. In this study we examine measurable/mappable parameters like surface geology or near-surface shear wave velocity to try and reduce some of the uncertainty in the ground motion predictions. Typically, an attenuation relation specifies motions for different soil types, often as simply "rock" or "soil." Average amplification factors based on residuals to predicted rock ground motion are calculated for different surface geologic classes in the Southern California region using strong motion data. These amplification factors are given at spectral periods of 0.1, 0.3, 1.0, and 3.0 seconds and in four ranges of ground motion level from very weak to very strong. When treated in a self-consistent manner, the low level strong-motion amplification factors are consistent with amplification factors from weak motion site response studies. At large ground motion levels, the strong-motion amplification factors are consistent with non-linear site response predicted by analytical geotechnical models. These amplification factors can then be used in probabilistic seismic hazard calculations to incluse the site response on a regional mapping scale. In addition, using the amplification factors, the effects of surface geology can be included in making contour maps of ground shaking from earthquakes as they happen, and directly after the event by interpolation between stations where real-time data is being collected.

Probabilistic Seismic Hazard in Southern California: 3-D Basin Effects

OLSEN, K.B. and ARCHULETA, R.J., Institute for Crustal Studies, UC Santa Barbara, Santa Barbara, CA 93106, kbolsen@crustal.ucsb.edu.

We have used 3D/1D 0–0.4 Hz peak velocity ratios to construct amplification maps for the Los Angeles basin for nine earthquake scenarios: rupture on the Elysian Park, Santa Monica, Palos Verdes, San Andreas near LA from north-west and south-east, and Newport-Inglewood faults, and approximations of the 1933 Long Beach, 1987 Whittier-Narrows, and 1994 Northridge earthquakes. The earthquakes were simulated as elastodynamic propagating ruptures with constant slip on the faults in two different velocity models (115 km by 95 km by 34 km): a 1D regional (rock) model and one including the 3D structure of the Los Angeles and San Fernando basins, assembled by Magistrale and others. Ratios of 3D/1D peak velocity ratios vary considerably between the scenarios in the LA basin. In particular, the amplification tends to increase with distance from the causative fault to the basin structure. The peak velocity ratios for the nine scenario earthquakes are combined into an average LA basin amplification map. The LA basin is outlined by an average peak velocity ratios ratio of 2 with a maximum value of 4.1. The sites associated with the largest mean 3D basin amplification effects are located above the deepest parts of the basin. Log standard deviations are less than 0.9. The amplification is caused by a combination of effects from the 3D basin structure and the sediment impedance. After applying 1D corrections for the sediment impedance amplification effects (up to 1.7), the maximum amplification averaged over sites above similar basin structure is 2.4, associated with sites above the deepest part of the basin. Durations are significantly increased by the 3D basin structure. The largest 3D–1D durations are obtained for the Santa Monica and San Andreas earthquakes, for sites above the deepest part of the basin.

Probabilistic Seismic Hazard Analysis of Southern California

MAHDYIAR, M., VortexRock Consultants, 3710 Windsong Cr., Yorba Linda, CA 92886, mahdyiar@email.msn.com. ABRAHAMSON, N., Pacific Gas and Electric Co., Geosciences Department, P.O. Box 770000, Mail code N4C, San Francisco, CA 94177, nabraham@holonet.net.

The primary objective of this study is to evaluate different regional seismicity models for southern California in terms of their ground motion hazards using different attenuation equations and taking into consideration the regional site conditions and basin effects information. Five different seismicity models for southern California are investigated: 1) The CDMG/USGS model, 2) the historic seismicity model; 3) the smooth historical seismicity model; 4) the strain rate model; and 5) a cascade earthquake model based on the CDMG/USGS fault segments. Each model produces different regional ground motion hazard in southern California. The probabilistic seismic hazard analysis (PSHA) is used to compare and evaluate these models against each other. The CDMG/USGS regional seismicity model is reconstructed based on the related information on their web-site.

The Inherent uncertainties in the source models translate to large uncertainties in seismic hazard values. The largest uncertainty, and the hardest to resolve, is the frequency of very large earthquakes, both on the major faults and in the regions between them. Allowing for very large earthquakes tends to reduce the ground motion hazards with typical return periods used for engineering design purposes. The seismicity models that balance a given moment budget are very sensitive to the choice of maximum magnitude of the seismic zones. Including large magnitude earthquakes, either by increasing the maximum magnitude or by cascading adjacent faults, will consume large amount of moment budget and would decrease the rate of moderate size earthquakes and thus the hazard.

Site classification matters, especially because models for attenuation and site effects are closely linked. The differences between available models are pronounced, sometimes exceeding a factor of 2, at very short periods and in Tertiary and Mesozoic rock, where site conditions are treated differently in different models. Differences between models are less pronounced at longer periods and for sites on Quaternary sediments. Basement depth is also an important factor that is not well represented by surface soil conditions. Including basin depth using a very simple empirical correction can affect the predicted spectral acceleration by a factor of two in some cases.

A New Probabilistic Earthquake Hazard Model for California: Comparison with Recent USGS Hazard Maps

SCHNEIDER, John F., MENDEZ, Andres J., ZEGHAL, Mourad, LI, Yong, and WU, Libo, Impact Forecasting, L.L.C., 230 West Monroe Street, Suite 9000, Chicago, Illinois, 60606, johns@if.aon.com

We have developed a new probabilistic earthquake hazard model for California. The Impact Forecasting (IF) model generates probabilistic estimates of ground motion, including site effects, in terms of response spectral acceleration or Modified Mercalli Intensity (MMI). For generic rock conditions (i.e., soft rock), the IF model is similar to the one developed by the California Division of Mines and Geology and US Geological Survey, and implemented in recent hazard maps (Frankel et al, 1996). However, some differences exist in the details of implementation which lead to modest differences in the predicted hazard.

The IF source model is based on two types of event distributions: 1) characteristic earthquakes, which are assigned to faults with uniform distribution of occurrence with magnitude, and 2) background events, which are assigned to either faults or area sources with truncated exponential distribution. For ground motion, four attenuation relations are presently used: Abrahamson and Silva (1997), Idriss (1991, 1994), Sadigh et al (1993, 1994), and Boore et al (1997). Site amplification factors were developed for six site categories, comprised of combinations of surface-geologic units, based on average near-surface (30m) shear-wave velocities. Site amplification factors for these categories were determined from nonlinear site response analyses of randomized soil-profile properties. The model accommodates uncertainty in predicted hazard in terms of both random (inherent to nature) and knowledge (due to model uncertainty and lack of knowledge) variables.

We present comparisons of the IF model for rock motions to the USGS (Frankel et al, 1996) hazard maps. For Sa(.3 s) and 10% probability of exceedance in 50 years, the USGS model yields on average 20% higher hazard. The differences are largely attributable to the choice of ground motion attenuation relations, and secondarily to the manner in which earthquake area sources and variance in ground motion relations are treated in the model.

A Method for Producing Probabilistic Seismic Landslide Hazard Maps for Southern California

JIBSON, R.W., and HARP, E.L., U.S. Geological Survey, Golden, CO 80225, jibson@gldvxa.cr.usgs.gov

The 1994 Northridge earthquake is the first earthquake for which we have all of the data sets needed to conduct a detailed regional analysis of factors related to triggered landsliding. These data sets include (1) a comprehensive inventory of triggered landslides, (2) hundreds of strong-motion records of the main shock, (3) detailed (1:24,000-scale) geologic mapping of the region, (4) extensive data on engineering properties of geologic units, and (5) high-resolution digital elevation models of the topography. All of these data sets have been digitized and rasterized at 10-m grid spacing in the ARC/INFO GIS platform. Combining these data sets in a dynamic model based on Newmark's permanent-deformation (sliding-block) analysis yields estimates of coseismic landslide displacement in each grid cell resulting from the ground shaking generated by the Northridge earthquake. The modeled displacements are then compared with the digital inventory of landslides triggered by the Northridge earthquake to construct a probability curve relating predicted coseismic displacement to probability of failure. Once calibrated with Northridge data, this probability function can be applied to predict the spatial variability of slope-failure probability in any ground-shaking scenario of interest. Because the resulting hazard maps are digital, they can be updated and revised with additional data that become available, and custom maps that model any ground-shaking conditions of interest can be produced when needed.

Tuesday AM, March 17, 1998—Room 235
The Tenth Anniversary of the Predicted Parkfield Earthquake
Presiding: Robert Wesson, *USGS*

HYDROLOGY AND/OR TECTONICS: RESULTS FROM THE PARKFIELD WATER-LEVEL MONITORING NETWORK

ROELOFFS, E., U.S. Geological Survey, 5400 MacArthur Blvd., Vancouver, WA 98661, evelynr@usgs.gov

Water-level monitoring at 11 wells (30-1570 m deep) near Parkfield has documented water level changes of tectonic origin and facilitated interpretation of borehole strain, creep, and other geophysical data. Water level responses to local earthquakes and fault creep events verify that most wells respond poroelastically to volumetric or areal strain, as anticipated. In one well, distant earthquakes produce non-oscillatory water level rises: if this phenomenon also takes place at seismogenic depths, it may be important for remote triggering of earthquakes. Water-level and strain changes at two sites before the 1985 M6.1 Kettleman Hills earthquake may have been earthquake precursors.

Currently, creepmeters, three-component borehole strainmeters, and two-color electronic distance measurements indicate deformation rates at Parkfield have changed since 1993. Hydrologic influences on these observations have been suspected because annual precipitation and groundwater recharge in 1993, 1995, and 1996 were significantly above average. At creepmeter XMD1, greater left-lateral motion during wetter winters is the reason why right lateral creep rate appears to have decreased. Right-lateral creep at WKR1 apparently increased in 1995, but after subtracting the average seasonal variation from the data, periods of accelerated creep are seen to coincide with heavy rainfall. Similar correction for seasonal effects at CRR1, however, reveals accelerated right-lateral creep surges that do not coincide with precipitation and are therefore almost certainly tectonic. Areal and volumetric tectonic strain rate variations are hard to detect because surface rainfall loading and poroelastically coupled aquifer pressure changes strongly influence these strain components. Changes in shear strain accumulation rate (Gladwin et al., 1997), however, are too large to be explained by poroelastic coupling to the observed aquifer pressure variations near Parkfield. After accounting for hydrologic influences, shear strain and creep data still imply a change in deformation rate near Parkfield since 1993.

Possible increase in fault slip rate at Parkfield in 1993 as inferred from deformation measurements from 1986 to 1997

J. Langbein, USGS, Menlo Park CA, langbein@usgs.gov, Gwyther, R.L., and Gladwin, M.T. (both at CSIRO, Pinjarra Hill, QLD, AU)

Prior to 1985, the deformation of the Parkfield region was measured annually with high precision Electronic Distance Meters (EDM), and in real-time with 7 creepmeters. With the initiation of the Parkfield Earthquake Experiment, we have extended the geodetic coverage spatially, temporally, and with better precision. Currently, we use a two-color EDM to measure twice weekly the lengths of 17 baselines in the region of the San Andreas fault that spans the anticipated rupture zone of the next Parkfield earthquake between Middle Mountain and Gold Hill. In addition, we have increased the number of creepmeters in this zone to 12. In order to increase the precision of our measurements of deformation at the periods between minutes to weeks, 9 borehole strainmeters have been installed; seven of these instruments are in the active zone between Middle Mountain and Gold Hill. Three of these instruments measure the 3 strain components and the remainder measure volumetric strain only. With between 10 and 12 years of observations on many of our instruments, we now have established an excellent baseline to judge any changes in rate of deformation and importantly, to judge the coherence of these changes between instruments. To date, we have recorded both on creepmeters and nearby strainmeters many instances of fault-slip that occurs over the period of minutes to 1 day. However, the most controversial signals are those that occur over periods of months to years since these signals are often difficult to distinguish between random-walk noise, hydrologic changes in the water table, or tectonic changes. We have now documented rate changes initiating in 1993 on several EDM baselines, adjacent creepmeters, and tensor strainmeters. All of these changes are greater than that expected from normal background fluctuations. Even though the rate change roughly coincides with the end of a 7 year period of sub-normal rainfall, the spatial coherence of these changes is consistent with an increase in the rate of fault slip on a part of the San Andreas fault. Although these rate changes are well resolved, there are neither enough observations nor a large enough signal to clearly resolve the amount and location of the source area responsible for the observed changes.

The Parkfield Experiment: A New View of Fault-Zone Process.

NADEAU, R.M., and MCEVILLY, T.V., Berkeley Seismological Laboratory and Center for Computational Seismology, Lawrence Berkeley Nat. Lab, University of California, Berkeley, CA 94720, @seismo.berkeley.edu

Since the 1980s, ideas on fault slip and microearthquake occurrence, as well as expectations for earthquake precursory changes, have been profoundly altered by the data acquired over the past ten years as part of the Parkfield Experiment. Given the performance attainable with a densely spaced borehole network of seismometers, we have sharpened our view of the ongoing deformation process in the San Andreas fault zone at Parkfield, with striking results. The fault zone at the nucleation region of the Parkfield repeating M6 events displays abnormally high Vp/Vs. The active slip surface, defined by over 6000 hypocenters, exhibits an unpredicted organization, with seismic moment release from over 60% of the seismicity confined to less than 1% of the fault area, and concentrated on a few hundred very small (~5–10 m radius) distinct patches, most of which are loci for sequences of regularly repeating, nearly identical (characteristic) earthquakes. Recurrence intervals, as short as a few months at M~0, are proportional to event size for a sequence. This property when combined with the geodetically determined fault slip rate, reveals a scaling relationship among moment, area, slip and recurrence time that appears to hold from M0 to M6. Temporal changes in wave propagation appear to occur primarily in the shallow crust and are small to insignificant at depth while significant deep changes are observed both in the overall seismicity patterns and in changing recurrence intervals which accompany larger nearby events and apparently reflect change in the local strain rate. This unprecedented degree of process definition enriches substantially the field of experiments and hypothesis tests that can be considered in the proposed deep drilling project at Parkfield, and illustrates that ten years of site characterization is reasonable for drilling to a seismogenic target.

Parkfield Earthquake: Not Likely this Year

JACKSON, D.D. and KAGAN, Y.Y., Southern California Earthquake Center, University of California, Los Angeles, CA 90095-1567, djackson@ucla.edu

The probability of a moderate earthquake at Parkfield is officially taken to be about 10 percent per year, according to a recent report by Roeloffs and Langbein (*Rev. Geophys.* **32**, 315, 1994). This figure is near the middle of several published estimates, all based on three assumptions: (1) the characteristic earthquake hypothesis, (2) quasiperiodic earthquake recurrence on the "Parkfield segment," and (3) that moderate earthquakes in 1857, 1881, 1901, 1922, 1934, and 1966 were all characteristic Parkfield earthquakes. Davis *et al.* (*BSSA* 79, 1439, 1989) showed that even if these assumptions are adopted, allowing for the open interval since 1966 decreased the estimated probability to a value of about 7 percent per year in 1989. The equivalent rate is now about 5 percent per year. However, the three basic assumptions must be questioned. As applied to the Pacific Rim, the characteristic earthquake hypothesis has failed important statistical tests, and has not been statistically validated anywhere. Without the characteristic hypothesis, quasiperiodic recurrence loses its meaning. Moreover, geodetic studies by Segall and others show that the 1934 and 1966 earthquakes had quite different rupture distributions; and evidence for the locations and magnitudes of the first three events is largely circumstantial. Without the three assumptions, the Parkfield region can be interpreted as an area which by chance endured a larger than average number of earthquakes in the last century and half. Its selection for special study may be largely a result of that chance. Assuming that the "Parkfield Study Region" has earthquake magnitudes distributed according to a truncated Gutenberg-Richter distribution with a maximum magnitude of about 8 and a rate sufficient to release all of the long-term slip on the San Andreas, the probability of a magnitude 6 or larger event there is less than 1 percent per year.

Short-Term Exciting, Long-Term Correcting Models for Earthquake Occurrence Times

SCHOENBERG, F.R., Department of Statistics, University of California, Berkeley, CA 94720, frederic@stat.berkeley.edu; Bolt, B.A., Departments of Geology and Geophysics and of Civil Engineering, University of California, Berkeley, 94720

The elastic rebound theory of Reid suggests that earthquake occurrences are well-dispersed over long periods of time. More recently, however, several authors including Kagan and Ogata have stressed that earthquakes exhibit short-term clustering behavior. This observation is important for seismic hazard estimation. A class of probability models incorporating both features is proposed here, in which the conditional intensity is increased in the short run following an event, but exhibits a self-correcting decrease in the long run. Members of the class are shown to provide satisfactory fit to a catalog of microearthquakes in Parkfield, California.

Tuesday AM, March 17, 1998—Room 235
Structure and Deformation in Subduction Zones
Presiding: Geoff Abers, *Univ. of Kansas* and **Susan Schwartz,** *UCSC*

A Global Survey of Slab Structures and Internal Processes Using a Combined Data Base of High-Resolution Earthquake Hypocenters, Tomographic Images and Focal Mechanism Data

ENGDAHL, E.R., US Geological Survey, DFC, Box 25046, Stop 967, Denver, CO 802225, engdahl@gldfs.cr.usgs.gov; VAN DER HILST, R.D., MIT, Cambridge, MA 02139, hilst@mit.edu; KIRBY, S.H., US Geological Survey, Menlo Park, CA 94025, kirby@isdmnl.wr.usgs.gov; and EKSTROM, G., Harvard, Cambridge, MA, ekstrom@geophysics.harvard.edu

Nearly 100,000 events globally that are well-constrained teleseismically by arrival times reported to the ISC and to the USGS/NEIC for the period 1964–1997 are relocated using the ak135 reference model. Hypocenter determination is significantly improved by using the arrival times of regional and teleseismic P and S phases, the core phases PKiKP and PKPdf, and the teleseismic depth phases pP, pwP and sP in the relocation procedure. The new data base, which is complete to about Mw 5.2 and includes all events for which moment tensor solutions are available, has immediate application to high-resolution definition of structures and processes in subduction zones worldwide.

We gain new insights about subduction zones globally by combining the new catalog with the results of tomographic imaging, volcano locations, Harvard CMT focal mechanism data, and inferences about the mineral physics. Along arc geometrical symmetry of most subduction zones permits us to display the relevant data in arc-centered curvilinear cross sections. Intermediate-depth intraslab earthquakes tend to occur in narrowly defined zones near the top surfaces of slabs with tension or pressure axes oriented parallel to the local slab dip, suggesting control by pre-existing faults and by metamorphic processes in the crust and shallow upper mantle of the subducting slab. Deep earthquakes, however, tend to occur within cold slab interiors, consistent with failure in a region of olivine metastability. We examine the diversity and peculiarities of subduction zones globally, as well as the relationships between the observed earthquake distributions and plate age, descent rate, presence of volcanic features, and other geophysical factors.

Upper Mantle S-Velocity Structure of South America from Portable and Permanent Seismic Stations

VAN DER LEE, S., JAMES, D.E., SILVER, P.G., Carnegie Inst. of Washington, DTM, Washington DC 20015, USA, suzan@dtm.ciw.edu

We have mapped the 3-D *S*-velocity structure of the crust and upper mantle of South America by applying partitioned waveform inversion (Nolet, 1990) to broadband (10–160 s) seismic data from events at regional and continental scale distances. The events were recorded by the stations of the GSN and of the portable networks BLSP92, BANJO, BLSP95, VEN92 and SEDA.

Our image shows low to extremely low velocities beneath the Paraná;, Chaco and Pantanal basins. In contrast we have imaged high velocities beneath the western Amazon basin. In some regions we have also imaged the high-velocity anomaly of the subducting Nazca slab with good resolution.

Our image of the subducting Nazca slab agrees well with the Benioff zone in that it shows steeper subduction around 20° S and shallow subduction towards 30° S. Structure beneath the Andes cannot be determined unambiguously, as crustal thickness trades off to some extent with mantle velocities. To resolve this problem we constrain crustal thicknesses using independent seismic data in the inversion. The resulting velocity models indicate extremely low velocities in the mantle wedge and abnormally low crustal velocities in the thick Andean crust.

Shallow mantle structure and evolution of the Andean Subduction zone at 20° South

Stephen C. Myers[1], Susan Beck, George Zandt, Terry Wallace
Department of Geosciences, University of Arizona, Tucson, AZ
[1]Now at: Geophysics and Global Security, Lawrence Livermore National Laboratory, Livermore, CA, 94550 myers@s42.es.llnl.gov

Tomographic images of velocity and attenuation (Q) for P- and S-waves in the shallow mantle across the Bolivian Andes at 20°S reveal a complex geologic environment. Under the volcanic arc of the Western Cordillera (WC), the primary seismic anomaly is high Vp/Vs (>1.8). The high Vp/Vs is interpreted as extreme hydration associated with subduction processes. In the backarc region, the overall velocity and Q of the mantle wedge under Bolivia have higher values than other subduction zones. Underneath the Altiplano (Al), seismic velocities of 8.3 km/s (Vp) are imaged from the Moho to a depth of ~150 km. Additionally, most of the Eastern Cordillera (EC) is underlain by Vp~8.1 km/s, Qp>1000 mantle lithosphere. However, at the EC/Al boundary, a low velocity (Vp~7.8 km/s) and high attenuation (Qs<50) mantle anomaly underlies the largest ignimbrite volcanic field in the study area (Los Frailes). The overall high velocity and Q in the backarc are attributed to downwelling lithosphere caused by upper-plate shortening, and the EC/Al seismic anomaly is interpreted as asthenospheric mantle wedge material that forms a window in the lithospheric mantle.

The spatial correlation between surface volcanism and shallow mantle seismic anomalies suggests that these features developed together. The volcanism associated with the EC/Al seismic anomaly began at about 25 to 30 Ma, contemporaneous with a large pulse in tectonic shortening. This suggests that the shallow mantle anomaly at the EC/AL boundary formed at about the same time. Peak volcanism occurred after shortening ceased in the region, about 12 Ma, and continued until at least 3 Ma. In the study area, Tertiary volcanism has been confined to a relatively narrow band, about 50 km wide, which corresponds to the width of the EC/AL seismic anomaly. The long-lived volcanism suggests that the window in the South American lithosphere has been maintained for at least 25 Ma, despite at least 125 km of upper-plate shortening since 12 Ma. These observations necessitate the semi-continuous removal or destruction of lithospheric material as it is fed into the EC/AL boundary region by tectonic shortening processes.

**Some of this work performed under the auspices of the U.S. Department of Energy by the Lawrence Livermore National Laboratory under contract number W-7405-ENG-48*

Termination of Subduction and the Deformation of South Island, New Zealand

FRANCIS, T. WU and ERYN KLOSKO, SUNY Binghamton, New York, 13901, wu@sunquakes.geol.binghamton.edu

The tectonics of the South Island (SI), New Zealand, is made complex by the apparent termination of the Hikurangi subduction zone in northern SI and the resumption of clearly identifiable subduction in the Puysegur zone of the southern SI. In between these zones, the region is usually described as undergoing collision. But often it is assumed to be underlain by a subduction zone, dipping either eastward or westward as the continuation of the southern or the northern zone, respectively. The existence of an active subduction zone in this section is, however, questionable. The available seismicity data show a paucity of events below about 20 km (Eberhart-Phillips, 1995). Within this section, the Chatham Rise on the east and the Lord Howe Rise on the west appear to be directly in contact. There is now clear evidence that the crust under this region has thickened noticeably (Stern et al., 1997). In fact the thickening can readily take into account over 50% of the convergence in the estimated lifetime (5–8 m.y.) of the collision zone. The high erosion rate can account for a major portion of the remaining convergence. Thus there is no need for subduction in this section. In the extreme north of SI, west of the southernmost portion of the Hikurangi subduction zone, strike-slip faulting dominates to the east and thrust faulting dominates in the west, as shown by recent large earthquakes, indicating strain partitioning (Anderson et al., 1993). The presence of island-normal compression in this region can perhaps be explained by continental subduction at the southern end of the Hikurangi zone (Eberhart-Phillips and Reyners, 1997). Recent island-wide SKS splitting study (Klosko, 1998) show that the fast directions are nearly parallel to the structural trend of the island. This apparent coherency of trends argues for a common mechanism that produces the deformation.

Observing Dispersion of Regional Body Waves in Subducted Slabs: A Signal from Subducted Crust?

ABERS, G.A., University of Kansas, Geology Department, 120 Lindley Hall, Lawrence KS 66045; g-abers@ukans.edu

Subducting plates have long been known to affect seismic wave propagation at a variety of scales. Recently, several studies have shown that along-strike propagation of body waves can lead to frequency-dependent propagation times (dispersion) at frequencies at and above 1 Hz. Although the cause of the dispersion is likely complex, several properties implicate the contrast between subducted oceanic crust and the surrounding mantle. This dispersion is observed and quantified here for a number of circum-Pacific subduction zones, using regional records made by nearby Global Seismic Network stations. Body wave dispersion is quantified using a filter bank approach which provides estimates of frequency-dependent delay times. The times are compared to predictions for a simple wave guide, and give estimates of wave guide thickness and velocity contrast relative to surrounding rock. In this preliminary effort, records are analyzed for paths 2–12 degrees long and sources 100–250 km deep. The first results show that slabs in Alaska, the Aleutians, Marianas and Solomon Islands all generate "normal" dispersion (high frequencies are delayed relative to low frequencies). Delays of 1–8 s occur at frequencies above 1–3 Hz and suggest the presence of a narrow wave guide that is 3–10% slower than the surrounding mantle. By contrast, records from New Zealand of Tonga earthquakes show "reversed" dispersion, a result found by several previous workers. The "normal" dispersion results suggest that in most arcs the oceanic crust does not fully react to form eclogite, as an eclogite layer would not be noticeably slower than surrounding peridotite. Parameters are consistent with persistence of a blueschist zone to great depth in some portion of subducting crust, perhaps the gabbroic layer, although other possibilities exist. The New Zealand data remain enigmatic.

Tuesday PM, March 17, 1998—Forum Room
Developments in Ground Motion and Ground Failure for Engineering Applications
Presiding: Andres Mendez, *Impact Forecasting*

Inversion of Source Parameters and Site Effects from Strong Motion Records Using Genetic Algorithm Approach—Aftershocks of the 1995 Kobe Earthquake

MOYA, C.A. and IRIKURA, K., Disaster Prevention Research Institute, Kyoto University, Gokasho, Uji, Kyoto 611-0011, JAPAN, moya@egmdpri01.dpri.kyoto-u.ac.jp

We inverted low frequency flat-levels and corner frequencies of displacement source spectra as well as site effects from aftershock records of the 1995 Hyogo-ken Nanbu, Kobe, earthquake using genetic algorithms. The data used here consists of velocity strong-motion records at 11 CEORKA stations from about 40 after-shocks with M 3.5 to M 4.9. First, the quality factor, Q, of propagation-path media in this study area were obtained by means of a linear inversion for the observed spectra. Next, we assumed an omega-n-squared model to find the low frequency flat-levels, the corner frequencies, and high frequency decay n for selected events which would minimize the standard deviation of the site effects at all stations. Two of the stations are placed on rock. We found that the omega-squared model gave the minimum standard deviation. The site effects for both rock sites by this inversion showed a significant amplification at high frequencies, which is in a good agreement with a 1-D numerical simulation considering weathered layers near surface. The seismic moment and stress drop were estimated based on the Brune's method (1970). In general, the relation of the seismic moments versus the corner frequencies follow the scaling law Mo ∝ fc^{-3}. The stress drop distribution along the fault zones presents some heterogeneities which are related with the slip distribution by the waveform inversion (Sekiguchi et al., 1998) and the high-frequency radiation distribution by the envelope inversion (Kakehi et al., 1996).

Effects of Randomization of Source Parameters for Estimating Strong Ground Motion with Empirical Green's Functions

LIU, P.-C. and ARCHULETA, R.J., Institute for Crustal Studies, UCSB, Santa Barbara, CA 93106, pcliu@crustal.ucsb.edu

The complexity of the earthquake rupture convolved with complex path effects and site response produces the high-frequency strong ground motion. It is difficult to model the detailed source process and wave propagation deterministically in such a way as to reproduce waveforms that match the phase of accelerograms. However, we can avoid some of these difficulties in the estimation of strong ground motion by randomizing some source parameters and by using small earthquake recordings as empirical Green's functions. We take rupture velocity, rise time, and density of high-frequency radiation on the fault into consideration and describe them as random variables. The probability distributions of these random variables are determined through numerical tests such that the source spectra of large earthquakes obey Aki-Brune omega-square spectrum. The ground motion for a large earthquake is produced by summation of the convolved impulse response with the randomized source parameters of each subfault. The impulse response is the deconvolution of small earthquake records by it's source function which is also assumed to follow the omega-square model. This procedure can use all the available empirical Green's functions at a site and can also account for the directivity of the source. This estimation is not biased by a single record, and different possible source-receiver path effects are included. We use this procedure to compare ground motion from the 1994 Northridge earthquake with a suite of ground motion estimates based on randomized source parameters. We have computed average values and confidence interval of peak acceleration, time history envelopes, Fourier amplitude spectra, and response spectra. In most cases the estimated results are in good agreement with the observed strong-motion records.

Correlation of Rise Time with the Style-of-Faulting Factor in Strong Ground Motions

SOMERVILLE, P.G., Woodward-Clyde, Pasadena CA 91101-2560, U.S.A., pgsomer0@wcc.com and SATO, T., Izumi Research Institute, Shimizu Corporation, 2-2-2 Uchisaiwai-Cho, Tokyo 100, JAPAN, satom@ori.shimz.co.jp

In empirical ground motion attenuation relations, there is a well established difference in ground motion amplitudes between reverse and strike-slip faulting mechanisms for crustal earthquakes. In these models, ground motions for reverse earthquakes typically exceed those for strike-slip earthquakes by a factor ranging from about 1.3 to 1.4. To date, no physical explanation for this systematic difference, which we call the style-of-faulting factor, has been proposed. We have found a correlation between rise time and faulting mechanism that may explain the style-of-faulting factor. We measured the rise times of ten crustal earthquakes for which multiple time window slip models are available. These multiple time window slip models were derived from strong motion and teleseismic data by Hartzell and co-authors, and Wald and co-authors. The rise time was measured by dividing the total slip on each fault element by the maximum slip velocity, and averaging the resulting values over the fault plane. The maximum slip velocity is derived from the largest slip among the individual time windows. The rise times for all of the events, as well as for the five strike-slip earthquakes and the five reverse earthquakes analyzed separately, are consistent with self-similar scaling with seismic moment. For a given seismic moment, the rise times for reverse earthquakes are on average about half as long as those for strike-slip earthquakes. Strong motion simulations show that halving the rise time causes an increase of about a factor of 1.4 in ground motion amplitudes. This increase is consistent with the style of faulting factor in empirical strong motion attenuation relations.

Broadband Simulation of Ground Motions in the Santa Monica Area for the Northridge Earthquake: Effects of Shallow Basin-Edge Structure

GRAVES, R.W. and PITARKA, A., Woodward-Clyde Federal Services, Pasadena, CA, 91101, USA, rwgrave0@wcc.com, axpitar0@wcc.com

Strong motion recordings in the Santa Monica area from the 1994 Northridge earthquake are characterized by large amplitudes and extended durations of shaking. In this region, the basin-edge geology is controlled by the active strand of the westward striking Santa Monica fault. Despite having similar surface geology, sites to the north of the fault show relatively modest amplitudes, whereas sites to the south of the fault exhibit significantly larger amplitudes, with a clear and immediate increase in amplification occurring at the fault scarp. The strong correlation of amplification pattern with the fault location suggests that the underlying basin-edge geology is controlling the ground motion response. To investigate the significance of the basin-edge structure, we have used 2D and 3D finite difference ground motion simulations. Constraints on the basin-edge structure come from geologic cross sections and seismological observations. The simulations indicate that the shallow basin-edge structure (1 km deep) formed by the active (northern) strand of the Santa Monica fault has the greatest influence on ground motions. This structure creates a large amplification immediately south of the fault scarp, in very good agreement with mainshock damage patterns and S-wave amplification measurements. This large amplification results from constructive interference of direct waves with the basin-edge generated surface waves and is quite similar to the basin-edge effect observed during the 1995 Kobe earthquake. In addition, we have found that focusing effects created by the deeper, lens-like structure (3 km deep), which is formed by the inactive (southern) strand of the Santa Monica fault, have a much smaller effect on ground motions and, in particular, these deep focusing effects cannot explain the large motions observed immediately south of the fault scarp.

STRONG GROUND MOTION FROM SURFACE WAVES GENERATED AT THE EDGE OF DEEP SEDIMENTARY BASINS

JOYNER, W.B., U.S. Geological Survey, Menlo Park, CA 94025,
joyner@samoa.wr.usgs.gov

It is widely recognized that long-period surface waves generated by conversion of body waves at the boundaries of deep sedimentary basins make an important contribution to strong ground motion. The amplitude of surface waves is commonly said to decay as the one-half power of distance. That statement is true only for laterally homogeneous media and then only in the frequency domain. The decay in the time domain is greater because of dispersion. With lateral heterogeneity, as with a surface wave generated at the edge of a sedimentary basin, the situation is different. The focusing effect of the low surface-wave velocity in the basin dramatically reduces the geometric spreading of the surface wave. To a first approximation the wave behaves as if it were generated by a line source in a two-dimensional medium. A study of pseudovelocity response spectra of records from the 1971 San Fernando earthquake shows that late-arriving surface waves with group velocities of about 1 km/s dominate the ground motion for periods of 3 s and longer. The rate of amplitude decay for these waves is less than for the body waves and depends significantly on period, with smaller decay for longer periods (essentially zero at 6 s for the horizontal component perpendicular to the basin edge). This relationship suggests that the amplitude can be modeled by anelastic attenuation with decay proportional to the exponential of distance multiplied by an attenuation coefficient. Data from the 1994 Northridge earthquake show similar characteristics, particularly for the component perpendicular to the basin edge. The data from both earthquakes were fit by equations of the form

$$y = \frac{a}{R_E} \exp(-bR_B)$$

where y is the pseudovelocity response, R_E is the component of distance between the source and the edge of the basin, and R_B is the component in the basin. The standard deviation of the natural logarithmic residuals is about 0.5 for the San Fernando earthquake and somewhat less for the Northridge earthquake. The relationship for the San Fernando earthquake predicts ground motion larger than existing attenuation relationships. The difference increases with R_B/R_E ratio and with period, reaching approximately a factor of four at 5 s period for $R_B = 60$ and $R_E = 22$ km. The relationship for the Northridge earthquake gives lower values than the one for the San Fernando earthquake by factors of two to four and gives values larger than existing attenuation relationships only for the component perpendicular to the basin edge at long periods and high R_B/R_E ratios. The surprisingly large difference between the San Fernando and Northridge earthquakes can be explained, at least in part, by directivity. These results indicate that inclusion of anelastic attenuation may be essential in modeling ground motion in deep sedimentary basins.

Near-Field Peak Ground Motion Scaling for Rock Versus Real Rock: How Do PHA and PHV Scale with Increasing Rock Foundation S-Wave Velocity?

O'CONNELL, D.R.H., Seismotectonic and Geophysics Section, U.S. Bureau of Reclamation, Denver, CO 80225, geomagic@seismo.usbr.gov.

Finite rupture simulations of a M 6.5 blind thrust earthquake using 1D Green's functions (GF) suggest that near-field peak horizontal accelerations (PHA) and velocities (PHV) for a 2.4 km/s S-wave rock site will be half those of a 0.64 km/s S-wave rock site, a typical S-wave velocity for rock sites in southern California. A finite rupture simulation of the M 6.7 Northridge earthquake using 1D GFs produces ground motions at 38 stations that underpredict observed PHA/PHV ratios by a factor of two. Convolving site-specific scattering functions from microearthquake recordings with 1D GFs at each point-source integration point of the finite fault produces PHA/PHV ratios (and PHA and PHV estimates to 10 Hz) consistent with observed Northridge near-field ground motions. Thus, PHA may decrease more slowly with increasing rock S-wave velocity than PHV because site-specific scattering dominates higher frequencies that often control PHA. The lack of detailed velocity logs for many strong motion sites, makes it difficult to determine an empirical PHA versus rock S-wave velocity relation from existing strong motion data.

Based on near-field modeling of PHV to 10 Hz, it is necessary to included site-specific responses in ground motions simulations to determine the scaling of PHA with rock S-wave velocity. Site-specific scattering functions are convolved with 1D GFs in finite rupture simulations to evaluate the effects of site-specific GF complexity on PHA/PHV scaling between a typical southern California "rock" site (0.64 km/s) and a northern California "real rock" site (2.4 km/s). Since site-specific 1D GFs probably do not contain all first-order factors effecting PHA, plane-waves are propagated through shallow 3D velocity models derived from borehole velocity information to estimate frequency-dependent amplitude scaling as a function of the lateral thickness of a high S-wave velocity foundation.

DISAGGREGATION OF SEISMIC HAZARD

BAZZURRO, P. and CORNELL, C. A., Dept. of Civil and Environmental Engineering, Stanford University, Stanford, CA, 9305-4020; paolo@surge.stanford.edu, cornell@ce.stanford.edu.

The probablistic seismic hazard at a site is the annual frequency of exceeding ground motion intensity level x, where intensity is typically measured in terms of the spectral acceleration at the natural period of the structure of interest. The conditional distribution of the magnitude and distance of the event given that level x is exceeded is referred to as the disaggregated hazard; it is therefore a display of the relative contributions to the hazard of all possible future events. An event (magnitude and distance) that dominates this function, for example, is a logical candidate for a "deterministic" or "scenario" or "design" event. Because of the insights that it provides disaggregation has quickly become a popular by-product in probabilistic seismic hazard analysis (PSHA) studies. Several recent guidelines specify that it be a product of any PSHA.

Nonetheless it is apparent that several subtleties of disaggregation, subtleties that may alter one's conclusions if not understood, are not widely appreciated by the producers and recipients of this useful tool. This presentation will cover such issues as: representation of this density function by mass functions, uniform versus variable discretization intervals, use of log distance rather than distance as the representative variable, amplifying the independent variable vector to include "epsilon" (a term representing scatter about the mean attenuation function) and/or latitude and longitude, and selection criteria for the "scenario" or representative event(s) (via the mode or mean, for example), and the potential dependence of these events upon the other issues in this list.

The discussion will be illustrated by applications to simple generic case studies and to a realistic representation of a downtown Los Angeles site involving many surrounding sources of future earthquakes.

There is not a unique, "correct" disaggregation. (The authors recommendations will be given, however.) At a minimum the message is that the PSHA analyst must always report explicitly what he has presented in the disaggregation he presents. This is seldom the case today.

A Deterministic-Stochastic Approach to Strong Motion Synthesis for Hazard Assessment

MENDEZ, A.J., Impact Forecasting, L.L.C., 230 West Monroe Street, Suite 9000, Chicago, Illinois, 60606, andresm@art.aon.com

A methodology is presented for the synthesis of high-frequency strong ground motion based on the stochastic simulation method of Boore (1983) and the isochron formulation of Bernard and Madariaga (1984) and Spudich and Frazer (1984). In this hybrid approach, the high-frequency oscillations observed in actual ground motion records are generated stochastically, while the envelope of these oscillations is calculated in a deterministic fashion from a simple kinematic description of rupture on an extended fault plane.

In a typical application of stochastic modeling, such as Boore's, synthetic acceleration time histories are generated by windowing white Gaussian noise with an envelope function that has a simple mathematical representation. After this the signals are filtered in the frequency domain so as to exhibit the desired spectral characteristics of earthquake ground motion. In the present technique, the isochron formulation is used as the physical basis for generating realistic envelopes resulting from the rupture of an extended fault plane. The ground motion envelopes have durations and amplitudes which take into account how the energy released by the propagation of a rupture throughout an extended fault is propagated to any given site.

The methodology is meant to be implemented using only a limited number of parameters to describe the source (dimensions and geometry), propagation medium (wave velocities), and site (site transfer function). Strong motion envelopes can be easily and quickly generated from a large number of plausible rupture scenarios of an extended fault. The envelopes are then "filled in" using the stochastic component of the methodology. Seismic input parameters of interest can be obtained from the synthetics; and more importantly, the scatter in their values directly reflects the different physical assumptions used in constructing the scenarios. This hybrid technique is illustrated through its application to recent California earthquakes. Comparisons between strong motion records and synthetic time histories are presented in terms of: envelope shapes, Husid plots of normalized Arias' intensity, and response spectra.

"Parametric-Historic" Procedure for Probabilistic Seismic Hazard Analysis

KIJKO, A., and GRAHAM, G., Council for Geoscience, Geological Survey of South Africa, Private Bag X112, Pretoria 0001, South Africa, kijko@geoscience.org.za.

A new methodology for probabilistic seismic hazard analysis (PSHA), has been developed. The approach combines the best features of the "deductive" (Cornell, 1968) and "historic" (Veneziano et al., 1984) procedures. It can be called a "parametric-historic" procedure.

The maximum regional magnitude m_{max} is of paramount importance in this approach and we present some of the statistical techniques which can be used for the evaluation of this important parameter.

The approach used permits the combination of historical and instrumental data. The historical part of the catalogue contains only the strongest events, whereas the complete part can be divided into several subcatalogues, each assumed complete above a specified threshold of magnitude. Uncertainty in the determination of magnitude has also been taken into account.

In addition the technique differs from the classical Cornell-based approaches, in that it assesses seismic hazard at individual sites without employing the subjective judgment that is involved in defining seismic source zones, in those cases where specific active faults have not been identified or mapped, and where the causes of seismicity are not well understood.

An example of the application of the new PSHA methodology is also presented.

Past and Future Seismicity Modelling by Spatial Smoothing

LAPAJNE, J.K., ZABUKOVEC, B., and ZUPANCIC, P., Geophysical Survey of Slovenia, Ministry of the Environment and Physical Planning, Ljubljana 1000, Slovenia, janez.lapajne@gf.sigov.mail.si.

The most important and, often, the only input for modelling seismicity in a given area is a seismological database represented by one or more appropriately-prepared complete (sub)catalogues. Usually spatial models of past seismicity are simply represented by corresponding epicentral maps, which do not take into account the uncertainty of epicenter locations. We suggest using a distribution that incorporates the uncertainty of epicenter locations as a spatial model of past seismicity. To demonstrate the preparation of such distributions, two complete subcatalogues of the Slovenian earthquake catalogue were used. In both cases the distribution of past seismicity was obtained by circular symmetrical smoothing of epicenters in which the radius of smoothing was proportional to the assessed errors of their locations. In the smoothing procedure the entire observed area was divided into grid cells of about 11 km square. Modelling of future seismicity is based on the assumption that future earthquakes will take place in the vicinity of past earthquake locations. Thus an expected distribution of future earthquake epicenters may simply be created by an appropriate further smoothing of a distribution of past seismicity. For this purpose we applied fault oriented elliptical smoothing of past seismicity based on presupposed orientations of seismogenic faults. The axes of the ellipse of smoothing were proportional to the assessed subsurface rupture lengths. The calculated distributions of expected future seismicity may be used either for the delineation of seismic source zones or directly for the evaluation of seismic hazard. In the last case grid cells should be used as seismic point sources.

Probabilistic Seismic Hazard Maps of Alaska

WESSON, R.L., FRANKEL, A.D., MUELLER, C.S., HARMSEN, S.C., and LAHR, J.C.

Probabilistic seismic hazard maps have been prepared for Alaska portraying ground motion values (peak ground acceleration and spectral amplitude at periods of 0.2, 0.3 and 1.0 seconds) at probabilities of exceedance of 2%, 5% and 10% in 50 years. Preparation of these maps followed the same general strategy as that followed for the U.S.G.S. seismic hazard maps of the contiguous United States, combining hazard derived from spatially smoothed historic seismicity with hazard from fault-specific sources. Preparation of the Alaska maps presented particular challenges in characterizing the hazard from the Aleutian megathrust. In the maps of the contiguous United States the rate of seismicity for recognized active faults was determined from slip rates estimated from geologic data. This approach is not appropriate for the megathrust because it has been demonstrated that a significant fraction of the subduction occurs aseismically. The characteristic earthquake hypothesis, based on recurrence rates determined from geologic data, is appealing for the portion of the megathrust that ruptured in the 1964 Alaskan earthquake, but is demonstrably inappropriate for the western portion of the megathrust. Consequently the hazard from the western portion was estimated based on a truncated Gutenberg and Richter model derived from historic seismicity, and the hazard for the 1964 zone was estimated from a combination of a Gutenberg and Richter model derived from historic seismicity and the characteristic earthquake hypothesis with recurrence rates estimated from geologic data. The easternmost portion of the megathust in the vicinity of Yakataga presented particular difficulty because of geologic complexity and limited data. The resulting maps will be discussed and deaggregations of the hazard will be presented for Anchorage, Fairbanks, Juneau and other points.

Peak Ground Motions from the Second Major 16 December 1811 New Madrid Earthquake

JOHNSTON, ARCH C., The University of Memphis, CERI, Memphis TN 38152, johnston@ceri.memphis.edu

The three main 1811–12 New Madrid earthquakes (**M** 7.8–8.1 ± 0.3) control the seismic hazard for much of the central U.S., but all ground motion estimates have been from qualitative measures in terms of intensities. Two accounts, however, are precise enough to allow peak ground velocity and acceleration estimates. The Louisville report of J. Brooks is especially useful since it includes frequency: "*... time about 80 returns to the same point per minute and uniform.... the greatest stretch of motion, whilst regular, was 4 to 5 inches.*" The New Madrid report does not include frequency but is clearly free-field: "*I hurried home... but the agitation of the earth was so great it was with much difficulty I kept my balance—the motion of the earth was about twelve inches to and fro.*"

Assumptions that 1) the reported displacements are peak-to-peak, 2) the Louisville (and more dubiously New Madrid) motions were sinusoidal, and 3) a frequency of at least 1 Hz is necessary to upset one's balance for a 12-inch differential displacement yield the following strong ground motions. Louisville (1.3 Hz): peak displ., pgd=5.1–6.4 cm; pgv=42–53 cm/s; pga=0.36–0.45 g. New Madrid (1.0–1.5 Hz): pgd=15.2 cm; pgv=96–144 cm/s; pga=0.61–1.38 g. Both locales are Class C soil sites.

Both historical accounts were for the second major earthquake at daybreak on 16 Dec. 1811. Use of the faulting scenario of Johnston & Schweig (1996) yields distances from the source fault of 18–30 km for New Madrid and 400–450 km for Louisville. The New Madrid results agree well with recently published ground motion relations for the Central U.S. for an earthquake of mid-7 **M**. The Louisville results are anomalously high, however, suggesting that Brooks' displacements may not have been free-field or may actually have been for the larger 2:15 a.m. mainshock.

Ground Motion Models in the Eastern and Central United States from National Seismographic Network Data

SAIKIA, C.K., P.G. SOMERVILLE, H.K. THIO and A. PITARKA, Woodward-Clyde Fedarl Services, 566 El Dorado St., Pasadena, CA 91101, cksaiki0@wcc.com

The objective of this study is to characterize earthquake source ground motion attenuation characteristics in the eastern and central United States using broadband recordings of the National Seismographic Network (NSN). A basin feature of the empirical attenuation data from the NSN is a decrease in the rate of attenuation centered at a distance of about 100 km, and typically extending from about 75 km to several hundred km. Using a crustal model derived from the NSN data, we were able to match the shape of the empirical attenuation using synthetic seismograms. We used synthetic seismograms to investigate the sensitivity of the attenuation relation to various parameters for a point source model of the earthquake. These parameters include the focal mechanism of the earthquake; the depth of the source in the crust; the Q model of the crust, and the presence of scattering in the crust. We found that for long period ground motions, for example as represented by peak velocity, variations in focal mechanism produced large variations in calculated ground motion amplitudes. We found that the attenuation at close distances is strongly dependent on the focal depth of the earthquake. At distances larger than about 30 km, the shape of the attenuation is less sensitive to the focal depth, except for shallow earthquakes for which trapping of energy in the shallow low velocity region causes gradual attenuation. Also, for deeper earthquakes, there is some influence because changes in the critical distance for reflected phases from the lower crust. We found that the sensitivity of ground motion amplitudes to changes in the Q model of the crust only became significant at distances larger than about 75 km. Based on empirical model and the synthetic seismograms, we developed an attenuation model that includes two shoulders (regions of steep slope). The first shoulder occurs within several tens of km from the source, and the second shoulder occurs at several hundred km from the source. The two shoulders are separated by the region of more gradual attenuation.

Tuesday PM, March 17, 1998—Room 235
Explosion and Impact Event Analyses and Monitoring
Presiding: Chris Young, *Sandia National Laboratory*

An Explanation for Degassing Explosions at Karymsky Volcano, Kamchatka, Russia

JOHNSON, J.B. and LEES, J.M., Geophysics Program, University of Washington, Seattle, WA 98195, eljefe@geophys.washington.edu; Department of Geology and Geophysics, Yale University, New Haven, CT 06510, lees@love.yale.geology.edu.

During the summer of 1997, Karymsky Volcano produced summit explosions about six times each hour. A typical episode lasted one to three minutes, produced gas and ash columns several hundred meters high, and ejected some incandescent material. To better understand the source mechanisms responsible, a three component broad-band seismometer and infrasonic microphone were deployed 1760 meters from the active vent for ten days.

The seismic data shows a striking uniformity between explosive events. In each explosion, the same distinct emergent seismic wavelet is identifiable at the onset and is followed 4.15 s ±0.1 s later by an impulsive acoustic arrival. The deviation in differential travel times is explained by changing atmospheric conditions, not a changing source location or mechanism. These events are interpreted as vent-clearing explosions of variable amplitude which enable several minutes of degassing to commence.

The continued degassing is generally manifested as either a series of regular one second 'chugging' explosions, or as a steady 'jetting'. The seismic signature for chugs appears as short duration harmonic tremor with integer overtones. Though commonly explained as fluid oscillations confined in a volume, we believe that our 'harmonic tremor' may simply be an effect of repeated gas bubble bursts at the surface. In contrast, the jetting is non-harmonic in nature and contains generally higher frequencies. A critical question is how vent/plug geometry and gas flux influence these competing degassing behaviors.

To address this question, we will analyze the amplitude-frequency relationship of seismic and acoustic data. We observe a positive correlation of seismic and acoustic signal strengths. We would expect that the lapse time between eruptive episodes dictates these amplitudes and subsequent degassing behavior. Finally, we intend to compare our findings with seismic data collected a year before when degassing was more vigorous.

CHARACTERISTICS OF SEISMIC SIGNALS FROM THE COLLAPSE OF UNDERGROUND CAVITIES

William R. Walter, and Kevin Mayeda, Lawrence Livermore National Laboratory, Geophysics and Global Security Division, L-205, Livermore, Ca., 94551, bwalter@llnl.gov

The sudden collapse of underground cavities have generated seismic signals as large as magnitude 5.4. Though much less common than ordinary tectonic earthquakes, there have been at least half a dozen magnitude 3.8 and greater mine collapses in the 1995-1997 time period. These included events in Kentucky, Alabama, and Wyoming as well as events in Germany and Russia. The relatively shallow depth of these sources, combined with an expected significant volumetric component, can make these events look like explosions by some measures, raising incorrect suspicions under the Comprehensive Test Ban Treaty. We are studying the point source mechanisms of these events via waveform modeling as well as examining the behavior of regional discriminant measures compared with nearby earthquakes.

A particularly interesting source of cavity collapse data comes from the collapses that followed underground nuclear tests at the Nevada Test Site. Because the explosions and collapses are co-located, direct comparisons between explosion and collapse point-source mechanism as well as discriminant behavior can be made. Preliminary results indicate that post shot collapse long period surface and body waves are well fit by a closing crack model. The same model also fits most of the large mine collapses and can be used to estimate collapse dimensions. Post shot collapses appear deficient in high frequencies compared with the explosions. Relative measures of post-shot P/S amplitudes at high frequencies indicate much variability but generally fall in between those of earthquakes and explosions.

*This research was performed under the auspices of the U.S. Department of Energy by Lawrence Livermore National Laboratory under contract number W-7405-ENG-48.

REPRESENTING SHORT-PERIOD REGIONAL P/S DISCRIMINANTS FOR CTBT MONITORING IN THE MIDDLE EAST

RODGERS, A., W. WALTER, Lawrence Livermore National Laboratory, L-205, Livermore CA 94551, rodgers@s34.es.llnl.gov; and T. LAY, University of California, Santa Cruz, Earth Sciences Department, Santa Cruz CA 95064.

Regional phase amplitude ratios have proven to be effective for discriminating earthquake and explosion sources and will play a critical role in monitoring a Comprehensive Test Ban Treaty (CTBT). However, P/S discriminants are highly regionally dependent due to variations in geology, topography, and elastic and anelastic lithospheric structure. Blockage and/or inefficient propagation of Sn and Lg can make these phases unusable for discrimination. Thus, successful monitoring of a CTBT will likely require calibration of regional phase amplitude ratios and phase blockage for each station.

We measured regional phase amplitude ratios (e.g. Pn/Lg, Pg/Lg, Pn/Sn, Pg/Sn) and signal-to-noise ratios for stations AAK, ABKT, ANTO, BGIO, GNI, KEG, KIV and NIL in the Middle East. Measurements were made on instrument deconvolved displacement seismograms in the frequency domain in four bands (0.75-1.5, 1.5-3.0, 3.0-6.0 and 6.0-9.0 Hz). Individual P/S ratios which pass a signal-to-noise test show large scatter, however, systematic trends can be observed. Low frequency (< 3.0 Hz) ratios show the largest variability, while many high frequency ratios (> 3.0 Hz) fail the signal-to-noise test. Maps of the individual P/S ratios indicate systematic regional variability related to tectonic and topographic structure. In order to gain predictive models of P/S amplitude ratio behavior, several representations of the data were investigated. Firstly, the individual data were plotted and smoothed with a cap-averaging scheme. This treatment of the data depends on the choice of a cap radius. The resulting maps tend to under-represent the true variability of the data. For station ABKT, which lies near a major tectonic and topographic boundary, the data can be subdivided into azimuthal sectors. Within each sector the scatter of the P/S ratios are well modeled with a simple distance trend. Multivariate regression of the P/S ratios with distance and path specific crustal waveguide parameters (e.g. mean and rms elevation, mean sediment and crustal thickness) allows us to determine the most important factors which control the data variability. The results of these various investigations will be presented and discussed. *Research was performed under the auspices of the U.S. Department of Energy by the Lawrence Livermore National Laboratory under contract W-7405-ENG-48.*

Calibration of International Data Center (IDC) Magnitudes for Event Screening Using the M_s/m_b Criterion

MURPHY, J.R. and BARKER, B.W., Maxwell Technologies, Reston, VA 20191, jrm@maxwell.com, bwb@maxwell.com

The M_s/m_b discriminant has proved to provide the most robust teleseismic event screening procedure for shallow seismic events. It is based on the observation that M_s - m_b is typically less than about −1 for underground nuclear explosions and greater than about −1 for crustal earthquakes. These generalizations are based on classical m_b and M_s values such as those published by the U.S. NEIC and other agencies. Unfortunately, such prior experience is not directly transportable to the IDC in that it has now been conclusively demonstrated that the m_b and M_s values estimated at the IDC are systematically different from those published by the NEIC for the same events. Since IDC magnitudes have been determined for only a few underground nuclear explosions, an indirect approach is required to calibrate the IDC M_s/m_b event screening criterion. Evaluation of the time dependencies of the average annual differences between the NEIS m_b and M_s values and the corresponding logarithms of the Harvard moment estimates for the same shallow earthquakes occurring over the period 1977 to 1997 indicate that the NEIS m_b and M_s determinations have been remarkably stable, on average, since about 1981. Analysis of NEIS m_b and M_s values for earthquakes and underground nuclear explosions which have occurred since 1981 indicate that an M_s - m_b threshold value of about −1.0 adequately separates the two populations for events having NEIS m_b values of around 5.5. Extension of the derived NEIS M_s/m_b event screening threshold at m_b = 5.5 for applications to the entire range of m_b values reported by the IDC is complicated by the fact that the M_s - m_b differences are known to be a function of m_b for both earthquakes and explosions, with the differences increasing with decreasing magnitude in both cases. Analyses of a large database of underground nuclear explosion data, followed by a transformation to account for the average differences between IDC and NEIS m_b and M_s values, leads to the following relation for the interim IDC M_s/m_b event screening criterion: M_s(IDC) = 1.25m_b(IDC) - 2.20. Application of this criterion to a large sample of 1226 1997 shallow earthquakes for which IDC m_b and M_s values have been determined indicates a false alarm rate of less than 1%.

A Procedure for Estimation of Source and Propagation Amplitude Corrections for Regional Seismic Discriminants

TAYLOR, S.R., HARTSE, H.E., Los Alamos National Laboratory, MS C335, Los Alamos, NM 87545, taylor@lanl.gov, hans@geophysics.lanl.gov

We outline a procedure for the estimation of frequency-dependent source and propagation amplitude corrections for regional seismic discriminants (Source Path Amplitude Correction - SPAC). For a given station and phase, a number of well-recorded earthquakes are inverted for source and path corrections. The method assumes a simple Brune (1970) earthquake-source model and a simple propagation model consisting of a frequency-independent geometrical spreading and frequency-dependent power-law Q. The inverted low-frequency levels are then regressed against mb to derive a set of corrections that are a function of mb and distance. Once a set of corrections is derived, effects of source scaling and distance as a function of frequency are applied to amplitudes from new events prior to forming discrimination ratios. The resulting discriminants are normally distributed and amenable to multivariate feature selection, classification, and outlier techniques. To date, most discrimination studies have removed distance corrections once a particular amplitude ratio is formed (Distance Corrected Ratio - DCR). DCR generally works well for phase ratios taken in a particular frequency band. However, when different frequency bands are combined (for phase spectral ratios or cross spectral ratios), significant source-scaling effects (e.g. corner-frequency scaling) can remain, causing the discriminants to vary as a function of event size and to be non-normally distributed. It is then often necessary to construct non-physical transformations in an attempt to make the discriminants multivariate normal. The SPAC technique can be used to construct discriminants that are multivariate normal by using simple physical seismic source and propagation models. Moreover, phase amplitude residuals as a function of frequency can be spatially averaged and used as additional path-specific corrections to correct for additional propagation effects such as phase blockages.

Nonstationary Bayesian Kriging: Application of Spatial Travel-Time Corrections to Improve Seismic Location

Craig A. Schultz, Stephen C. Myers, Stanley D. Ruppert, Lawrence Livermore National Laboratory[1], L-205, Livermore, CA 94551, schultz9@llnl.gov; James Hipp, Christopher J. Young, Sandia National Laboratory[2], PO Box 5800, Albuquerque, NM 87185, cjyoung@sandia.gov

Seismic characterization works to improve the detection, location and identification of seismic events by correcting for inaccuracies in geophysical models. These inaccuracies are caused by inherent averaging in the model and, as a result, exact data values cannot be directly recovered at a point in the model. Seismic characterization involves cataloging reference events so that inaccuracies in the model can be mapped at these points and true data values can be retained through a correction. Application of these corrections to a new event requires the accurate prediction of the correction value at a point that is near, but not necessarily coincident with the reference events. Given that these reference events can be sparsely distributed geographically, both interpolation and extrapolation of corrections to the new point are required. In this study, we develop a closed form representation of Bayesian kriging (linear prediction) that incorporates variable spatial damping. The result is a robust nonstationary algorithm for spatially interpolating geophysical corrections. This algorithm extends local trends when data coverage is good and allows for damping to an *a priori* background mean when data coverage is poor. Benchmark tests show that, when the correlation structure of the correction surface is stationary and nonstationary damping is incorporated, the technique gives a reliable prediction of the correction value along with an appropriate uncertainty estimate. Tests with travel-time residual data show that combining variable damping with an azimuthal coverage criterion reduces the large errors that occur with more classical linear prediction techniques, especially when values are extrapolated in poor coverage regions. In the travel-time correction case, this technique generates both seismic corrections along with uncertainties in the corrections. Application of this algorithm to calibrate regional networks allows for significant improvement of locations.

Testing the DOE Model for Improving Seismic Event Locations Using Kriged Traveltime Corrections

YOUNG, C.J., HIPP, J.R., SHEPHERD, E., and MOORE, S.G., Sandia National Laboratory[1],MS1138, Albuquerque, NM 87185, cjyoung@sandia.gov; SCHULTZ, C.A.and MYERS, S.C., Lawrence Livermore National Laboratory[2], L-205, Livermore, CA 94551, schultz9@llnl.gov

The U.S. National Laboratories, under the auspices of the Department of Energy, have been tasked with improving the capability of the United States National Data Center (USNDC) to monitor compliance with the Comprehensive Test Ban Treaty (CTBT). The seismic location algorithm used by the USNDC has the capability to generate very accurate locations by applying geographically dependent traveltime corrections, but to date none of the means proposed for generating and representing these corrections has proven to be entirely satisfactory. We demonstrate a new method for generating and applying the traveltime correction data which we believe can meet the performance and quality requirements of the USNDC. The method consists of two parts. First, the residual data and error estimates from "ground truth" events are interpolated using a Nonstationary Bayesian Kriging Technique (described in a talk by Schultz et al.) to densify them. The densified data set is then spatially indexed and stored in a fast-access database. When an accurate location is needed, the densified data is retrieved and a quick interpolation is performed using a fast interpolation method. To test our model, we use a set of synthetic events that were created to have traveltimes consistent with a radial base model plus perturbations from randomly generated spherical-harmonic surfaces. We show that if these events are located with the interpolated corrections, the locations are dramatically improved.

[1]This research was supported by the U.S. Department of Energy under Contract DE-AC04-94AL85000. Sandia is a multiprogram laboratory operated by Sandia Corporation,a Lockheed Martin Company, for the U.S. Department of Energy

[2]This research was performed under the auspices of the U.S. Department of Energy by Lawrence Livermore National Laboratory under contract number W-7405-ENG-48.

Maximum Spectral Energy Timing Method for Epicenter Determination And Location Errors Reduction. Part II: P-Waves.

YACOUB, N.K., U.S. Air Force Technical Applications Center/TTR, 1030 S. Hwy A1A, Patrick Air Force Base, Florida, 32925-3002; 407-494-2251; nazieh@rayleigh.tt.aftac.gov.

Location of seismic sources is subject to random and systematic errors. The random error is attributed, in part, to inaccuracies and inconsistencies in the method for measuring the arrival time for the signal. The systematic error is attributed to travel time residuals between global travel time models and the actual travel time in the earth. The goodness of a determined epicenter depends on the size of these errors and is reflected in the location parameters, which are the mislocation vector, the error ellipse, and the origin time residual. Maximum spectral energy timing addresses the random error by improving the accuracy and the consistency for measuring the arrival time. P-wave maximum spectral energy arrival times (spectral timing) are used to determine the epicenters for 26 nuclear explosions of well known locations. To compare the accuracy and the consistency of spectral timing to that of conventional technique, these epicenters are also determined by means of P-wave first breaks, using a common network of stations for each explosion. Mislocation vector magnitudes between the actual locations and the determined epicenters are calculated. On the average, the vector magnitude determined by the spectral timing method is 50% of that determined by the P-wave first break method. Because the same set of stations are used for each explosion, there is no change in the parameters for the coverage ellipse error. However, all the epicenters determined by the spectral timing are within the error ellipse, while many of the epicenters determined by the P-wave first break timing fall outside the error ellipse.

Recent Developments in SAC2000

Doug Dodge, Mike Firpo, and Peter Goldstein
Geophysics and Global Security Division, Lawrence Livermore National Laboratory

SAC2000 is the rebirth and evolution of Lawrence Livermore National Laboratory's (LLNL's) Seismic Analysis Code (SAC) developed during the 1980s for a variety of geophysical applications. SAC2000's strengths include its ability to process a diverse range of data types, its extensive, well-documented signal processing capabilities (both on-line and on the web at: http://www-ep.es.llnl.gov/tvp/sac.html), its macro language, and its ability to do both batch and interactive processing. Its extensive usage (> 300 institutions worldwide) has also made it much easier for researchers to develop collaborative research projects. SAC2000's extensive signal processing capabilities include: data inspection, signal correction, and quality control, unary and binary data operations, travel-time analysis, spectral analysis including high-resolution spectral estimation, spectrograms and binary sonograms, and array and three-component analysis.

Recent developments in SAC2000 include: compatibility with the widely used SEED data format instrument responses, map making capabilities via an interface to GMT, a three-component polarization and phase identification tool, an external interface that allows users to define their own commands, and an interface to MATLAB that allows the user to use MATLAB commands and scripts on SAC data from within SAC2000. We have also implemented many commands to enhance user efficiency and made numerous improvements and enhancements to individual SAC commands. Our work on SAC2000 is motivated by the need for easy and efficient access to and processing and interpretation of large amounts of data contained in CSS3.0-based Oracle databases or CSS3.0 flat files. Based on these needs, we have developed a new, internal data structure for SAC2000, capable of representing all the information in our databases. Currently SAC2000 can read from those databases, and work is in progress to allow SAC2000 to update the databases as well. Given the variety of data that are currently possible in SAC2000 and other programs, and the likelihood that additional parameters will be needed in the future, we have designed SAC2000's new format to be easily extendible and anticipate incorporation of significant extensions to the CSS3.0 schema.

This research was performed under the auspices of the U.S. Department of Energy by Lawrence Livermore National Laboratory under contract number W-7405-ENG-48.

In Search of a Robust 3 Component Bearing Estimator

J.P. CLAASSEN, Cooperative Monitoring Technologies Dept, Sandia National Laboratories[1], NM 87185-0655, jpclaas@sandia.gov.

As the monitoring thresholds of networks are reduced, bearing estimates become more important to associating detections and locating events. Current methods of estimating bearings on 3-component station data typically lack consistent precision. A technique which extracts co-lateral information useful to making estimates has been identified and explored. A common estimation framework is used to define the optimal time-frequency windows, to make the bearing estimates themselves, and to withdraw helpful metrics. It is theorized that the use of windows having optimal polarization properties will result in estimates having all the available precision.

The approach features a quadrature filter bank whose individual filters are based on Slepian wavelets [1] with a slight but important modification. The quadrature signal components are used to construct a series of rectangular observation matrices centered on the current sample. The degree of polarization, the linearity of the dominant particle motion, the eigen energy concentration, and a pseudo SNR are withdrawn from each observation matrix. Bearings are estimated from consecutive samples having good polarization properties. Among the available estimates, the choice of the best estimate is currently guided by a simple information theoretic premise, although continuing investigations may reveal alternative methods of combining or selecting estimates.

In this presentation the methodology and properties of the estimator are described and illustrated. The potential for making better bearing estimates is addressed and discussed.

[1] Lilly, J.M. & J. Park, Multiwavelet Spectral and Polarization Analyses of Seismic Records, *Geophysical Journal International*, **122**: 1001–1021, 1995

[1]Sandia is multiprogram laboratory operated by the Sandia Corporation for the US Dept. of Energy under contract DE-AC-94AL85000

Tuesday, 8:30 AM–5:00 PM
Glenn Miller Ballroom
Posters
Shallow High-Resolution Seismology for Environmental and Seismic Hazard Studies

High-Resolution Seismic Imaging of Strata Buried by Basalt Flows, Bellemont, Arizona

RYMER, M.J., CATCHINGS, R.D., and GOLDMAN, M.R., US Geological Survey, 345 Middlefield Rd., MS 977, Menlo Park, CA 94025, mrymer@isdmnl.wr.usgs.gov

Conventional seismic reflection imaging in areas with large velocity-impedance contrasts, such as interlayered basalt and sediments, is exceedingly difficult due to penetration limitations. High-resolution seismic reflection imaging in seismically difficult areas can be equally or more challenging than conventional seismic reflection imaging. Bellemont, located about 18 km west of Flagstaff, Arizona, is one such seismically difficult area due to the alternating layers of clay and Cenozoic basalt in the upper 100 m. Limited drilling in the Bellemont area has been used to characterize subsurface stratigraphy and structure, but the cost of drilling can be prohibitive and provides laterally limited information.

To aid in toxic waste remediation efforts by characterizing the subsurface in the Bellemont area, we used combined seismic reflection and refraction techniques to obtain high-resolution images and velocities. Seismic data were acquired using 0.45-kg explosive sources buried at depths of about 5 m. Geophone and shot spacings were 3m and 6 m, respectively, yielding maximum folds of between 100 and 125. The data show thick accumulations of interlayered basalt and clay, overlying upper Paleozoic limestone and sandstone strata of the Colorado Plateau. Locally, the stratigraphic sequence is faulted and downdropped by as much as several tens of meters.

Both the seismic reflection/refraction data and borehole data indicate consistent structure near the boreholes; however, the seismic reflection and refraction data further indicate lateral structural variations that greatly differ from that interpreted from the widely spaced boreholes. These data show that seismic methods can be used in seismically challenging areas and show the utility of using seismic methods to characterize the subsurface for environmental remediation efforts.

Correlation of 1- to 10-Hz Earthquake Resonances with Surface Measurements of P- and S-Wave Reflections and Refractions in the Upper 70 M

WILLIAMS, R.A., STEPHENSON, W.J., ODUM, J.K., MEREMONTE, M.E., CRANSWICK, E., and FRANKEL, A.D. (U.S. Geological Survey, Denver Federal Center MS 966, Box 25046, Denver, CO 80225, USA; williams@gldvxa.cr.usgs.gov)

Resonances observed in earthquake seismograms recorded at some sites in Seattle and central U.S. are strongly correlated with the near-surface structures determined from shallow seismic reflection and refraction surveys of the same

sites. In Sherman Oaks, Calif., correlation of earthquake resonances with shallow impedance boundaries is less certain because calculated and observed resonances do not match as closely. We also observed near-surface resonances in Santa Cruz, Calif., in similar previous studies. Sledgehammer impacts were used to generate reversed profiles along an 87-m-long geophone array at each site. The array consisted of 30 vertical and horizontal sensors spaced at 3-m intervals. We recorded a high-amplitude S-wave reflection 250 m northeast and 300 m east of the Seattle Kingdome earthquake recording station. The reflection two-way traveltime is about 0.23 to 0.27 s (about 18- to 22-m depth) and appears to mark the boundary between overlying alluvium (Vs <180 m/s) and a higher velocity material (Vs about 400 m/s). This reflecting boundary probably causes a strong 2-Hz resonance that is observed in the earthquake data for the site near the Kingdome and accounts for the highest amplitude ground motion at this site above 1 Hz. In the central U.S., we recorded S-wave reflections from a high-impedance boundary (the S-wave velocity increases from about 200 m/s to about 2000 m/s) at about 45-m depth. The traveltime for this reflection corresponds to a strong fundamental resonance at about 1.5 Hz. Two other prominent peaks in the spectrum at 3.9 and 6.2 Hz are probably harmonics generated by this simple impedance structure, which taken together with the fundamental, account for the highest amplitude shaking at this site above 1 Hz. In Sherman Oaks, a strong resonance at about 4 Hz is consistently observed on earthquake seismograms, and is possibly explained by a 3.25- to 3.9-Hz resonance calculated from an areally consistent impedance boundary at about 10-m depth as determined by S-wave refraction data. These results show that imaging near-surface reflections from the ground surface can locate impedance structures that are important contributors to damaging ground shaking in an earthquake.

Use of Combined Seismic Reflection and Refraction High-Resolution Imaging for Environmental, Water Resource, and Earthquake Hazards Investigations

CATCHINGS, R.D., RYMER, M.J., and GOLDMAN, M.R., US Geological Survey, 345 Middlefield Rd., MS 977, Menlo Park, CA 94025, catching@andreas.wr.usgs.gov

We combined high-resolution seismic reflection and refraction techniques to characterize the subsurface for environmental, water resource, and earthquake hazards investigations. High-resolution seismic reflection images provide details of stratigraphic variations and faulting relations, whereas seismic refraction data provide: (1) constraints on the physical nature of the subsurface (bedrock vs. sediment, dry vs. saturated), (2) depth control due to detailed velocity characterization, and (3) a better seismic reflection stack due to enhanced near-surface statics information. High-resolution seismic reflection images are compared with velocity models determined from inversion of first arrivals. The combined reflection and refraction images reveal lateral variations where aquifers, aquitards, paleochannels, or faults are present. When both high-resolution P- and S-wave data are available, we use Vp/Vs and Poisson's ratios to map features not always apparent in either stacked seismic images or velocity models.

Seismic data are presented from studies in a wide variety of geologic conditions and compared with results obtained from borehole data. Included are examples from the Colorado Plateau (upper Paleozoic limestone and sandstone); another site with similar materials, but capped by upper Cenozoic basalt flows; alluvial, fault-bounded Quaternary basins within the San Andreas fault zone; fluvial and lacustrine deposits of regional extent in the Mojave Desert, California; and Quaternary estuarine deposits adjacent to San Francisco Bay.

High-Resolution Seismic Imaging of Quaternary Faulting Across the Commerce Geophysical Lineament, Southeast Missouri

STEPHENSON, W.J., ODUM, J.K., and WILLIAMS, R.A., U.S. Geological Survey, Box 25046, MS 966, Denver, CO 80225, stephens@gldage.cr.usgs.gov; PRATT, T.L., U.S. Geological Survey, University of Washington, Building WB-10, Seattle, WA 98195; HARRISON, R., U.S. Geological Survey, MS 928, Reston, VA 22092; HOFFMAN, D., Missouri Department of Natural Resources, Box 250, Rolla, MO 65401

High-resolution seismic reflection data acquired at three southeast Missouri sites along the surface projection of the Commerce Geophysical Lineament, defined by linear northeast-trending basement magnetic and gravity anomalies extending for over 400 km, reveal a complex history of faulting and deformation that extends into Quaternary time. Near Qulin, Missouri, approximately 20 m of apparent vertical displacement has occurred, possibly as recent as mid-Quaternary. Roughly 100 km to the northeast, data acquired on the east side of Idalia Hill, Missouri, reveal a series of reverse and probably right-lateral strike-slip faults. About 100 km further northeast in the Benton Hills, near Thebes Gap, seismic data image a complicated series of anticlinal and synclinal fault-bounded blocks in the subsurface immediately north of the main Commerce fault. Much of the observed deformation imaged in the upper 400 m of these data appears to have occurred since post-Cretaceous time, with a significant portion of it apparently occurring since the Tertiary. Collectively, these data along with geomorphic and surface-geologic evidence suggest: 1) the existence of at least one major seismogenic structure in southeast Missouri that lies outside the main bands of New Madrid Seismic Zone seismicity; and 2) this structure has been active in the Quaternary and possibly the Holocene. The structure (or structures) causing the subsurface deformation along the Commerce Geophysical Lineament may thus pose another previously-unknown seismic hazard to the Central United States.

Seismic Surface Wave Tomography for Near-Surface Structures

LONG, L.T., School of Earth and Atmospheric Sciences, Georgia Institute of Technology, Atlanta, GA 30332, tim.long@eas.gatech.edu; KOCAOGLU, A.H., Dept fo Geophysics, Mining Faculty, Istanbul Technical University, Maslak 80626, Istanbul Turkey, argun@sariyer.cc.itu.edu.tr; and DOLL, W.E., Oak Ridge National Lab, Environmental Sciences Division, P.O. Box 2008, Oak Ridge, TN 37831, d8e@ornl.gov

The objective of surface wave tomography for near-surface structures is to facilitate interpretation of structures associated with the burial of wastes or the dispersion of underground contamination. Surface waves from 2 to 50 Hz are sensitive to the 1 to 10 meter depth range. By using tomography, the group velocity can be determined from measurements made outside a suspected waste site, minimizing the need to take measurements on top of a waste site. Tomography is used to determine the distribution of group velocities over the study area as a function of frequency. The vertical velocity structure at any point in the study area is then obtained from the frequency dependence of its surface wave group velocity. Interpretation of the dispersion curves depend critically on knowledge of the structure. For a test site at the Oak Ridge National Laboratory, Tennessee, inverse dispersion for frequencies from 10 to 25 Hz were observed. A theoretical layered model demonstrated that a velocity inversion was not needed to explain the dispersion. Measurements of group velocity are inherently limited in precision by the trade-off in time and frequency resolution. We have used a combined phase-correlation, group velocity technique to improve precision. Surface wave tomography was able to define the significant features of the test site.

Rapid 3D Refraction Traveltime Tomography with a Variable Grid

Zhang, Jie, Blackhawk Geometrics, Golden, Colorado 80401, jie@blackhawkgeo.com

We have developed a rapid 3D refraction traveltime tomography technique that applies graph theory to calculate first-arrival refractions in the forward calculation and the Gauss-Newton method with Tikhonov regularization in the inversion. Rapid performance is obtained through the use of a fast algorithm for wavefront traveltime calculation and a dynamically varying grid representing the slownesses for inversion. The model is coarsely parameterized in the early inversion stage and a low-order graph template is applied for the raytracing calculation. The use of the sparse grid ensures extremely fast performance. The slowness model is dynamically reparameterized with increasing fineness in accordance with the convergence rate of the rms traveltime residuals. During the later stages of the inversion we also switch to a higher-order graph-template for more accurate traveltime calculation. This reparameterization procedure may take place three or four times during the entire inversion. The use of a coarse model parameterization in the early iterations also provides for a stable solution of the ill-posed inverse problem, i.e., the solution is independent of the initial model.

Hydrostratigraphic Characterization using Shallow Seismic Reflection Profiling, Northwestern Monterey County, California

UNDERWOOD, D.H., SILVER, E.A., LEWIS, S.D., FISHER, A.T., Earth Sciences Department, University of California, Santa Cruz

Groundwater is the principal source of municipal and agricultural water in coastal northwestern Monterey County. Detailed characterization of the properties and distribution of eolian, fluvial, and alluvial fan sediments that comprise the hydrostratigraphic system is necessary to optimize groundwater resource management. We imaged key sections of a shallow aquifer system within one of this region's groundwater basins using high-resolution seismic reflection profiling. Downhole geophysical data, including vertical seismic profiles (VSPs), and hydrogeologic measurements, will be integrated with the seismic reflection data to cross-correlate interpretations and to assess the limits of spatial extrapolation. Our investigative approach and results may hold regional significance since hydrostratigraphic systems in similar depositional settings are typical along the California coast.

The seismic study area is located within the northern part of former Fort Ord, spanning approximately 5 km^2. Previous investigations indicate that the hydrostratigraphy of the shallowest 80 m generally consists of two water-bearing sand units of varying coarseness and silt content. These aquifers are separated by a clay package comprising up to three clay layers, interlayered with variably graded sand. One main objective of the seismic profiling is to map the lateral continuity and properties of this clay package. A peak-to-peak dominant reflector frequency of 120 Hz yields a practical vertical resolution of approximately 2 m. Processing steps to address strong groundroll, residual static variations, and combination of VSP-derived velocities into the NMO correction model are being refined. Preliminary interpretation of these data suggest significant variability in the seismic character of the clay package, possibly indicating differences in hydrogeologic properties.

Soil Properties and Bedrock Fracture Distributions from Shallow Seismic Observations

ALEXANDER, S.S., FALKENSTERN, D.M., GEBBIE, T.J. and ZEISLOFT, M., Department of Geosciences, The Pennsylvania State University, University Park, PA 16802, shel@geosc.psu.edu

Observations of P and Rayleigh waves have been used for several environmental applications in central Pennsylvania. Soil properties and bedrock fracturing distributions were measured along sets of shallow refraction/reflection profiles in two watersheds with shale bedrock and one watershed with limestone bedrock. Empirical relationships from in situ measurements were used to relate P-velocity to fracture density and hydraulic permeability in the shale bedrock areas. Discrete, separated fractures characterize the limestone bedrock area. These bedrock fracture distributions control the shallow subsurface flow of groundwater and are important for mitigation of non-point-source groundwater pollution from human activities such as farming. In the areas studied, related research is being carried out by the U.S. Department of Agriculture to assess the effectiveness of riparian vegetation in reducing the concentrations of nitrates that enter the streams from nearby farms. The seismic results are used to constrain models of the 2- or 3-dimensional hydrogeologic flow and estimate the proportion of the flow near a stream that can interact with the root systems of the riparian vegetation. Significant lateral variability in soil properties and bedrock fracturing was observed in both the shale and limestone settings. The observed systematic decrease in fracture density in shale bedrock near streams should increase the effectiveness of riparian vegetation by channeling most of the flow into the soil zone. However, in the limestone bedrock area riparian vegetation appears to be effective only in localized zones where no bedrock fractures were found. The data also show that first-, second- and third-order stream locations are not controlled by fracturing in the shale bedrock. Rayleigh wave dispersion observations provide spatial resolution of soil and bedrock properties on a scale of a few meters.

Tuesday, 8:30 AM–5:00 PM
Glenn Miller Ballroom

Posters
GPS and Seismology

Integration of the Northern Basin and Range (NBAR) and Wasatch Front GPS Networks for Crustal Deformation in and Around the Southern Intermountain Seismic Belt

BENNETT, R.A.and DAVIS, J.L., Harvard-Smithsonian Center for Astrophysics, 60 Garden Street, MS 42, Cambridge, MA 02138, rbennett@cfa.harvard.edu, MEERTENS, C.M., and SMITH, R.B., Department of Geology and Geophysics, University of Utah, Salt Lake City, Utah 84112, WERNICKE, B.P., Division of Geological and Planetary Sciences, California Institute of Technology 170-25, 1201 E. California Blvd., Pasadena, California 91125

The southern Intermountain Seismic Belt, including the central and southern Wasatch fault zone and the Sevier Desert area, marks the transition from an actively extending lithosphere with a relatively low seismogenic thickness in the Basin and Range province in the west, to the more stable lithosphere with greater seismogenic thickness of the Rocky Mountains-Colorado Plateau to the east. The details of the crustal deformation pattern associated with this transition have not yet been resolved. Combined GPS and terrestrial geodetic measurements near the Wasatch fault [Martinez *et al.*, *GRL*, in press, 1998] yield an estimate of strain accumulation of 51±9 nstrain/yr, oriented nearly east-west. This value is significantly higher than the 10±1 nstrain/yr average obtained for the entire, ~750 km wide, northern Basin and Range from the NBAR GPS network [Bennett *et al.*, *GRL*, in press, 1998]. To further investigate the nature of this transition in crustal deformation, we have begun a combined analysis of data from both the NBAR and Wasatch Front continuous GPS networks. Together these networks provide a dense (10–50 km), wide-aperture (~100 km) sampling of the crustal velocity field across the Wasatch and surrounding faults of west-central and northern Utah. Preliminary NBAR results from ~16 months of monitoring across the Wasatch Fault zone suggest rates that are on average lower than the campaign GPS results, but at this time agree within error. We will report on the new crustal deformation results from this work and explore their relationship to the observed geology and seismicity.

Institutional Collaborations for Joint Seismic and GPS Measurements

PERIN, B.J., MEERTENS, C.M., University Navstar Consortium / UNAVCO, Boulder, CO 80301, USA, perin@unavco.ucar.edu, chuckm@unavco.ucar.edu; NEUHAUSER, D.S., BAXTER, D.R., and MURRAY, M.H., University of California, Berkeley, Berkeley Seismological Laboratory, Berkeley, CA 94720-4760, USA, doug@seismo.berkeley.edu, ray@seismo.berkeley.edu, mmurray@seismo.berkeley.edu; BUTLER, R., Incorporated Research Institutions for Seismology / IRIS, Washington, DC 20005, rhett@iris.edu

There has been long-standing interest in making combined seismic and Global Positioning System (GPS) measurements for geophysical studies for scientific, logistical, and cost benefits. Seismic and GPS instruments measure motions on different time scales but are complementary in improving understanding of earthquake processes, plate motions, inter-plate deformation and plate boundary deformation. Various groups within the Incorporated Research Institutions for Seismology (IRIS) and the University Navstar Consortium (UNAVCO) have been working jointly for almost two years to realize the cost and efficiency benefits of joint seismic/GPS measurements. This collaboration includes developing the technical capability to use existing VSAT bandwidth to relay co-located GPS measurements to appropriate regional GPS data centers, the integration of multi-vendor GPS receivers with seismic data loggers used both within the Global Seismic Network and regional arrays, and joint development of the data management and communications hardware and software, including advanced data archiving tools. For example, UC Berkeley with IRIS funding developed extensions to the SEED standard to incorporate GPS data into a SEED real-time data stream and has ported the GPS acquisition software to the Quanterra's MSHEAR software. This allows Quanterra dataloggers to expand their functionality as geophysical dataloggers by acquiring, logging and telemetering real-time GPS data along with seismic and other geophysical datasets such as temperature and barometric pressure. Both IRIS and UNAVCO are committed to promoting and extending the benefits of joint use of infrastructure and the mutual scientific benefits of combined seismic and GPS measurements in the solid-Earth sciences research community.

A Technique for Measuring the Timing Accuracy on GPS-Based Seismic Waveform Recorders

KROMER, R.P., Sandia National Laboratories, Albuquerque, NM, 87185-0655, rpkrome@sandia.gov; MCDONALD, T.S., Applied Physics Incorporated, Albuquerque, NM, 87110, tsmcdon@sandia.gov.

Sandia National Laboratories has developed a technique for measuring the time-tag accuracy to within approximately 100ns for some GPS-based seismic waveform recorders. A prototype Portable GPS Timing Reference provides an independent source of phase-locked 'Slow-Code' pulses as the input signal to the waveform recorder under test. For unaliased data acquisition systems, the Whittaker reconstruction of the continuous response signal is used to obtain a very accurate estimate of the reference time, which can be compared to the appropriate data sample time-tag for an accurate reading. A detailed description of the test theory and procedures will be presented, along with the test results for a few commercial seismic waveform recorders.

Tuesday, 8:30 AM–5:00 PM
Glenn Miller Ballroom
Posters
North American Lithosphere and Asthenosphere

Receiver Function Studies from Digital Broadband Data Recorded at El Paso, Texas

KILBRIDE, F.E.A., and DOSER, D.I., University of Texas at El Paso, El Paso, Texas, 79968, United States, kilbride@geo.utep.edu.

Since November 1994, the collection of earthquake data has been underway in a number of localities: El Paso and Lubbock, Texas; Chaco Canyon, New Mexico; and Canyon de Chelley, Arizona. The objective of this collection is to digitally record earthquakes from around the world which can be analyzed for receiver functions, shear-wave splitting and surface-wave dispersion to give insight into the crustal structure beneath or between the receiver stations. Preliminary processing of the dataset from El Paso has determined over 150 events. After event identification and verification, approximately 60 events were catalogued with epicentral distances suitable for receiver function generation. Receiver functions from similar back azimuths and epicentral distances were then stacked to enhance signal-to-noise ratio. Composite receiver functions can be subdivided by back azimuth into two major groups: South America (Columbia, Peru, and Chile) and the western Pacific (Japan, Kuril Islands, Kamchatka, Aleutian Islands). Receiver functions from each subset show similar character with phase delays 10 to 25 seconds after the P arrival which are a function of the ray parameter. The dissimilarity between the subsets of receiver functions from South America and the western Pacific can be modeled as azimuthal variation in Earth structure beneath the recording station at El Paso.

New Maps of North American Crustal Structure

CHULICK, G.S., Department of Chemistry and Physics, Purdue University Calumet, Hammond, IN 46323, chulick@calumet.purdue.edu; MOONEY, W.D., USGS, MS 977, 345 Middlefield Rd., Menlo Park, CA, 94025, mooney@andreas.wr.usgs.gov.

The past decade has seen the acquisition of large amounts of fresh seismic data and substantial advancements in computer graphic techniques. Hence, it is time for new seismic crustal maps to be prepared for the North American continent. A preliminary set of such maps have been prepared and are presented here. They were constructed using SEISPROF, a comprehensive catalog of seismic crustal data (Chulick, 1997). Amongst these maps are: (1) crustal thickness (h_c: mean = 36.9 km, S. D. = 8.6 km, n = 965), (2) average crustal compressional velocity including sediments (V_c: mean = 6.29 km/s, S. D. = 0.32 km/s, n = 940), (3) average crystalline crustal compressional velocity (V_{cc}: mean = 6.43 km/s, S. D. = 0.23 km/s, n = 616), and (4) sub-Moho compressional velocity (P_n: mean = 8.03 km/s, S. D. = 0.20 km/s, n = 876). These maps are an update on earlier such maps, and we discuss similarities and differences. We find evidence for weak (1%) anisotropy in P_n beneath the Superior-Grenville-Appalachian Provinces.

Chulick, G. S. Comprehensive Seismic Survey Database for Developing Three-Dimensional Models of the Earth's Crust, *Seism. Res. Lett.*, **68**, 734 (1997).

Tuesday, 8:30 AM–5:00 PM
Glenn Miller Ballroom
Posters
Seismic Hazards from the Rocky Mountain Region to the Great Basin: Results from Seismology and Paleoseismology

Surficial Geologic Mapping and Paleoseismic Investigations on the West Cache Fault Zone, Cache County, Utah

BLACK, B.D., and SOLOMON, B.J., Utah Geological Survey, 1594 West North Temple, Suite 3110, Box 146100, Salt Lake City, Utah, 84116-6100.

The West Cache fault zone (WCFZ) in Utah extends for about 56 kilometers (35 mi) along the west side of Cache Valley from the Utah-Idaho border to about 6 kilometers (4 mi) south of Wellsville. The WCFZ consists of three east-dipping normal faults that include; from north to south, the Clarkston, Junction Hills, and Wellsville faults. Quaternary geology of the region is dominated by late Pleistocene Bonneville lake-cycle deposits and late Quaternary alluvial-fan deposits. Detailed geologic mapping of the fault zone suggests the most recent displacement is late Pleistocene or younger. Surficial evidence for Holocene surface faulting is ambiguous. To define the timing and size of prehistoric earthquakes on the WCFZ, we investigated two trench sites on the Clarkston and Wellsville faults, and a natural stream-cut exposure on the Junction Hills fault. Fault lengths in the WCFZ range from 11–25 kilometers (7–16 mi), but net slip per event on all the faults is similar and ranges from 3.2–3.7 meters (10.5–12.1 ft). Preliminary paleoseismic data from these sites show the most recent event on the faults occurred about: (1) 3,650 years ago on the Clarkston fault, (2) 8,450 years ago on the Junction Hills fault, and (3) 4,500 years ago on the Wellsville fault. One radiocarbon age estimate is pending that will provide a limiting age for the penultimate event on the Wellsville fault. These data suggest that the faults may behave independently, although evidence for a possible younger earthquake on the Junction Hills fault may be obscured. The difference in Bonneville shoreline elevations across a transverse fault between the Junction Hills and Clarkston faults suggests independent surface rupture between these two faults.

Some Sensitivity Studies of Probabilistic Seismic Hazard Estimates for New Mexico

Lin, K.W., Sanford A.R., and Tsai, I.C., Geophysical Research Center and Earth and Environmental Science Department, New Mexico Institute of Mining and Technology, Socorro, NM 87801, klin@griffy.nmt.edu

We have estimated seismic hazard throughout New Mexico using instrumental data collected from 1962 through 1995. Based on the distribution of seismicity, we divided the whole area into two source zones, an ~6000 km^2 area located in the central Rio Grande rift which was designated as the Socorro Seismic Anomaly (SSA), and the remainder of the state (RNM). A total of 477 independent earthquakes with $M_D \geq 2.0$ (133 within the SSA) were used to obtain a universal b for the entire state. For this computation, we assumed a Poisson distribution with upper and lower bound magnitudes of 6.5 and 2.0, and a magnitude bin size of 0.1. We divided the state into 20 km x 20 km areas and evaluated seismic hazards on the basis of these blocks. Seismic hazard estimates were obtained by combining the temporal probability of occurrence with the spatial probability of occurrence and a relation between ground acceleration and magnitude (Joyner and Fumal, 1985). Results have been presented in the format of maximum horizontal ground accelerations at 10% probability of exceedance in a 50 year period. We have determined variations in these seismic hazard estimates arising from uncertainties in (1) the fitted slope b and (2) the maximum magnitude earthquake assumed in the recurrence relationship. The variation of the fitted slope b for the whole area, 0.6675±0.0314 (1 s.d.), resulted in minimal changes on the level of seismic hazard estimates. For example, the highest level of estimated ground acceleration for the entire area ranged only ±0.006g (1 s.d.) from a mean value of 0.212g. Changes in maximum magnitudes had larger but still moderate effects on the overall estimates of seismic hazard. The decrease in the highest level of seismic hazard obtained by reducing the maximum magnitude from 6.5 to 6.0 was -0.009g and the increase in hazard by increasing the maximum magnitude to 8.0 was +0.04g.

We have examined the effects of incorporating pre-instrumental data from 1860 through 1961 on seismic hazard estimates for the SSA. The fitted slope b derived from the pre-instrumental catalog for the SSA yielded a slighter lower value, 0.6454, than that obtained from the instrumental data but within the range of the first standard deviation. The annual seismic density per km^2 for events of magnitude 4.0 or greater, the starting magnitude for seismic hazard estimates, differs only 7% between instrumental and pre-instrumental data. Thus no major changes in hazard estimates are expected by including pre-instrumental data into the evaluation process.

Stress Interaction and its Application to the Earthquake Hazard Analyses of the Wasatch Fault, Utah

CHANG, Wu-Lung, and SMITH, Robert B., Dept. of Geology and Geophysics, University of Utah, Salt Lake City, Utah 84112, wchang@mines.utah.edu

Stress interaction amongst adjacent faults is often cited as an evidence for systematic space-time variations in aftershock distributions and background seismicity. An earthquake would be expected to change the static stress on neighboring faults that can in turn affect fault loading or unloading and therefore influence the timing of future earthquakes. This study focused on stress interaction analyses on the Wasatch fault zone (WF), Utah, the longest continuous, active normal fault in the United States. It is located on the eastern edge of the Basin and Range Province and extends along the Wasatch Front populated corridor of 1.6 million people. The WF has not experienced a large magnitude earthquake (M>7) in historic time and the last scarp-forming event occurred 400 years ago based upon paleoseismic data. Trench data showed that 19 scarp-forming events were experienced in the past 6,000 years on six segments of the fault. In this study, we first reinterpreted the ages and lengths of coherent ruptures along with the locations of corresponding trenches to determine a new time-space distribution of Holocene paleoevents, which is needed to generate a history of scarp-forming earthquakes. A three-dimensional, elastic boundary element methodology (after Simpson, USGS) was applied to calculate the static stress changes, or changes of Coulomb Failure Function (CFF), on fault segments that may interactively induce earthquakes on adjacent fault planes. Based on the paleoearthquake chronology, our stress-interaction modeling showed that several paleoevents ruptured through the hypothesized fault segment boundaries of the WF into nearby segments and are good evidence for multi-segment ruptures. Using these results, fault slip obtained from the trench data was then applied to model the rupture length, maximum displacement and magnitude of each prehistoric earthquake. These give a new distribution of paleoearthquakes for the WF that has been unavailable due to the lack of moderate to large modern earthquakes, which is important to the implementation of seismic risk assessment along the populated Wasatch Front. In addition, we found that azimuthal variations of the Wasatch fault can produce the similar order of magnitude changes in shear stress, that adds an additional complexity to the hazard problem. These data, along with GPS results, are used to evaluate new earthquake hazard probabilities that will be discussed.

Microearthquake Field Study of the Front Range of Colorado

SHEEHAN, A.F., HUGHES, N.D., and JONES, C.H., Department of Geological Sciences and CIRES, University of Colorado at Boulder, Boulder, Colorado 80309, afs@mantle.colorado.edu.

Though the products of past tectonic activity are structurally evident along the Front Range of Colorado, modern seismicity has been relatively quiet, though not completely inactive. An earthquake of approximate M 6.6 occurred in north-central Colorado in 1882, and a cluster of moderate injection-induced earthquakes occurred in 1967. Despite the ample geologic evidence for Quaternary fault movements, the seismicity of the Front Range has remained largely unstudied. During the fall of 1996, a local seismic network was deployed near Boulder to record local activity as part of a Field Geophysics course at the University of Colorado. The seismic deployment consisted of three short period three component seismometers with digital recorders. Station spacing was approximately 15 km. The sensors were in place from Sept. through Nov. 1996, with a single station left in place through the present. The stations were supplemented by stations in Golden and Idaho Springs, CO, operated by the USGS. Twenty-three small seismic events were located withing a 50-mile radius of Boulder during the first 3 months of the deployment. The earthquakes ranged from magnitude 0.5 to 2.0 on the Richter scale. The levels of microseismicity for the Colorado network are found to be midway between levels for California (high) and New England (low). A NW-SE trend of seismicity was found west of Golden. The majority of other events were located fairly randomly, though more in the mountains (west) than in the plains (east). A cluster of three events was located near a known mine, and more work is needed to eliminate blasts from our catalog. Further analysis of this microseismic distribution can help isolate faults which may still be active and perhaps to locate previously unknown faults. An understanding of fault locations and activities will lend insight into the modern tectonics of the area.

Tuesday, 8:30 AM–5:00 PM
Glenn Miller Ballroom

Posters

California Seismicity and Structure

3D Subsurface Data of the Ventura Basin: Testing the Reliability of 2D Models to Infer Deep Fault Structure in the Western Transverse Ranges

NICHOLSON, C., VALENTINE, D., KAMERLING, M.J., Institute for Crustal Studies, University of California, Santa Barbara, CA 93106-1100; and HOPPS, T.E., Rancho Energy Consultants, Inc., Santa Paula, CA 93060

In the Ventura basin, faults and folds accommodate high rates of oblique crustal strain and uplift rates exceed 10 mm/yr. These faults represent a significant seismic hazard, yet much of what is known about these faults and folds has been inferred from 2D balanced cross section models. To test the reliability of these 2D models to predict 3D subsurface structure, we have been evaluating a unique 3D dataset provided by the Ventura Basin Study Group (VBSG). The VBSG study consists of 17 structure contour maps and 84 interlocking cross section data panels based on nearly 1200 deep-penetration (1–5 km) wells. Many of these wells drill active fault and fold structures associated with major fault systems, including the San Cayetano, Oak Ridge, Red Mountain, and Santa Susanna faults. This integrated 3D study is based on wire-line logs, mud logs, paleontological reports, core analyses, and surface maps. Each data panel typically ties in 4 directions to define the sides of a 3D data volume or cell. Any 2D or 3D kinematic model of the basin and its associated fault and fold geometry must incorporate these data, if it is to be successful. Based on the VBSG drillhole data and combined with seismicity and other subsurface datasets, our preliminary results show that although the 2D models have proven useful in other tectonic regions where convergence is more uniform along strike, these models consistently fail to adequately resolve significant subsurface structure in this area. Active buried or blind faults typically have steeper dips, deeper depths, and non-planar geometry—features not replicated in many of the 2D models—and several active faults are missing or are misidentified in the 2D models. The primary reasons for this failure are the inappropriate assumptions used in the 2D models that ignore fundamental aspects of the regional tectonic deformation that includes significant strike-slip or out-of-plane motion, crustal rotations, large variations in depositional thickness and material strengths of rocks, basin subsidence, and pre-existing fault structure that preclude for the most part the simple ramp-flat geometry often adopted by the 2D models. A preliminary digital version of the VBSG dataset is now available from our website at http://www.crustal.ucsb.edu/hopps/.

Late Quaternary Growth of the San Joaquin Hills Anticline—A New Source of Blind Thrust Earthquakes in the Los Angeles Basin

MUELLER, K.J., Department of Geological Sciences, University of Colorado, Boulder, CO 80309, Karl@lolita.colorado.edu; GRANT, L.B., Division of Natural Sciences, Chapman University, Orange, CA 92668, lgrant@chapman.edu; GATH, E., Earth Consultants International, 2522 N. Santiago, Orange, CA 92867, gath@worldnet.att.net

Structural and geomorphic analysis of marine terraces and stream drainage networks suggest the San Joaquin Hills anticline in the southern Los Angeles Basin is an active fold. Marine Stage 5a–13 terraces incised into the SW-dipping flank of the fold form well defined platforms which can be traced around the NW-dipping plunge panel of the fold. Two terraces (Stage 7 and 9) can be traced onto the NE-dipping flank of the fold where they are folded downward to the east. Structural models of fault-related folds for different blind fault geometries suggest the terraces are being deformed by fault-bend folding above a NE-vergent thrust ramp. Stream networks support the interpretation of folding above a NE-vergent ramp and are unique indicators of fold kinematics. For a laterally propagating fault-bend fold, the plunge panel is consumed by fold limbs across active axial surfaces. Drainage networks mapped on the youngest part of the forelimb (produced by consumption of the plunge panel) record a short-lived disequilibrium condition where channels are oriented parallel to strike. Older portions of the forelimb display drainages which have reestablished new channels consistent with its NE dip. Map patterns of the stream channels in disequilibrium suggest the east edge of the plunge panel is an active axial surface, consistent with material moving through the top of the ramp on a NE-vergent blind thrust. Rates of uplift derived from U-series dating of corals from deposits which overlie the terrace platforms yield independent and consistent determinations of 0.25mm/yr. A fault slip rate of 0.51mm/yr is indicated for a 30 degree dipping fault, similar to a NE-vergent thrust imaged on seismic reflection profiles from the adjacent offshore area. This high-level fault lies above the well-imaged Oceanside detachment, a Miocene low-angle normal fault that dips NE. Cross sections permit the interpretation that the blind thrust beneath the San Joaquin Hills is linked at depth with the detachment as part of a wedge structure, now reactivated as a SW-vergent fault system. For earthquakes originating at the base of the seismogenic crust on the wedge structure, magnitude and recurrence must be consistent with the large fault area (~2400 square km) and slow slip rate.

Seismicity of the Southern Sierra Nevada from Two Portable Experiments

EDWARDS, J., and JONES, C.H., Dept. of Geological Sciences, CB 399, Univ. of Colorado, Boulder, CO 80309-0399, cjones@mantle.colorado.edu

The southern Sierra Nevada contain the highest elevations in all of California but the cause for this are still unknown. Shear motion occurs to the west and east along the San Andreas fault and the Eastern California Shear Zone, respectively. Additionally, extension lies to the east in the Basin and Range, producing a very interesting and complex tectonic setting. Large historic ruptures have occurred in the region as well, including the 1872 Owens Valley earthquake (M ~8), and the 1952 Kern Co. earthquake (Ms 7.7). We ran networks of 16 portable, triggered short period seismometers (1988) and 24 portable, continuously-recording broadband seismometers (1997). The 1988 data produced about 100 earthquakes located within 50 km of the nearest portable seismometer. Epicenters of these earthquakes show a swarm in the Owens Valley and a line of seismicity just east of the Kern Canyon. The 1997 data produced about 400 earthquakes. These data shows diffuse seismicity along the Sierran Front, east of the Kern Canyon, and some in the western foothills. The band of seismicity running north-south east of the Kern Canyon may be a continuation of the Durrwood Meadows Swarm of 1983–4. Earthquake depths appear to be much deeper (to about 20 km bsl) in the western foothills than elsewhere (<~10 km), suggesting that the crust in the foothills is still cold to these depths. We will present focal mechanisms from these experiments that delineate the relative contribution of transform and extensional faulting to deformation in this region.

Tuesday, 8:30 AM–5:00 PM
Glenn Miller Ballroom
Posters
Seismic Methods

A 3-D Mantle Model from Free-Oscillation Data

RESOVSKY, J.S., and RITZWOLLER, M.H., Geophysics Group, Department of Physics, Campus Box 390, University of Colorado, Boulder, Boulder, CO 80309-0390, resovsky@abdu.colorado.edu

Differences between recent global mantle models demonstrate considerable uncertainty in the amplitude and geometry of structures in the mid-mantle (700–1800 km depth), even at the longest wavelengths. Our recently compiled database of normal mode structure coefficients provides important new constraints on this part of the Earth. We illustrate the nature of these constraints by inverting the structure coefficients for a new mantle shear-velocity model at degrees 1 through 8. This new model is characterized by: (1) improved fits to long-period seismic spectra; (2) improved constraints on the amplitude spectrum of structure in the mid-mantle; and (3) improved resolution of dynamic characteristics such as the rise of plume-like structures through the mantle and the continuation of upper mantle features into the mid-mantle.

Modeling Wave Propagation Through Heterogeneous Media Using the Extended Local Rytov Fourier Method: Effects of Random Heterogeneity on Regional Waveforms

FEHLER, M.C., and HUANG, L.-J., Geological Engineering Group, Los Alamos National Laboratory, Los Alamos, NM 87545, fehler@lanl.gov, ljh@lanl.gov

Approaches for modeling wave propagation in complex media consist of computationally intensive methods such as finite difference that can model realistic structures over a relatively small number of propagation wavelengths, and less computationally intensive methods such as reflectivity that can model relatively simple structures. We develop an extended local Rytov Fourier method for fast simulation of primary forward acoustic wave propagation in a heterogeneous medium. The method is computationally fast and can reliably model effects of both deterministic and random structures. We employ this method to investigate the effects of various types of structures on regional seismic waveforms. Investigators in Japan have described a broadening and delay of the arrival of the peak envelope of initial arrival packets observed from deep earthquakes (Obara and Sato, 1995). The envelope characteristics vary with tectonic region of the propagation path. The observations are explained as being due to multiple forward scattering between the source and receiver. Observed differences among seismograms recorded in different tectonic provinces are attributed to differences in the form of the autocorrelation function that describes the random heterogeneity of the medium through which the waves propagate. The model does not include spatial variation in the deterministic component of the structure. Using our local Rytov propagator, we investigate the effects of inclusion of variations in the deterministic part of the structure along the propagation path. We also investigate the differences in envelope characteristics caused by differences in the form of the autocorrelation function of the random portion of the velocity structure and changes in the relation between velocity and density with depth in the medium.

SPECTRAL INVERSION OF REGIONAL WAVES FROM EARTHQUAKES IN PRESENCE OF RANDOM AND MODEL ERRORS

JIAKANG XIE, Lamont-Doherty Earth Observatory, Columbia University, Route 9W, Palisades, NY 10964; 914-365-8553; xie@lamont.ldgo.columbia.edu.

Spectral inversions for source moments (M_0), corner frequencies f_c and path Q using high-frequency regional phases, such as Lg, suffers from errors caused by the random and systematic deviations of the observed spectra from the idealized, theoretical models. The large random and modelisation erros may jeopardize Q measurements at lower frequencies, at distances up to a few hundred km or more. These errors were previously reduced by minimizing the unknown parameters, so that a highly overdetermined inverse problem can be formed. This minimization of unknowns, however, can be demonstrated as being frequently insufficient to suppress the errors, when the source is an earthquake and distance small.

Using the formulation of Tarantola (1986), we can formulate the inverse problem as one that maximizes the posterior probability density function, in the presense of modelisation errors and apriori knowledge on the unknown model parameters. That formulation suggests that various improvements of the stability and reliability of the estimated model parameters can be achieved, one of such improvements is the use of apriori knowledge. We have implemented a few improvements, and applied the improved inverse method to Lg spectra from the 1995, western Texas earthquake sequence. The resulting estimates of M_0, f_c and path Q parameters are more reliable. Ultimately with the growing data base, a more thorough understanding on the statistical properties of the regional wave spectra will be needed to achieve a higher reliability of the the spectral inversion.

High Frequency Ground Motion Scaling from Regional Array Data in Central Italy and Germany

MALAGNINI, L., MACEIRA, M., HERRMANN, R., Department of Earth and Atmospheric Sciences, Saint Louis University, St. Louis, MO, luca@eas.slu.edu; KOCH, K., BGR, Inst for Geosciences and Natural Resources, Hannover, Germany, koch@sdac.hannover.bgr.de

High frequency ground motion in the 0.25–15 Hz band from broadband deployment in Italy and the German Regional Seismic Network (GRSN) are processed to study distance scaling of Fourier velocity spectra and filtered gound velocities. Observed data are fit to the model

$$\log A = \text{Excitation} + \text{Site} + \text{Distance}$$

where the Distance function is a piecewise linear interpolator. The Italian data set currently consists of 640 waveforms from 141 events. Although sparse, there are sufficient data to define distance scaling to 200km. Comparison to similar processing on a Southern California data set shows greater spatial attenuation in central Italy! Processing is starting on the 13 station, 624 event GRSN data set.

The purposes of the investigation multiple: use of regional network data, characterization of regional differences in high frequency ground motion distance scaling, and ultimately relating these to differences in the crustal waveguide structure and *Q*.

Applying Waveform Correlation Event Detection and Location at Regional and Local Scales

ASTER, R.C., New Mexico Tech, Socorro, NM, 87801, USA, aster@nmt.edu; WITHERS, M.M., University of Memphis, Memphis, TN 38152, USA, withers@ceri.memphis.edu; YOUNG, C.J., Sandia National Laboratories, Albuquerque, NM, 87185, USA, cjyoung@sandia.gov

We report on development and testing of a Local Waveform Correlation Event Detection System (LWCEDS) for the state of New Mexico. LWCEDS is an adaptation of WCEDS; a matched filtering algorithm designed for global

CTBT monitoring applications at Sandia National Laboratories and New Mexico Tech. The algorithm correlates near-real-time data, which have been preprocessed to enhance phase arrivals, with a master image composed of theoretical phase arrival envelopes as functions of time and distance. The algorithm presently performs a 10 km-spacing, 1 second, statewide space-time grid search on triggered data streams to find the maximum correlation between the data and the master image and thus obtain hypocenter and origin time estimates without the need of explicit phase identification. For events in the relatively high seismicity Socorro region, a 1 km-spacing, 0.1 second local grid search is subsequently conducted over a range of possible hypocenter depths to refine hypocenter estimates. In this case, the master image includes phase arrival envelope information from reflections off of the Socorro midcrustal magma body. A preliminary system has been in operation since July 1997 and has correctly discriminated approximately 85 percent of the 1000 events in the NMT archive during the last half of 1997. A modified version of the IRIS/JSPC DATASCOPE package allows immediate analyst verification and refinement of the automatically estimated hypocenters through the review of inferred arrival times and relocation. A CSS3.0 database is automatically updated by the analyst review. This research was supported by the U.S. Dept. of Energy under Contract Number DE-AC04-94AL85000 and by the New Mexico Dept. of Public Safety. Sandia is a multi-program laboratory operated by Sandia Corporation, a Lockheed Martin Company, for the U.S. Dept. of Energy.

An Automatic Method for Determination of Lg Arrival Times Using Wavelet Transforms

TIBULEAC, I.M. and HERRIN, E., Department of Geological Sciences, Southern Methodist University, Dallas, Texas, TX 75275-0395, ileana@passion.isem.smu.edu; herrin@passion.isem.smu.edu

The regional phase Lg is used to estimate location and magnitude for sources closer than 1500 km. The complexity of Lg waveforms makes it difficult to consistently determine Lg arrival time, thus affecting source location with a single station or array.

This study tests an automatic method for timing Lg arrivals using wavelet transforms to decompose the Lg signal into its components localized both in time and scale. A Continuous Wavelet Transform (CWT) using a Daubechies order two (db2) wavelet is applied to 10 seconds of raw data, containing the start of Lg. Initial positioning of the window is obtained using the standard Lg travel time tables. The coefficients at scale 8 from the db2 decomposition are squared and the resulting time series is represented by an approximation of the 4'th level Discrete Wavelet Transform (DWT) using a Haar wavelet. A threshold detector is then applied to the resulting time series to determine the Lg arrival time.

The method was tested using well located earthquakes (USGS) and explosions from known mines (mb less than 4.0), recorded on the vertical components at TXAR (Lajitas, Texas) and PDAR (Pinedale) arrays. Preliminary results show that the Lg arrival time is automatically picked with a standard deviation of less than 1 second (~7 km location error). Performance of the method is analyzed relative to the epicentral distance and magnitude of events, and different wavelet decomposition parameters.

AUTOMATIC PHASE REPICKING FOR IMPROVED HYPOCENTER LOCATIONS IN LARGE DATA SETS

ROWE, C.A., ASTER, R.C., Dept. of Earth and Environmental Sciences and Geophysical Research Center, New Mexico Tech, Socorro, NM 87801; FEHLER, M.C., PHILLIPS, W.S. and ALDE, D.M., Geo-Engineering Group, Los Alamos National Laboratory, Los Alamos, NM.

We report on the development of a software package for automatically improving P and S picks in large seismic data sets having initial, rough location estimates, and which contain appreciable numbers of events exhibiting similar waveforms. Individual trace components are first assessed for waveform similarity and roughly aligned, if appropriate, through time-domain correlation, where trace windows are iteratively adjusted. For significantly similar waveform pairs, coherency-weighted fitting of the cross-spectral phase allows for a subsequent refinement of pick corrections to subsample precision. Once all feasible interevent lag corrections and their standard deviations have been calculated, we use these multiple constraints to find RMS adjustments for pick times within similar event trees. For multicomponent seismograms, S-wave correlations may be enhanced by rotating components to maximize energy in the plane orthogonal to the approximate ray path estimated from preliminary event locations. Difficulties in obtaining automatic estimates of S-wave picks can be further reduced by limiting the extent of the cross-correlation window based on estimates of Poisson's ratio and hypocentral distance.

The test data used in the development of the package consists of over seven thousand microearthquakes resulting from injection experiments at the Soultz, France Hot Dry Rock geothermal field. The seismograms are from four-component borehole seismometers and a borehole hydrophone, which we have converted to three-component orthogonal seismograms. A subset of the original, rough picks for this data were laboriously and exactingly re-picked in earlier work. These repicked results provide a high-quality set of relocations, delineating fine-scale, planar, intersecting joint features, against which to compare the results of the automated technique applied to the original picks.

Tuesday, 8:30 AM–5:00 PM
Glenn Miller Ballroom
Posters
Seismic Systems and Instrumentation

Earthworm Collaborative Development Report

DIETZ, L., KOHLER, W., LUETGERT, J., PITT, M., U.S. Geological Survey, Menlo Park, CA 94025; dietz@usgs.gov; BITTENBINDER, A., BOGAERT, B., KETCHUM, D., USGS, Golden, CO 80401, alex@usgs.gov; LOMBARD, P., Geophysics Program, Univ. of Washington, Seattle, WA 98195, lombard@geophys.washinton.edu; JOHNSON, C.E., Science and Technology International, Hilo, HI 96730; carl@sti.hawaii.com; CHAVEZ, D. Engineering Services & Software, San Diego, CA 92121; 619-587-2765; email: dec@essw.com; KRAGNESS, D., Morgan Hill, CA 95037,davek@garlic.com; MOON, B. and ROHAY, A. Pacific Northwest National Laboratory, WA 99352, ac_rohay@pnl.gov.

The Earthworm seismic processing system was first developed at the USGS Menlo park in collaboration with Carl Johnson to produce an earthquake notification system. Since that development, a number of regional seismic networks have adopted the Earthworm system or created derivative networks, the NOAA-USGS CREST project has adopted the Earthworm architecture for its processing system, and the Council of National Seismic Systems has established an Advisory Board to guide further developments. Consequently, the USGS Earthworm team began joint efforts with a number of other institutions and individuals, resulting in a suite of new features for the Earthworm System:

Wave_viewer: An interactive Windows graphics program which provides a remote trace-viewing capability for examining trace data from real time to several weeks old. Data may be browsed, or viewed event-by-event.

RCV and *VDL*: These programs permit turn-key, two-way trace data exchange between regional networks and the USNSN.

Import_ida: This program enables an Earthworm to connect to any number of IDA data servers, retrieve and process IDA data.

Wave_serverIV: This Earthworm module, jointly developed by USGS and UofA Fairbanks, stores selected trace data in circular buffers (up to 2GB per channel) and provides a multi-threaded network server capable of serving requested trace segments. A suite of client utility functions and a variety of client programs are being developed.

earth2uw: This program, developed in conjunction with UofW Seattle, provides an interface between Earthworm and the UofW post-processing system. The program has been written to facilitate adaptation to other formats; SAC and AH interfaces are being worked on.

Other developments include the port of Earthworm to Windows NT, an Oracle/EW integration, and a module that produces record sections for web display.

A Dial-Up System for Rapid Retrieval of Remote Digital Strong-Motion and Event-Triggered Seismic Data

WOOD, C., VIKSNE, A., and COPELAND, D., U.S. Bureau of Reclamation, Seismotectonics and Geophysics Group, Denver, CO 80225, chris@seismo.usbr.gov, aviksne@do.usbr.gov, dcopeland@do.usbr.gov

We have developed and implemented a low-cost, fully automated system that retrieves seismic waveform data from event-triggered, digital data loggers at remote sites, and does so in near real time. Standard dial-up telephone lines, modems, and an inexpensive interface device are used to telemeter data from remote sites to a central-site data collection computer. Event triggers from one or more data loggers that are connected to an interface device (called a triggered modem controller, or TMC) cause the TMC to establish a dial-up connection with the central-site computer. The TMC also provides the computer with the means to remotely switch between data loggers. The delay from an event trigger to completion of data retrieval is usually five minutes or less. Several features were incorporated into the TMC (developed for us under contract) to make dial-up communications flexible and robust, including programmable scripts for modem and computer handshaking, call retries with an exponential back-off, and remote configuration and diagnostics. Software for the central-site computer system was developed to run on UNIX workstations, and supports several models of commercially-available data loggers. Calls from multiple remote sites can be handled simultaneously, limited only by the number of incoming phone lines and modems. In addition to data retrieval, the system performs automatic remote configuration and periodic state-of-health monitoring of the instrumentation. Specific remote sites may also be operated in a polling-only mode if immediate data retrieval is not necessary, permitting data retrieval during lower-cost, off-peak hours. The system is being used to retrieve data from 60 digital strong-motion instruments at 42 dams and other lifeline facilities located throughout the western United States. It has also been successfully used in temporary site-response and aftershock studies to provide remote access to seismic data loggers with broadband seismometers.

Performance of Modern Broadband Seismic Instrumentation

UHRHAMMER, R.A., University of California, Berkeley, CA, 94720-4760, bob@seismo.berkeley.edu

Most modern broadband seismic stations, either due to the presence of high microseismic background or cultural noise levels or due to immoderate environmental conditions in the seismic vault, do not fully exploit the capabilities of modern very-broadband seismic sensors. As a demonstration of the capabilities of a modern very-broadband seismometer, coupled to a high resolution (24 bit) digital data logger and installed in a nearly ideal seismic vault, we examine in detail the performance of the Berkeley Digital Seismic Network (BDSN) station sited at Yreka (YBH). YBH is located in a remote hard rock mining drift, in the Klamath National Forest (430 km north of Berkeley and 120 km from the coast), with no significant cultural noise sources located within a radius of 10 km. Consequently, YBH has the lowest background noise level and also the most thermally stable vault of any BDSN station. We examine the seismometer performance and characterize the background noise Power Spectral Density (PSD) over the 8+ decade frequency range from 60 nHz to 8 Hz. At YBH we also record, with 1 Hz sampling, the seismometer temperature and atmospheric pressure with high resolution. We further improve the noise performance of the very-broadband seismic sensors using an adaptive filtration algorithm to remove the temperature and pressure correlatable effects from the seismic signal and effectively lower the seismic background noise PSD (>10 dB) to levels well below the Peterson 1993 seismic low-noise model. Examples shown include the recording of: gravitational tides (4–24 hour periods), graver mode eigenvibrations (periods longer than 2500 seconds), and, several earthquakes.

Self-Noise Spectra and Shake Table Tests of the Wilcoxon 731-4A and the Kinemetrics FBA-23DH Accelerometers

RODGERS, P.W., SWAIN, S.T., and STEIDL, J.H., Institute for Crustal Studies, Univ. of Calif., Santa Barbara, CA 93111. rodgers@crustal.ucsb.edu

Self-noise data are computed for the Wilcoxon 731-4A and Kinemetrics FBA-23DH accelerometers. The data used are ambient seismic noise data from colocated, downhole (75 m), three component accelerometers. Recording was done with the Quanterra Q4120 24 bit data logger. The self-noise spectra are presented in units of both power density spectra and acceleration in a one-half octave bandwidth. Peterson's new low noise model (NLMN) is included for comparison.

Shake table data are presented comparing the responses of the 731-4A and the FBA-23DH. Inputs used are sinewaves of various frequencies. Random inputs in the range 1 to 50 Hz are used to compute the spectral coherence between the two accelerometers. The amplitude linearity between the two accelerometers in the range 0.1 to 0.5 g's is presented.

Response, Calibration, and Noise of the Homemade Hardware Store Broadband Leaf-Spring Vertical Seismometer.

Sean-Thomas Morrissey, St. Louis University, Dept. of Earth and Atmospheric Sciences, 3507 Laclede Ave, St. Louis, MO, 63103; sean@eas.slu.edu.

A vertical seismometer with a very broadband velocity response has been assembled from hardware store items and consumer electronic components. Since it is a fully fedback broadband system, its' response and calibration are tightly controlled regardless of the flexibility of the mechanical design. The instrument has been configured for a flat velocity response from 90 seconds to 30 hz, although this is readily changed to suit local site conditions.

The response is initially determined by knowledge of four mechanical parameters of the sensor and four electronic components of the feedback system. The mechanical parameters (M, Tn, Gn, Rd) are very stable, and the electronic parameters are set by known component values, as indicated by the transfer function. This response is readily confirmed by comparison with the FFT of the output from a step displacement calibration pulse. The overall response is further confirmed by calibration on a shake table.

The expected site for installing the sensors is a quiet corner of the basement. Even so, moderate local, regional, and teleseismic events are readily recorded. The Power Spectral Density (PSD) of the noise of such a less-than-optimum site is well within the USGS noise models.

The stability and reproducibility of this broadband response means that every school or personal site that regularly maintains these sensors and the associated PC data acquisition system is capable of providing valuable data for ground motion, attenuation, and tomographic studies at a close spatial resolution that cannot be realized by established networks.

Wednesday AM, March 18, 1998—Forum Room
The U.S. National Seismic System
Presiding: Steve Malone, *Univ. of Washington* and **Harley Benz**, *USGS*

The Council of the National Seismic System—The First Five Years

MALONE, S.D., Geophysics Program, University of Washington, Seattle, WA 98195, steve@geophys.washington.edu

Seismic networks within the United States, as elsewhere, have traditionally cooperated in an informal and ad hoc way. However, because of historically diverse goals, funding sources and interests US networks have proliferated with diverse characteristics. The large variety of station type and density, recording techniques and formats, location procedures and speed, reporting formats and types has made even informal cooperation increasingly difficult and has made network products difficult for end users to use.

In 1993 the USGS sponsored a meeting attended by many US seismic network operators to discuss a formal consortium for improving cooperation and coordination between networks. Agreement was reached on the need and a charter drafted to define the purpose and goals of this *Council*. Five years later over 30 institutions representing almost all operators of seismic stations in the US have signed the charter and are formal members of the *Council*. Resolutions have been passed by the *Council* for specific projects to improve the coordination of information between networks and to standardizing their products. Progress to date implementing some of these includes a standard way of making a network's recent earthquake catalog available on the Internet (19 networks), a composite catalog combining and removing duplicate entries (12 networks), and waveform data available from a major data center in SEED format (5 networks). Projects recently initiated include the establishment of a procedure to very rapidly distribute earthquake information to other networks and to the public following significant events and a review board to help direct the development of regional network recording and data exchange computer systems. A WEB page with information about the **CNSS** can be found at *http://www.cnss.org*.

ORB: A New Real-Time Data Exchange and Seismic Processing System

HARVEY, D.J., QUINLAN, D.M., VERNON, F.L., Boulder Real Time Technologies, Inc., 2305 Broadway, Boulder, CO, 80304-4106, USA, danny@brtt.com; VERNON, F.L., University of California, San Diego, vernon@palapa.ucsd.edu; HANSEN, R., University of Alaska, Fairbanks, roger@eq.giseis.alaska.edu

Within the last several years, a new and effective real-time system for transporting and processing seismic data has been developed. This system is based upon an Object Ring Buffer (ORB) and makes use of standard TCP/IP protocols and POSIX compliant system utilities. Each ORB is implemented as a set of disk files that contain a circular data packet buffer along with indexing information. Each ORB is managed by a single server process. ORB client processes communicate via standard TCP/IP sockets and therefore can run on any host that is accessible through the internet. ORBs are data neutral and have no packet size, time ordering, or data format restrictions. We have found the system to be very robust, efficient and cost effective for real-time data transport both locally and over long distances (such as Boulder to Fairbanks). In addition to transporting data, the ORB acts as the underlying infrastructure for a complete real-time seismic processing system that includes detection, network triggering, event association, and preliminary location and magnitude estimates. The system is currently in operation at the University of Alaska, Fairbanks, for processing Alaska Network data, at the University of California, San Diego, for processing Anza Network data and by various IRIS member institutions in support of the IRIS Broadband Array project, currently deployed in Northwestern Colorado.

Crest and the U.S. National Seismograph Network

OPPENHEIMER, D., DIETZ, L., and KOHLER, W., USGS, Menlo Park, CA 94025, oppen@usgs.gov; BITTENBINDER, A., BOGAERT, B., BULAND, R., and BENZ, H., USGS, Lakewood, CO 80225, alex@usgs.gov; WEAVER, C. and MALONE, S., Geophysics, Univ. of Washington, Seattle, WA 98195, craig@usgs.gov; HANSEN, R., Geophys. Inst., Univ. of Alaska, Fairbanks, AK 99775, roger@giseis.alaska.edu; OKUBO, P., USGS, Hawaii National Park, HI 96718, pokubo@usgs.gov.

Through funding provided by NOAA, the USGS has implemented a project called Consolidated Reporting of EarthquakeS and Tsunamis (*CREST*) to upgrade seismic equipment and monitoring facilities of 6 regional seismic networks (RSN's) operating in Cascadia, Alaska, and Hawaii. The purpose of the upgrade is to provide seismic data rapidly to the Alaska and Pacific Tsunami Warning Centers (TWC's) to improve their ability to evaluate the tsunamigenic potential of earthquakes. We are developing software for the RSN's, TWC's, and US National Seismic Network (USNSN) to provide the TWC's with continuous seismograms from 20 stations surrounding the Pacific Basin and, after an event, to provide seismograms from a larger set of stations, phase information, hypocenters, magnitudes, shaking maps, mechanisms, and spectra within a few minutes. Because issuing tsunami warnings is critical to public safety, we will transmit information between *CREST* networks and the TWC's via dedicated communications links to ensure bandwidth, although data exchange via the Internet is also possible. In addition, we plan to send only parametric data independently via satellite. For redundancy, data from a subset of the *CREST* stations will also be sent via satellite to the USNSN for independent processing and transmission to the TWC's. Earthworm software will be the basis for the data acquisition, processing, and exchange for *CREST.* Software is being developed to interface the Earthworm system to non-Earthworm systems in use at some institutions. The *CREST* project can be considered a *de facto* model for a national, real-time, seismic network. Integration of other RSN's into the system would make it possible to provide the nation with greatly improved real-time information on earthquake activity.

SCSN/TriNet: Modern, Multi-Functional Real-Time Seismic Network

HAUKSSON, E., CLAYTON, R., HAFNER, K., HEATON, T., HUTTON, K., KANAMORI, H., MAECHLING, P., (Seismo. Lab., California Institute of Technology, Pasadena, CA 91125 USA), and JONES, L., GIVEN, D., MORI, J., WALD, D., (USGS, Pasadena, CA 91106 USA)

Caltech, USGS and CDMG have been funded to create a new generation of seismic network in southern California to be called TriNet. The purpose of TriNet is to record and analyze earthquake ground motions, and distribute that information quickly, to improve our understanding of earthquakes and their effects, to contribute to improving building codes and structural design, and to facilitate emergency response. The CDMG element concentrates on engineering applications while the Caltech/USGS element (SCSN/TriNet) concentrates on seismological and emergency response aspects. SCSN/TriNet must have new capabilities, including rapid acquisition and processing of data streams exceeding 2 Mbytes/s, real-time ground motion estimations and hardened data distribution channels. The system specifications for SCSN/ TriNet address achievement of five goals: First, operate a hardened seismic network, that allows documenting the distribution of ground motions and robust to operate in the largest possible earthquakes. Second, cooperate with other agencies working to mitigate the earthquake hazard. Third, create an easily accessible database Fourth, distribute information about an earthquake rapidly to save lives and property. Fifth, develop a pilot early warning system and conduct social science research on the use of such data to be ready to implement when funds for future SCSN/TriNet enhancements, including sufficient stations, are obtained. The specifications detail the sensors, data loggers, siting and telemetry, the software needed for data acquisition, real-time and post processing and archiving, research projects to achieve real-time ground motion estimation and early warning and systems for data distribution. Progress to date includes, installation of 55 broadband digital stations and 25 strong motion stations. Prototypes of products such as ground motion intensity maps (ShakeMap), paging of peak accelerations to CUBE, and continuous ground motion displays have been developed.

The Canadian National Seismic Network in Western Canada

BALDWIN, R.E., BEVERLEY, K.I., ROGERS, G.C., Geological Survey of Canada, Pacific Geoscience Centre, Sidney, BC, V8L 4B2, CANADA, baldwin@pgc.nrcan.gc.ca

Modernisation of seismic monitoring in Canada, begun in 1992, is now nearly complete. The Canadian National Seismograph Network (CNSN) currently consists of over 100 sites telemetered continuously to parallel data analysis centres located near Victoria, BC and in Ottawa, ON. The core backbone consists of 28 three-component broadband stations recorded at both centres. These provide overall coverage of the country at a spacing of about 500 km. The core sites are augmented by short-period stations recorded by at least one of the centres, which monitor seismicity in the more active and populated areas.

Broadband sites employ Guralp CMG-3ESP, CMG-3T or Streckeisen STS-1VBB seismometers, while short-period sites primarily use the Geotech S-13. All stations employ 24-bit digitizers and GPS clocks on-site. Broadband digitizers run at 40 samples/s, while the short-periods run at 100. Data is compressed then assembled into 6 s packets for transmission. Many sites (including all broadband sites), provide for retransmission of corrupted data on request. Event detection employs an ST/LT trigger on binned frequencies, followed by an initial automatic location. The entire continuous stream of data is archived.

In western Canada, the CNSN maintains a denser station spacing in the Cascadia subduction region of southwest British Columbia, in the Queen Charlotte Islands, and, by arrangement with BC Hydro, at hydroelectric sites in the eastern part of the province. In these areas, instrument spacing is 50–100 km. Approximately 500 MB/d are archived to CD-ROM. Site details of the western portion of the CNSN and seismicity plots, updated daily, can be found at www.pgc.nrcan.gc.ca.

The NEIC Role in the NSS

BULAND, R. and BENZ, H.M., U.S. Geological Survey, Box 25046, MS967, Denver, CO 80225

The National Earthquake Information Center (NEIC) has a 25 year history of acquiring real-time waveform data from regional seismograph networks (RSNs) across the US, integrating information derived from this data to detect and locate seismic events, and providing a national monitoring capability for significant and/or felt earthquakes. This process has always depended on close cooperation between NEIC and RSN operators to minimize location errors and coordinate response. Data exchange between RSNs was also facilitated by this system, particularly between RSNs and the Tsunami Warning Centers (TWCs).

With the advent of the US National Seismograph Network (USNSN) providing high dynamic range, broadband data to the NEIC; the National Seismic System (NSS) coordinating seismograph network activities throughout the US; and public demand for more timely and accurate earthquake information, the national monitoring strategy has evolved rapidly. The NEIC is now in a position to exchange data with the RSNs and the RSNs as a group are increasing their role in rapid earthquake hazards response. The evolving exchange philosophy for real-time waveform data as well as both real-time and reviewed arrival time and hypocentral information involves direct network hub processor-to-network hub processor communications. Existing mechanisms for the hub-to-hub exchange of real-time waveform data are already being used to bring 9 broadband and 28 short period stations into the NEIC and return 39 broadband station feeds to RSNs including the TWCs.

To facilitate the real-time coordination of earthquake information release, steps have been taken to implement the coordination plan adopted by the NSS in 1997. In particular, the NEIC data structures have been modified to accommodate contributed hypocenter and magnitude information and the press release system is being modified to attribute earthquake parameters properly. When complete, it is intended that information released by the NEIC will reflect the most authoritative information available according to the NSS algorithm and be attributed to the proper network.

The New Madrid and Southern Appalachian Cooperative Seismic Networks: Outlook 1998.

WITHERS, M.M., JOHNSTON, A.C., University of Memphis, Memphis, TN 38152, USA, withers@ceri.memphis.edu; HERRMANN, R.B., HAUG, E.J., St. Louis University, St. Louis, MO, 63103, USA, rbh@slueas.slu.edu; POWELL C.A., University of North Carolina, Chapel Hill, NC, 27599, USA, cap@geosci.unc.edu, CHAPMAN, M.C., SNOKE, A.J., Virginia Tech, Blacksburg, VA, 24061, USA, chapman@ruamoko.geol.vt.edu

This presentation will report on progress occurring and outlook for two collaborative regional seismic networks operated by the Center for Earthquake Research and Information (CERI) at the University of Memphis and four other academic institutions. The Cooperative New Madrid Seismic Network (CNMSN) is operated jointly with St. Louis University and the Southern Appalachian Cooperative Seismic Network (SACSN) is operated in collaboration with Virginia Tech, and the University of North Carolina at Chapel Hill. The CNMSN design consists of 76 3-component short-period and 28 broadband stations; the SACSN includes 44 3-component short-period and 5 broadband stations. Each collaborating institution operates independently and thus datalogging and telemetry systems vary. Due to unavoidable telemetry requirements, CERI data are FM transmitted to remote nodes where they are digitized, and where the datalogging system "eqacquire" records triggered data segments. The short-period CNMSN network was completed in August, 1997 and half of the CERI component of the short-period SACSN network was operational by January, 1998. Efforts at CERI are now focusing on completing the broadband installations. We are also concentrating on streamlining methods for transferring waveform and parametric data between collaborating institutions. In 1998 we will also investigate methods to improve the real-time capability for data processing, exchange, and dissemination. These investigations will include a Mid-America Earthquake Center sponsored workshop, tentatively scheduled for September, 1998, to allow participation and input from scientists and engineers, emergency managers, industry and insurance representatives, and other interested parties. Research supported by the U.S. Geological Survey, Department of the Interior, under USGS award numbers 1434-HQ-98-AG-01929 and 1434-JQ-98-AG-01932.

Seismic Monitoring and Cooperation in the Puerto Rico Region

VON HILLEBRANDT-ANDRADE, C., HUERFANO, V. and LUGO, J., Puerto Rico Seismic Network, Dept. of Geology, University of Puerto Rico, PO BOX 9017, Mayaguez, Puerto Rico 00681-9017, staff_1@rmsismo.upr.clu.edu

The Puerto Rico Seismic Network (PRSN), which was set up in 1974, has been operating as part of the Geology Department of the University of Puerto Rico at Mayaguez (UPR-M) since 1987. To monitor the seismic activity in the region (17–20° N and 63.5–69° W, it runs a telemetered network of 14 short period stations. At the PRSN's facilities on the UPR-M campus, where the data are being received since 1997, traditional helicorders and two digital seismic acquisition systems (IASPEI and Soufriere) are run to record and archive seismic events. Several programs are used for the semi automatic analysis, location and reporting of recorded earthquakes. Between 1987 and 1997, the PRSN located over 6469 local earthquakes. In 1998, with funds from the Federal Emergency Management Agency (FEMA) and the University of Puerto Rico, the network will be expanded and upgraded to include nine digital telemetered broadband stations and a near real time seismic information system.

The PRSN is a member of two seismological cooperative organizations, the Council of National Seismic Systems (CNSS) and MIDAS, a Seismographic Consortium for the Caribbean. As part of the CNSS, the PRSN runs a finger quake utility with a listing of the 25 most recent events located in the region. Both seismic information and data compiled by the PRSN are exchanged and put on line through the MIDAS Electronic Seismic Data and Information Center which is managed by the PRSN. On the MIDAS home page (http:// midas.upr. clu.edu), interested parties can access information on MIDAS and short period and broadband seismic stations in the region (55–120° W amd 5° S - 33° N), as well as data and information on significant regional earthquakes (magnitude or MM Intensity grater than six), which are contributed by the over 17 seismological institutions participating in MIDAS. The 1900 - 1994 catalogue compiled by the Instituto Panamericano de Geografia e Historia for the MIDAS region will be placed on line and updated with the hypocentral information provided by the participating institutions.

The CNSS Composite Catalog

GEE, L., 475 McCone Hall, UC Berkeley, Berkeley CA 94720-4760; MALONE, S., University of Washington; NEUHAUSER, D., UC Berkeley; OPPENHEIMER, D.; USGS, Menlo Park; BULAND, R., USGS, Golden; and members of the CNSS

Traditionally, every seismic network - whether regional or national - has produced an earthquake catalog as part of its monitoring effort. In many cases, these catalogs have been difficult to access and use. As part of its contribution to the National Seismic System, the CNSS has encouraged member networks within the United States to contribute their respective earthquake catalogs for the purpose of creating a single, composite catalog.

The CNSS composite catalog is a world-wide earthquake catalog which is created by merging the master earthquake catalogs from contributing CNSS member institutions and then removing duplicate entries for the same earthquake. Each contributing seismic network is assigned a geographical region where that networks's solutions are considered authoritative. If more than one network supplies a hypocenter for the same earthquake, only one solution for that earthquake is included in the catalog, based on rules which give priority to the authoritative network. As of Jaunary 1998, 10 regional networks and the NEIC are actively contributing earthquake catalogs and another 3 networks will soon start. Each network updates their catalog on an appropriate time scale. For the NEIC and most of the networks in the western United States, catalogs are updated daily. For networks in less seismically active areas, catalogs may be updated monthly. A Web- based interface allows on-line catalog searches (http://quake.geo.berkeley.edu/cnss/cnss-catalog.html) and the entire catalog is available via anonymous ftp at quake.geo.berkeley.edu. Usage of the CNSS catalog materials accounts for 6000–7000 hits per month at the Web site, with 800–1000 of these conducting catalog searches.

A total of 1,411,600 earthquakes have been contributed to the CNSS composite catalog for the time period 1910–1997, producing 1,317,000 unique events. Approximately 25% of the catalog is for regions outside the US. A detailed look at the last five years indicates that, for the US mainland, the overall catalog seems complete at the M=2.0 level, although the level of completeness varies from region to region. The NEIC catalog alone is complete at the M= 3 1/4 level for the US and at M= 4 3/4 for the rest of the world. Statistics and map comparisons indicate that the US is well monitored by the combination of the National Seismic Network supplemented by dense regional networks in the seismically active areas.

USEFUL PRODUCTS FOR ELECTRIC UTILITIES FROM INTEGRATED REGIONAL SEISMIC NETWORKS

SAVAGE, W.U., ABRAHAMSON, N.A., MCLAREN, M.K., Pacific Gas and Electric Company, Geosciences Department, Mail Code N4C, P.O. Box 770000, San Francisco, CA 94177, wus1@pge.com.

For magnitude 5 to 7+ earthquakes, very rapid information about an individual earthquake can significantly improve the efficacy of earthquake response for electric service restoration. Information is needed to answer three questions:

1. *What the heck happened?* The occurrence with approximate location of a potentially damaging earthquake needs to be distinguished quickly (within seconds) from other potential causes of utility service disruption (e. g. lightning, plane crashes).
2. *How large is the affected region?* Quickly distinguishing (within a few tens of seconds) a locally damaging seismic event (e. g. M5 to 6) from a Big One (e. g. M7 to 8) or from a minor event (e. g. M4) dramatically affects the nature of a system operator's initial response. It is necessary to make these distinctions rapidly: a rough but confident immediate description of earthquake size is worth much more than the delayed release of a precise magnitude value. New regional-network approaches are needed to provide useful size estimates to facilitate accurate earthquake response.
3. *How much damage occurred?* This is critical information for all responders. Strong-motion parametric data (PGA, PGV, spectral acceleration values) at or near sites of utility facilities can be compared with fragility curves by utility personnel to quickly assess likely types and amounts of damage. Similarly, parametric data from widely distributed strong-motion recorders can be used to create a broadly accurate map of damage to transportation systems and buildings. Utility emergency responders need this information (in a few tens of minutes) to efficiently deploy field personnel to alleviate life-threatening conditions and begin service restoration. Regional seismic networks can centralize the parametric data and distribute them to organizations who can perform the desired analyses (such as utilities or emergency response agencies).

Recent Earthquake Web Pages for California and Nevada at http://quake.usgs.gov/recenteqs/

SIMPSON, R.W., ELLSWORTH, W.L., MICHAEL, A.J., and OPPENHEIMER, D.H., U.S. Geological Survey, Mail Stop 977, 345 Middlefield Road, Menlo Park, CA, 94025, USA; simpson@gold.wr.usgs.gov, ellswrth@andreas.wr.usgs.gov, michael@andreas.wr.usgs.gov, oppen@alum.wr.usgs.gov

We have created WWW pages to display information about earthquakes in California and Nevada within minutes of their occurrence. The pages are based on a merged catalog, automatically generated as events are reported by the contributing networks (USGS, UCB, Caltech, UNR). Three principles guided design of the pages: (1) keep things simple so that updates occur quickly, (2) keep pages and maps small (in bytes) to reduce load on our WWW server after felt events, and (3) keep things standard given the variety of browsers used to access the pages. In order to provide a zoom-in capability, we prepared 99 overlapping 2-degree gif basemaps covering CA and NV, as well as an overview index map of the two states. The update software (Bourne and Perl scripts) writes a set of drawing instructions used to plot the earthquakes on the gif basemaps. Text descriptions of events, fault plane solutions, and other information are linked by the update program to appropriate pages, which are then sent to a list of servers. After an event, relevant maps and pages are replaced - usually within a few minutes of origin time, and selected maps are emailed to Yahoo for use on their site. Every hour, all maps and pages containing earthquakes are updated. The full system is currently running on our server at "quake.usgs.gov" and the SCEC Data Center server at "www.scecdc.scec.org" (thanks to Katrin Hafner). Activity at Long Valley in December 1997 provided an extended stress test for the system. At times there were 2400 earthquakes on some 2-degree maps, and these pages on our server received as many as 80,000 hits per day. We hope, with collaboration from CNSS members, to improve the distribution system for making the merged catalog and to make the updating software and basemap-generation software available to anyone who would be interested in testing or using this approach.

Wednesday AM, March 18, 1998—Room 235
Eastern Hemisphere Structure and Faulting
Presiding: Laura Jones, *Los Alamos National Laboratory*

Slip Parameters for the Rann of Kachchh, India, 16 June 1819 Earthquake Quantified from Contemporary Accounts

Roger BILHAM, CIRES University of Colorado, Boulder CO 80309-0216

The 16 June 1819 Rann of Kachchh earthquake was felt throughout much of India. Significant vertical movements of the ground caused flooding of regions near sea level, damming of a distributary of the Indus river, widespread liquefaction, and a local tsunami, however, the geometry of the fault plane has hitherto remained obscure. Dislocation models based on deformation data gathered 7 and 25 years after the earthquake suggest that a near-surface reverse fault, slipped locally more than 11 m. The inferred 50–70° N-dipping fault plane beneath the Allah Bund is unfavorably steep for reverse faulting, presumably requiring high fluid pressures in the nucleation zone. A geometric moment magnitude of M=7.7±.2 is obtained from the inferred slip parameters, consistent with a magnitude estimated empirically from the intensity distribution. While a recurrence of the Kachchh earthquake is unlikely soon because of low inferred contractional strain rates in the region, the Indus Delta and Kachchh rift zones could host several ruptures contiguous with the 1819 event, with important consequences for the city of Karachi.

Seismicity of Northern Thailand: Past, Present and Future

BOTT, D.J., and WONG, Ivan G., Woodward-Clyde Federal Services, Oakland, CA 94607; PRACHUAB, Sumalee and WECHBUNTHUNG, Burin, Thai Meteorological Department, Bangkok, Thailand.

Despite its long historical earthquake record (+700 years), Thailand has not experienced any large, damaging earthquakes during historical times. Northern Thailand, however is more seismically active than southern and eastern Thailand, having suffered more than fifteen moderate-sized earthquakes ($M_L > 5$, MMI > VI) since about 1350 A.D., the largest being about M_L 6.5. The first instrumentally located earthquake (M 6.75) in the region occurred in 1925 in Laos but its reported locations differ by about a degree. Prior to 1925 only eight earthquakes have been identified in the region, based on sparse felt reports, four of which were felt in Chiang Mai. In 1963, a seismographic station was installed at Chiang Mai as part of the WWSSN. This improved the detection capability only for northern Thailand until a 10-station national network was installed and operated by the Thai Meteorological Department in the 1970s and 1980s. Since its inception, the network has only provided the capability to detect small to moderate-sized earthquakes and the location capability for larger events ($M_L > 4$) in northern Thailand. Further seismological analyses have been hampered by timing problems and poor azimuthal coverage of the network To better understand the nature of seismicity in the region, precise event locations are necessary, which would require a denser network (currently underway) and an improved crustal velocity model.

A historical principally instrumental catalogue compiled for Northern Thailand indicates low levels of diffusely distributed seismicity across the region, increasing northward towards the borders with Burma and Laos. There are no apparent associations with known active faults. Although the focal depth control is poor, moderate to high heat flow in northern Thailand suggests a typical continental seismogenic thickness of 15–20 km. We have calculated focal mechanisms of several recent felt earthquakes (M_L 4–5) in the region which indicate strike-slip faulting with approximate east-west oriented T-axes. Recurrence estimates for northern Thailand indicate a b-value of 0.9±0.1. The return period for M_L 6 and larger earthquakes ranges from 10 to 300 years with a best estimate of 60 years.

Historical and Recent Seismicity of Southwestern China

DOBER, M.C., VAN DUSEN, S.R., and DOSER, D.I., Department of Geological Sciences, University of Texas at El Paso, El Paso, TX 79968, dober@geo.utep.edu

The over 350 km long Xianshuihe-Anninghe-Xiaojiang fault system of southwestern China is a series of left-lateral strike-slip faults that accomodates a significant portion of the movement of India into the Eurasian plate. Over the past century it has been one of the most active strike-slip fault systems in the world. Four earthquakes of $M \geq 7$ have occurred since 1923 along the Xianshuihe branch of the fault system, and Holocene slip rates of up to 15 mm/yr have been observed along its segments. This study concentrates on determining the source parameters for $M \geq 4.5$ events occurring between 1923 and 1993 along the entire fault system, as well as for off-fault events, through use of earthquake relocation, first motion focal mechanism and body waveform modeling techniques. Preliminary studies of the Xianshuihe region indicate moderate events (M 4.5 to 6.5) are most likely to occur on smaller faults that are parallel or perpendicular to the main fault zone. One Mw=7.4 strike-slip event in 1948, however, is also an "off Xianshuihe fault zone" earthquake. Strike-slip focal mechanisms predominate for these moderate "off-main fault" events, with normal faulting also present. Events associated with the main Xianshuihe fault zone include two Mw > 7.0 strike-slip events in 1923 and 1973, as well as a Mw=6.7 normal faulting event in 1955 that appears to be associated with a fault stepover. All earthquakes have shallow (< 15 km) focal depths.

Predictions of the 1997 Strong Earthquakes in Jiashi, Xinjiang, China

ZHANG, Guomin, Center for Earthquake Analysis and Prediction, State Seismological Bureau, Beijing 100036, China; ZHU, Lingren, Xinjiang Seismological Bureau, Urumqi, Xinjiang, China; SONG, Xiaodong, Lamont-Doherty Earth Observatory of Columbia University, Palisades, NY 10964, USA, xsong@ldeo.columbia.edu; LI, Zhixiong, State Seismological Bureau, Bejing 100036, China; YANG, Maling, and SU, Naiqin, Xinjiang Seismological Bureau, Urumqi, Xinjiang, China; CHEN, Xuezhong, Center for Earthquake Analysis and Prediction, State Seismological Bureau, Beijing 100036, China.

A sequence of strong earthquakes hit Jiashi County, Xinjiang, China (40N, 77E) with a population of 280 thousands in 1997, after 10-month quiescence following the Ms6.9 earthquake on March 19, 1996 in the same area. From Jan. 21, 1997 through Oct. 18, 1997, 15 earthquakes occurred with Ms ≥ 5.0, seven of which has Ms ≥ 6.0. Such a sequence of strong earthquakes are rare around the world, but has occurred 6 times in the continent inside China in this century. Of the 15 Ms ≥ 5.0 earthquakes in the Jiashi sequence, seven short-term predictions were made, but the first shocks of the sequence (Jan. 21, Ms6.4, 6.3) were not predicted. Six of the seven predictions (Feb. 21, Ms5.0; Apr. 6, Ms6.3, 6.4; Apr. 13, Ms5.5; Apr. 16, Ms6.3; May 17, Ms5.4) were implemented by the local authorities and the public were noticed 2.5 hours to 4 days before the earthquakes, which caused 0 death; one earthquake (Apr. 11, 6.6) struck 30 minute after the prediction was made before actions could be taken by the local authorities, which caused 9 death. These predictions were based on composite observations of precursory anomalies in seismicity, electromagnetic fields, and crustal deformation, which were in turn compiled over the past 30 years in a nation-wide earthquake monitoring program under the supervision of the State Seismological Bureau of China. Examples of precursory anomalies include: (1)A clear seismicity pattern of "quiescence — foreshocks — main shock(s)" was observed for the Apr. 6 earthquakes (Ms6.3, 6.4), which was previously applied to the prediction of the famous 1975 Haicheng earthquake in Laoning, China. (2) Distinct decreases in b-values preceded the earthquakes on Mar. 1 (Ms6.0) and Apr. 6 ((Ms6.3, 6.4). (3) Sudden decreases in borehole strain preceded the earthquakes on Jan. 21 (Ms6.3, 6.4), Feb. 12 (Ms5.3), Mar. 1 (Ms6.0) Apr. 6 (Ms6.3, 6.4), Apr. 11 (Ms6.6), and May 17 (Ms5.4).

High Resolution Surface-Wave Dispersion Studies in China

JONES, L.E., and PATTON, H.J., Los Alamos National Laboratory, Los Alamos, NM 87545 USA, lejones@lanl.gov, patton@lanl.gov

As part of the effort to characterize surface-wave dispersion in China, we perform broadband dispersion measurements in a high-resolution survey of critical monitoring areas. Focusing on western China initially, with emphasis on events local to the Lop Nor site, we employ broadband data recorded on CDSN stations, and regional events (mb 4 and above). Our approach is twofold, emphasizing path-specific calibration of key stations and well-recorded reference events. Such calibration results in filters designed to extract surface waves in an automated fashion for use in surface-wave detection, Ms estimation, discriminants and further structural or attenuation studies. Tomographic inference then integrates longer period results from teleseismic data with results from broadband waveforms recorded at regional distances in China and Eurasia, providing group velocity curves for regions with sparse station distribution and little seismic activity. For this purpose, we draw on the tomographic results of Ritzwoller and Levshin (University of Colorado, Boulder). Initial path-specific dispersion studies at Chinese station WMQ show substantial azimuthal variation in the 10–30s range, reinforcing the need for careful determination of source regions, and for path-specific calibration. Positive travel-time residuals are found for basin paths, while negative residuals dominate for the Tien Shan fold belt. Large local variations in travel times may be due to complex wave propagation, such as multipathing.

Path Effects on Regional Phases in China

PHILLIPS, W.S., RANDALL, G.E., HARTSE, H.E. and TAYLOR, S.R., Los Alamos National Laboratory, Los Alamos, New Mexico 87545 USA
wsp@lanl.gov

We have evaluated path effects on regional seismic phases by geographically smoothing amplitudes recorded by stations of the Chinese Digital Seismic Network after correcting for source scaling (using m_b) and distance. Consistencies between the resulting geographical patterns for different stations suggest the smoothing has removed source radiation pattern effects reasonably well. Relationships with regional tectonic features and with independent measures of the path effect such as coda Q further support the assertion that the patterns represent the path effect. The smoothing will not remove effects of possible bias in m_b caused by laterally varying properties of the upper mantle. However, if path effects for regional and teleseismic raypaths correlate, an m_b bias will cause the patterns to underestimate actual variations in the path effect. The geographical patterns can be used to correct amplitude data to reduce scatter in magnitude estimates or discriminant ratios. To test this, we modified the smoothing procedure so that an event would not be allowed to affect its own correction factor. For 853 events recorded at station LZH in central China, path correction reduced variance up to 39% for L_g, but averaged only 10% for P-wave (P_n, P_g and P-coda) amplitudes. Path correction reduced variance up to 57% for P/L_g ratios, compared to the standard correction for distance alone. Interestingly, we found relatively strong L_g for paths originating in Myanmar and Laos, passing through the blockage in eastern Tibet. Unless an m_b bias is important, we will need to consider lateral refraction and other unusual propagation phenomena to understand such observations.

2-D Image of Seismic Attenuation of the Mantle from the Deep Seismic Sounding Profile "Quartz," Russia

MOROZOV, I.B., MOROZOVA, E.A., and SMITHSON, S.B., Department of Geology and Geophysics, University of Wyoming, PO Box 3006, Laramie, WY 82071-3006. morozov@uwyo.edu

We present a detailed 2-D image of the P-wave upper mantle attenuation down to about 500 km depth using nuclear explosion data from the ultra-long refraction/reflection profile "Quartz." Our analysis is based on a modified common spectrum technique followed by attenuation tomography and iterative ray tracing in the "Quartz" velocity structure obtained earlier. The resulting attenuation structure corroborates the earlier 1-D model for the Northern Eurasia, as well as our recent estimate based on the analysis of the teleseismic P_n phase, and provides significantly more detail than the existing models. The resulting upper mantle attenuation structure is characterised by Q values ranging from 400 to 1800. Down to the depths of 150 - 190, and probably, 400 km, the attenuation increases horizontally in SE direction, away from the Baltic Shield. Our model exhibits strong 2-D, vertical and horizontal attenuation contrasts. A significant attenuation increase at the boundary near the depths of 120 - 150 km can apparently be associated with the base of the lithosphere.

Pn Velocity Structure from South Western Europe to Western Asia

D. E. McNamara, C. Schultz and R. A. Hansen

The vast region of convergent margins, extending from the western reaches of Europe and the Mediterranean, eastward in to western Asia, is likely the most structurally and technically complex area in the world. Tectonic structures include: 1) large sedimentary basins such as the Persian Gulf, the Mediterranean Sea and the Caspian Sea; 2) high elevations such as the Zagros mountains, the Iranian Plateau, the Alps, Caucuses and Himalaya; 3) Stable continental shields of Northern Africa and the Arabian Peninsula; and 4) areas of active extension such as the Red Sea rift. The region is also characterized by abundant seismicity and active volcanism. Given the tectonic complexity of the region we can expect the lateral seismic velocity structure of the crust and upper mantle to be equally complex. For this reason, predicting the characteristics of regional waves, that dominantly travel within the crust and upper mantle, can be a formidable task. Since seismic waves that propagate at regional distances (<1800km) are becoming increasing important to verifying the CTBT it is, none the less, important to understand their propagation characteristics.

In order to place some constraints on regional wave propagation in the region we attempt to model the lateral variation of upper mantle P-wave velocity. To do this, we have inverted the travel times of over 50,000 first arrivals (from NEIC 1598 earthquakes at 749 stations, raypath distance=200-1600 km), in a backprojection tomography scheme. We assume that the first arrival in this distance range, Pn, is a head wave with a travel time that can be divided into three parts: a mantle leg that travels directly beneath the Moho, one crustal leg beneath the recording station and a second crustal beneath the source. For estimating lateral velocity perturbations, the region is divided into cells and a velocity is computed as a function of all rays traversing that cell. Preliminary results suggest significant lateral heterogeneity of upper mantle Pn velocity that correlate well with major tectonic features and previous geophysical results. Results from this study will be used to better define seismic parameters required to verify the CTBT.

Work performed under the auspices of the U.S. Department of Energy by the Lawrence Livermore National Laboratory under contract number W-7405-ENG-48.

Surface Wave Continental Tomography

LEVSHIN, A.L., RITZWOLLER, M.H., and VDOVIN O.Y., Department of Physics and CIRES, University of Colorado, Boulder, CO 80309, U.S.A., levshin@lemond.colorado.edu

We present the results of the dispersion characteristics of broadband (15 s - 200 s) fundamental surface waves propagating across three continents: Eurasia, S. America, and Antarctica. The ultimate purpose is to invert for high resolution, tectonic scale crustal and lithospheric models of these continents to depths of approximately 200 km. Intermediate period (15 s - 40 s) group velocity maps may also be used for path-oriented signal detection and enhancement within a nuclear test monitoring environment. More than 17000 three-component waveforms have been analyzed for Eurasia, and more than 10000 have been analyzed for S. America and Antarctica. The estimated group velocity maps exhibit greater detail than predictions from global models and hold new information about the structure and tectonics of these continents. Many known tectonic structures are observed in the group velocity maps. The dispersion signatures of numerous sedimentary basins across Eurasia and S. America are displayed clearly on short period maps (e.g., Tarim Basin, Ganges Fan and Delta, Persian Gulf, Tadjik Depression, S. Indus River, N. and S. Caspian Sea, Black Sea, E. Mediterranean Sea, W. Siberian sedimentary Complex, Lena River Complex, Barents Sea Shelf, Sechuan Basin, Adriatic Sea, North Sea, Ucayali-Madre de Dios, Chaco-Tarija, and Parana Basins). Other tectonic features observed include continental flood basalts of the Ethiopean and Deccan plateaus, significant thickening of the crust under high-altitude plateaus and mountain systems (Tibet, Pamir, Tien Shan, Altai, Zagros, Caucasus, Andes, Altiplano), shields and platforms (Baltic, Siberian, Kazakh, Indian, Arabian, Nubian, Guyana, Guapore, Sao Francisco, E. Antarctic craton), back-arc spreading (Seas of Japan and Okhotsk), down-going slabs (Hindu Kush, Himalaya).

The Propagation of Seismic Waves in North African and Mediterranean Lithosphere

DIAL, P., DOSER, D.I., KELLER, G.R., University of Texas at El Paso, El Paso, TX, 79968, USA, dial@geo.utep.edu, Fairhead, J.D., University of Leeds, Leeds, UK.

Preliminary research on lithospheric structure and seismic wave propagation on a regional scale is vital for a CTBT verification effort. This research focuses on the region of North Africa and the Mediterranean Basin. Geologically, the study area is a complex mixture of continental, oceanic, and transitional crustal domains. The study area contains Precambrian terranes intruded by Cenozoic volcanics (e.g., in the Hoggar, Tibesti, and Darfur domal uplifts) and compressional and extensional features associated with the convergence of the African and European plates (e.g., the Atlas Mountains, Betic Cordillera, and Alboran Sea). Three lithospheric gravity profiles have been constructed to obtain preliminary lithospheric structure across North Africa. The gravity profiles, along with previous geological and geophysical studies in the region, were used to construct **1-D velocity models** for modeling of the complete **regional seismic wavetrain**. A **reflectivity code** was used to generate synthetic seismograms, which were compared to observed seismograms at 8 WWSSN seismic stations in southern Europe and northern Africa. Nine large earthquakes (**M** > 5.0) and their aftershock sequences were used. Over 260 seismograms have been digitized and approximately **150 seismograms have been modeled** with the 1-D reflectivity code. Seismograms were only modeled for periods between 20 and 200 seconds. This method appears to adequately model seismic wave propagation character in the western Mediterranean Basin to an epicentral distance of 1300 km. Relatively low upper mantle velocities (7.7 - 7.85 km/sec) have been found beneath Iberia and the western Mediterranean. Crustal thickness varies between 25 and 35 km along the propagation paths studied.

Wednesday PM, March 18, 1998—Room 235
California Seismicity and Structure
Presiding: Edward Field, *USC*

EARTHQUAKE DEFICITS, SEISMIC MOMENT DEFICITS, AND M ≥ 6 SEISMICITY IN SOUTHERN CALIFORNIA SINCE 1903

HANKS, T. C. and STEIN, R. S., U.S. Geological Survey, 345 Middlefield Road, Menlo Park, CA 94025

The Working Group on California Earthquake Probabilities (WGCEP, 1995) concluded that the observed rate of M ≥ 6 and M ≥ 7 earthquakes in southern California is too low by a factor of 2. This conclusion is seemingly driven by the infrequency of great, Fort Tejon-size (M = 7.9) earthquakes in the WGCEP (1995) model calculations, thus forcing ≃ 70% of the seismic moment release rate to earthquakes of M ≤ 7.5. Noting this infrequency, Jackson (1996) perceived a seismic-moment deficit for southern California and the need for the "huge earthquake" (M = 8 to 9) to alleviate it. Meanwhile, a number of investigators took note of the eleven M ≥ 6 earthquakes in southern California from 1983 to 1994; a link between the M ≥ 6 earthquake deficit and an increasing rate of M ≥ 6 earthquakes was appealing. Thus, the following questions relevant to the occurrence of M ≥ 6 earthquakes in southern California since 1850 arise: Is there an earthquake deficit? Is seismicity increasing at the present time? Is there a seismic moment deficit? Is there a case for a "huge earthquake"? The answers to these questions would seem to be broadly affirmative within the U.S. earthquake-research community, and in the wake of the 1994 Northridge earthquake, they have had an enormous impact on the assessment of earthquake losses and mitigation strategies in California. We find, however, that there is nothing in the available data that sustains affirmative answers to any of these questions. Our analysis is founded on a catalogue of M ≥ 6 earthquakes in southern California since 1903. This catalogue yields a rate of M ≥ 6 earthquakes of 0.49 events/yr, 50% larger than for the WGCEP (1995) catalogue, and $b = 1.00$, the theoretical expectation for constant stress drop earthquakes. M ≥ 6 earthquake catalogues for southern California are unlikely to be complete prior to the early 1900's. The seismicity increase from 1983 to 1994 is the occasional expectation of a Poisson process. The rate of seismic moment release since 1850 is in balance with the accumulation rate, given likely uncertainties in either quantity. As such, the case for a "huge earthquake" is no more plausible seismologically than it is geologically (Schwartz, 1996).

An Integrated Seismic-Hazard Source Model for Southern California: No Deficit or M>8 Earthquakes Required

FIELD, E.H., Dept. of Earth Sciences, University of Southern California, Los Angeles, CA 90089-0740, field@usc.edu; JACKSON, D.D., Dept. of Earth and Space Sciences, University of California, Los Angeles, Los Angeles, CA 90024-1567, djackson@ucla.edu; DOLAN, J.F., Dept. of Earth Sciences, University of Southern California, Los Angeles, CA 90089-0740, dolan@usc.edu.

Previous attempts to integrate geological, geodetic, and observed seismicity data into a probabilistic-hazard source model have predicted a rate of magnitude 6–7 earthquakes significantly greater than the historical record. One proposed solution was that the apparent earthquake deficit is not real, but an artifact of the upper magnitude limit built into the models. However, this explanation was controversial because it required magnitudes larger than are supported by direct geological-evidence. Although several papers have addressed this issue, an alternative, integrated source model without an apparent deficit has not yet appeared. We present a simple geologically-based approach for constructing such a model, which agrees well with the historical record and does not invoke any unsubstantiated phenomena. In particular, we show that a careful adherence to the conservation of seismic-moment rate, an allowance for geologically-feasible multiple-segment ruptures, and accounting for magnitude uncertainties are among the important factors.

A Correlation Between Crustal Thickness and Cut-off Depth of Earthquakes in Southern California

Dapeng Zhao & Ta-Liang Teng (Dept. of Earth Sci., Univ. of Southern California, Los Angeles, CA 90089; dzhao@usc.edu); Hiroo Kanamori (Seismo Lab 252-21, Caltech, Pasadena, CA 91125)

It has long been recognized that the cut-off depth of the crustal earthquakes in southern California has a great spatial variation, ranging from 15 km to up to 30 km. In general, this variation has been explained in terms of the variation in temperature. The deep seismicity and crustal thickening in the Transverse Ranges are interpreted as a result of convergence due to the bend of the San Andreas Fault (SAF). In this study, we investigated the relationship between the crustal thickness and the cut-off depth of seismicity in the entire southern California region. We used the P and S wave arrival times recorded by *the Caltech-USGS Southern California Seismic Network* to relocate thousands of earthquakes. We used a 3-D velocity model which includes the Moho depth changes mapped by *Richards-Dinger and Shearer* [1997] (RS97) by stacking the Moho-reflected *PmP* phases from local earthquakes. Independently, *Zhu and Kanamori* [1997] used a teleseismic receiver function method and obtained a result that confirms the findings by RS97. The 3-D ray tracing method of *Zhao et al.* [1992] was used in the hypocentral relocation, which can deal with complex velocity discontinuities in the model. The relocated hypocenters result in a variance reduction by about 60%, and they show a more clustered distribution than the network locations. Our preliminary results show a striking positive correlation between the crustal thickness and the cut-off depth of the crustal earthquakes. The cut-off depth is deep (20-30 km) in the southern edge of Sierra Nevada, and central and western Transverse Ranges where the Moho depth is 31 to 38 km. In most of the Mojave Desert, the Los Angeles Basin and its offshore areas, the cut-off depth is shallow (about 15 km), in agreement with a thin crust (17-28 km). This correlation is also visible from the hypocenters located by the seismic network with a 1-D model. There is no significant change in the cut-off depth and the Moho depth across the SAF, though the *Pn* velocity of the uppermost mantle changes dramatically across SAF, according to the RS97 model.

Aftershocks from Rate and State Dependent Friction

GROSS, S.J., CIRES, University of Colorado, Boulder, CO 80309-0216, USA, sjg@quake.colorado.edu

In 1994 James Dieterich developed a seismicity model based upon rate and state dependent friction that well represents observed spatial and temporal aftershock distributions. Does the success of the Dieterich seismicity theory imply that Dieterich friction is a better model of fault friction than other friction relations? Some of the results of Dieterich seismicity theory can be derived from other friction relations, and some cannot. Results can be derived from simple graphical analysis of the slip curve followed by faults generating a constant rate of seismicity. A step in stress from the mainshock causes the slip speed to be increased suddenly, and then the state variables respond, driving faults closer to failure. The number of aftershocks is proportional to the background seismicity rate for most friction laws. A linear proportionality between the number of aftershocks triggered and the magnitude of the triggering stress step results from friction laws having a logarithmic dependence upon slip velocity and relatively rapid nucleation. I have used the proportionality between stress step and aftershock productivity to estimate loading rates for several large California earthquakes. These estimates of loading rate are not specifically dependent upon Dieterich friction. The temporal distribution of aftershocks is specific to the friction relation. Dieterich seismicity theory fits observations of aftershock decay well. The highest rate of aftershocks is generally observed within a few hours after the mainshock, and may be limited by the capacity of networks to record earthquakes during the coda phases of the mainshock. The nucleation time for early aftershocks must therefore be no more than a few hours, much shorter than the observed duration of aftershock sequences.

DOES THE CALIFORNIA GENERIC "AFTERSHOCK" MODEL ALSO REPRESENT FORESHOCK-MAINSHOCK OCCURRENCE?

REASENBERG, P.A., U.S. Geological Survey, 345 Middlefield Rd., Menlo Park, CA 94025, 650-329-5002, reasen@hayward.wr.ugss.gov)

After $M \geq 5$ earthquakes in California, the short-term probability for additional earthquakes is estimated by the U.S. Geological Survey and communicated to the state government and the public. The methodology for doing this uses a generic, stochastic short-term clustering model that is based on aftershock data observed after moderate ($M \geq 5.0$) earthquakes in California between 1933 and 1987. These aftershocks are, by definition, smaller than their respective mainshocks. In applications, the model is extended beyond its original magnitude range, and probabilities are estimated for "aftershocks" that are larger than their mainshock. Thus, the model is used as a "foreshock-mainshock" model, although it was derived solely from aftershock data. Is such an extension justified?

I tested the model in its foreshock-mainshock mode by comparing the model probabilities with corresponding frequencies of foreshock-mainshock pairs observed worldwide. Data were taken from the Harvard CMT catalog (1977-1996) and the Triep and Sykes (1997) compilation of shallow intracontinental earthquakes (1978-1994). Foreshock-mainshock pairs were assayed for a variety of magnitude and focal mechanism constraints. In the Harvard CMT data set, both $M \geq 6$ and $M \geq 7$ earthquakes occur after $M \geq 5$ foreshocks with approximately twice the frequency predicted by the California generic model — a difference explainable by model uncertainty. Mainshocks with thrust mechanisms were found to have a significantly higher rate of foreshock occurrence than strike slip and normal events. Because the Harvard CMT catalog is dominated by subduction zone earthquakes, this higher rate may not be representative of intracontinental zones, such as central and southern California, where the model is often applied. The Triep-Sykes catalog provides a smaller but, perhaps, more pertinent data set for use in calibrating the generic model. Results of foreshock-mainshock assays in this data set were not available at abstract time, but will be presented in the talk.

Moment Tensor Solutions of 1997–1998 Long Valley Earthquake Swarm

PASYANOS, M.E., TKALCIC, H., DREGER, D.S., University of California, Berkeley, CA 94720, mike@seismo.berkeley.edu; HILL, D.S. United States Geological Survey, Menlo Park, CA 94025.

The Long Valley Caldera (LVC) is located along the east side of the Sierra Nevada range in central California. The Long Valley volcanic system, which erupted 760,000 years ago, was responsible for the deposition of the Bishop Tuff and the 2–3 km subsidence of the chamber roof to form the 17 by 32 km oval depression of LVC. In May 1980, an earthquake swarm which included four magnitude 6 earthquakes occurred near the south moat of the LVC, and was accompanied by a 25-cm uplift in the center of the caldera. Since that time, there have been recurring earthquake swarms and continued uplift of the central section of the caldera (the resurgent dome). Most recently, the onset of nearly continuous swarm activity in early July has persisted through the date of abstract submission. This sequence of swarms has included several thousand events of $M \geq 2$, over 100 events of $M \geq 3$, and seven events of $M \geq 4$. Most of the activity has been confined to the south moat of the caldera east of Mammoth Mountain.

Regional moment tensor inversion methods have been used to estimate source parameters for moderate earthquakes in California for several years now (Romanowicz et al, 1992; Pasyanos, 1997). Two independent methodologies have been employed to both provide a check on the results and to help in calibrating the velocity models. We will be presenting moment tensor solutions calculated using the two methods for magnitude 4 and larger events occurring during the current swarm, as well as for nearby earthquakes located outside of the Long Valley region. We shall construct two catalogs of moment tensor solutions for these events. The first is a catalog of solutions constrained to have no volume change (double couple and compensated linear vector dipole (CLVD) only), while the second catalog will be comprised of unrestrained solutions (isotropic, CLVD, and double couple components). We hope to determine whether we can resolve physically significant, non-double couple components of the earthquakes. By comparing the solutions obtained for events outside of the caldera, presumably on tectonic faults, we hope to assess the significance of the non-double couple components which we have obtained in preliminary results. We shall also be investigating whether there is consistency in the non-double couple components determined by each of the two methodologies and how the results compare with first motion focal mechanisms obtained from the short-period Northern California Seismic Network.

Imaging Attenuation Structure and Source Properties at the Coso Geothermal Field

HOUGH, S.E., U.S. Geological Survey, 525 S. Wilson Ave, Pasadena, CA, 91106, hough@gps.caltech.edu; LEES, J., Yale University, New Haven, CT,06511; and MONASTERO, F., China Lake Geothermal Program, China Lake, CA 93555.

Source properties of small (magnitude –1 to 1) clustered events from the Coso geothermal region are analyzed using an empirical Green's function (EGF) method. Stress drop values of at least 0.5–1 MPa are inferred for all of the events; in many cases, the corner frequency is outside the usable bandwidth and the stress drop can only be constrained as being higher than approximately 3 MPa. P- and S-wave stress drop estimates are identical to the resolution limits of the data. These results are indistinguishable from results from numerous previous EGF studies of M2–5 earthquakes, suggesting a similarity of rupture processes that extends to events that are tiny, shallow (2–3 km depth), and induced (by injection). Whole-path Q estimates for P and S waves are determined using a multiple-empirical Green's function (MEGF) method (Hough, JGR, 1997) whereby spectra from a cluster of colocated events at a given station are inverted for a single attenuation parameter, t^*, with source parameters constrained from EGF analysis. This approach has been shown to mitigate signficant biases in both t^* and corner frequency that can arise using conventional methods (single spectrum and joint inversion). Finally, the t^* results are inverted for three-dimensional attenuation structure using a damped least-squares method (Lees and Lindley, JGR, 1994). Qs/Qp values greater than 1 are observed throughout the region, consistent with restriction of fluids to narrow conduits within the geothermal region. Significant lateral variability in attenuation structure is inferred; the central low-Q anomaly corresponds well to the extent of the high heat flow region.

Wednesday, 8:30 AM–5:00 PM
Glenn Miller Ballroom
Posters
Seismic Hazard Assessment

Average Annual Losses for Earthquakes in the Continental United States

NISHENKO, S.P. and JAMIESON, G., FEMA/Mitigation Directorate, 500 C Street SW, Washington DC 20472, stuart.nishenko@fema.gov; LAWSON, R.S., RMS Inc., 149 Commonwealth Drive, Menlo Park CA 94025

Much of our perception of the earthquake 'problem' in the United States is based on our understanding of the earthquake hazard - earthquake locations and the spatial distribution of strong ground motion - and not the earthquake risk, which is a product of the hazard, the building inventory and building vulnerability. Policy, land use and development decisions at the Federal, state and local level however, are essentially risk-based decisions. We present a new national analysis of seismic risk based on a nationally consistent loss estimation methodology ($HAZUS^{TM}$, a nationally consistent building inventory, and the new generation of USGS seismic hazard maps. The use of nationally consistent methodologies and databases facilitates comparison of results between various parts of the country and provides a common framework with which to develop policy decisions. The analytical resolution for this study is at the census tract level, with the final results aggregated to the county and state levels for the purposes of comparison. Total direct losses for the residential and general commercial building inventory were calculated using peak ground acceleration, peak ground velocity, and spectral acceleration (0.3 and 1.0 sec) for eight return periods (100, 250, 500, 750, 1000, 1500, 2000 and 2500 years). Total direct loss includes capital loss [structural, non-structural, contents and inventory] and income loss [relocation costs, lost wages and rental income losses]. In addition to absolute dollar values, risk is also presented in terms of dollar loss as a percentage of inventory value. The results of these analyses are used to compute the Average Annual Loss (the area under the loss curve defined by the above eight return periods - bounded by the 100 and 2500 year return periods). Average Annual Loss is introduced as a new decision criterion for evaluating and developing earthquake mitigation strategies.

New Developments in the UCSB Strong Motion Database

LINDLEY, G., TUMARKIN, A., and ARCHULETA, R., Institute for Crustal Studies, University of California, Santa Barbara, CA, 93106 e-mail: grant@quake.crustal.ucsb.edu

The UCSB Strong Motion Database is a relational database that has been available on the World Wide Web for over a year (http://smdb.crustal.ucsb.edu/). During that time significant improvements of the user access methods have been made and additional data has been added. The database is now nearly complete for California strong motion data, and allows the user to search on numerous parametric information related to the data. In addition, many of the download links from the Web site now point directly to CDMG and USGS FTP sites, allowing those agencies to maintain ultimate control over their data, while still allowing database users to download data via the Web site. Current access methods include a newly developed Java map program which allows the user to select a station or earthquake from a map to see a summary of available data. Other access methods allow the user to search the database based on specific parametric information such as the magnitude, epicentral or hypocentral distance, site geology, peak ground acceleration, etc. Future improvements will include refinement of the access methods, inclusion of global data, addition of new database parameters, and quality control to ensure uniformity and accuracy of the information in the database.

SITE CHARACTERIZATION AND SITE RESPONSE EFFECTS AT THE TARZANA, CALIFORNIA CSMIP STATIONS.

GRAIZER V. M., SHAKAL A. F. (California Division of Mines & Geology, Strong Motion Instrumentation Program, Sacramento, CA 95814; smipdata@consrv.ca.gov)

Amplification of ground motion has been observed at the Tarzana - Cedar Hill Nursery in many, but not all earthquakes, and for both strong and weak motion. Both the Whittier Narrows and Northridge mainshocks produced larger than expected motions at Tarzana. The peak acceleration and velocity during the Northridge mainshock were amplified by factors of 5 and 3, respectively, compared to nearby sites.

In January 1994 (one week after the Northridge earthquake) the California Strong Motion Instrumentation Program (CSMIP) installed an additional accelerograph at the foot of the small hill at a distance of about 150 m from the Tarzana - Cedar Hill station. Strong-motion data from 24 Northridge aftershocks with magnitudes $2.4<M<5.2$ were recorded and have been processed. Peak acceleration, velocity and displacement were often, but not always amplified by factors near 2 on the top of the hill during Northridge aftershocks. Also, response spectra were often amplified by a factor of 4.5 near 0.3 second (3.2 Hz).

In June 1997 CSMIP installed a third accelerograph on the top of Tarzana hill at the distance of about 50 m from the existing station as a transitional step to abandoning the original site because of planned construction. Comparison of strong-motion data shows a surprising variability between the records from these two close stations.

The Tarzana site was recently drilled to a depth of 100 m. Shear-wave velocity increases from 200 m/sec near the surface to near 750 m/sec at 100 m depth. The 20 m high hill was found to be well drained with a water table near 17 m. Modelo formation (extremely weathered at the surface to fresh at depth) is underlying the hill. The subsurface geology and velocities obtained allow classification of this location as a soft-rock site class C. In October 1997 CSMIP put a downhole instrument at the depth of 60 m at the new site.

The source of the site amplification that produces large motions at Tarzana is still under investigation. The topography, shear-wave velocity profile and three- dimensional structure of the site apparently all contribute to the higher amplification of ground motion at the Tarzana site. The difference between ground motion at the original site and the new site 50 m away adds new questions to the studies of site effects at Tarzana.

The studies of Tarzana were co-funded by CSMIP and by the National Science Foundation (NSF) through the Resolution of Site Response Issues from the Northridge Earthquake Project (ROSRINE).

Controls on Ground Failure in Alluvium: Lessons from the 1994 Northridge, California, Earthquake

PONTI, D.J., U.S. Geological Survey, 345 Middlefield Road MS 977, Menlo Park CA 94025, dponti@usgs.gov; CRAVEN, A.E., Stanford University, Stanford, CA, 94305, craven@pangea.stanford.edu; TINSLEY, J.C. III and HOLZER, T.L., U.S. Geological Survey, 345 Middlefield Road MS 977, Menlo Park CA 94025, jtinsley@usgs.gov, tholzer@usgs.gov.

The 1994 Northridge earthquake, which occurred on a blind fault, caused ground and pavement cracks in alluvium and damaged subgrade utilities near Newhall and in parts of the San Fernando Valley (SFV). Failures occurred in Holocene, fine-medium grained alluvial fans (from silt-rich Tertiary rocks), underlain by shallow (<9m depth) ground water. Most deformation, however, was confined to near-linear belts of cracks, up to 2 km wide and 5 km long, in Potrero Canyon (PC), Granada Hills (GH) and Reseda-Canoga Park (R-CP). Post-earthquake mapping and geotechnical investigations show that the deformation was caused by shaking-induced ground failure. Liquefaction seems to be the primary mechanism, but shear failure of saturated, normally-consolidated clayey silts of alluvial fan distal margins, may be important.

Several factors appear to have localized ground failure in susceptible deposits: the presence of fault zones, active fold axes and toe-slope alluvial fan silts, and rupture directivity. In GH, failures occurred along trend near the Mission Hills fault (MHF). The MHF did not reactivate in the earthquake, but serves as a ground water barrier (promoting liquefaction), and may also have focused or enhanced ground motions, as damaged residential structures concentrate near the MHF. AT PC, failures occurred directly up-dip of the seismogenic fault, near the active fold axis, where long-period ground motions were very high owing to rupture directivity. In R-CP, failures were confined to fine-grained, soft, young sediments along the toe-slope of the Santa Susana Pass Wash alluvial fan. The spatial distribution of ground failures in the SFV can be estimated using multivariate probit regressions that include various physical (depth to ground water, lithology, V_s) and ground motion parameters as independent variables. The best fit to the data is when peak velocity is used as the ground motion parameter, indicating that directivity may be important to localizing ground failure. Quantitative ground-failure-hazard estimates can be improved by using the distribution of alluvial fan facies and geologic structures, and ground motion scenarios that incorporate rupture directivity.

Estimates of Ground Accelerations at Point Reyes, California During the 1906 San Francisco Earthquake

ANOOSHEHPOOR, A., Seismological Lab., University of Nevada, Reno, Reno, NV 89557, rasool@seismo.unr.edu; HEATON, T.H., California Institute of Technology, Dept. of Civil Engineering MS 104-44, Pasadena, CA 91125, heaton_t@caltech.edu; SHI, B., and BRUNE, J.N., Seismological Lab., University of Nevada, Reno, Reno, NV 89557, bshi@seismo.unr.edu, brune@seismo.unr.edu

On April 18, 1906 the 5:15 San Francisco bound train was standing on a siding at Point Reyes when the Earthquake shook the area. According to the conductor the train gave a great lurch to the east, followed by another to the west which threw the train on its side. However, since the narrow gauge tracks at the station are in the Northwest-Southeast direction (nearly parallel to the San Andreas Fault) we believe that the ground motion experienced by the train's conductor was most likely in the Southwest-Northeast direction (perpendicular to the tracks), in agreement with another eyewitness account in Marin County (Bolt, 1968). These descriptions are consistent with a large horizontal fault-normal component associated with the rupture front.

We have developed an analytical solution for the rocking and overturning response of a two-dimensional, symmetric rigid block subject to a full sine-wave of horizontal ground acceleration. Assuming a full sine-wave shape for the fault-normal component of acceleration, we use this to estimate the peak ground acceleration at Point Reyes, California during the 1906 San Francisco earthquake that toppled the narrow-gauge train. Our results, for a 3% damping ratio, indicate that the minimum toppling accelerations at 1, 1.5, and 2 hz are about 0.35, 0.5, and 1.05 g, respectively.

Precarious Rock Constraints on Ground Motion from Great Earthquakes Along the San Andreas Fault, California

BRUNE, J.N., Seismological Laboratory, University of Nevada Reno, Reno, NV 89557, brune@seismo.unr.edu.

Groups of precariously balanced rocks are effectively earthquake strong ground motion seismoscopes that have been operating on solid rock outcrops for thousands of years, thus providing a constraint on the maximum ground motion that could have occurred during that time. In the Mojave Desert near Palmdale, California, near the Mojave Section of the San Andreas Fault, and in the adjacent San Gabriel Mountains, numerous precarious and semi-precarious rocks (as defined by Brune, 1996) were found extending from distances of 35 km from the San Andreas Fault to as close as 11 km, with a considerable number occurring at Lovejoy Buttes, a distance of about 14 to 17 km, thus potentially providing constraints on ground motion from large earthquakes over an important range of distances. The precarious rock data appear to be inconsistent with the assumptions made for recent PSHA maps about time variability of strong ground motion at a given site resulting from a sequence of rare large earthquakes. This in turn implies that the PSHA maps for long recurrence (low probabilities) are too high. If this conclusion is confirmed by more accurate analysis of the precarious rocks, it has profound implications for seismic hazard in California.

Non-Ergodic Probabilistic Seismic Hazard Analysis

ANDERSON, J.G., and BRUNE, J.N., Seismological Laboratory and Department of Geological Sciences, University of Nevada, Reno, NV 89557, jga@seismo.unr.edu

Most probabilistic seismic hazard studies treat uncertainty for large, low probability ground motion parameters incorrectly, with the result that the hazard at low probabilities may be seriously overestimated. The optimum distribution of uncertainty between aleatory (random) uncertainties and epistemic (knowledge) uncertainty must be determined from data, not assumed, and epistemic uncertainty cannot be treated as an ergodic uncertainty. The economic consequences of designing sensitive structures for low probability ground motions assuming ergodic vs. non-ergodic distributions are potentially huge.

Which Potential Earthquakes Dominate Seismic Hazard in the U.S.—A Regional Comparison

HARMSEN, S.C. and FRANKEL, A. U.S. Geological Survey, Denver, CO 80225. USA. harmsen@usgs.gov

We deaggregate probabilistic seismic hazard by distance and magnitude for the coterminous United States and for specific cities. We show national maps of mean and modal distance and magnitude for damped response spectral acceleration at periods 1 second (s), 0.3 s, and 0.2 s, and peak ground acceleration. Ground motions correspond to 2 per cent and 10 per cent per 50 years probability of exceedance. For the central and eastern US (CEUS), we also show maps of 2 s, 0.5 s, and 0.1 s mean and modal statistics.

In much of the US in or west of the Intermountain Seismic Belt (ISB), average and modal distances and magnitudes to a given site are controlled by nearby faults or by hazard associated with subduction of the Juan de Fuca plate. Average magnitudes and distances at sites of relatively high seismic hazard often differ little from modal values. In most parts of the western US east of the ISB, average distances and magnitudes represent contributions of many faults and historic and/or instrumental seismicity effects, with no particular source strongly controlling the average. In much of the CEUS, modal distances and magnitudes are determined by two major seismic hazards: characteristic earthquakes at New Madrid or Charleston. The domination by these two hazards extends to greater distances for longer period response. The Meers fault (SW Oklahoma) and Cheraw fault (SE Colorado) dominate over small regions. At some locations in the WUS, and more commonly in the CEUS, the influence of local low-magnitude seismicity and regional faults on hazard are relatively balanced. The multi-modal nature of the joint magnitude, distance distribution for such sites poses special challenges for those who use deaggregated hazard analysis to aid in preparation of design spectra.

STRESS DROPS IN EXTENSIONAL REGIMES

BECKER, Ann M., Woodward-Clyde, 7050 Union Park Center, Suite 370, Midvale, UT 84047, ambecke0@wcc.com; ABRAHAMSON, Norman A., Pacific Gas & Electric Company, 245 Market St., Room 410A, San Francisco, CA 94105

We compute Brune stress drops for both normal and strike-slip faulting earthquakes in extensional regimes based on the corner frequency to determine whether significant differences exist. The extensional data include strong motion records compiled by Spudich et al. (1996) and the 1995 Dinar, Turkey earthquake. The resulting set comprises 210 horizontal components from 140 sites in 24 earthquakes, a magnitude range of M_w 5.1 to 6.9, and Joyner-Boore distances ranging from 0 to 102 km.

A two-step inversion process was adopted that decoupled the solution for stress drop ($\Delta\sigma$) from kappa. Weights were applied to estimate the median $\Delta\sigma$ to effectively downweight poorly-constrained individual estimates in earthquakes with few records available for the inversion. Two sets of site amplification functions were used. One is based on profiles with average shear wave velocities in the top 30 m of 620 m/s ('rock') and 310 m/s ('soil'; Boore and Joyner, BSSA 1997). The second set is based on mean transfer functions for rock and shallow soil site profiles combined ('rock') and for deep soil site profiles ('soil'; Silva, pers. comm.).

Both transfer function sets yield similar weighted $\Delta\sigma$ values. Using the Boore-Joyner amplifications, the median values are 47 and 52 bars for normal and strike-slip faulting, respectively. Using Silva's transfer functions, the values are 45 and 59 bars. We conclude that the $\Delta\sigma$ differences between faulting styles are significant. The stress drop differences contribute to reducing ground motions in normal faulting to about 87% of strike-slip motions.

Probabilistic Seismic Hazard and Ground Motions in Alaska

WELLS, D.L., ROSIDI, D., and YOUNGS, R.R., Geomatrix Consultants, Inc., 100 Pine Street, 10th Floor, San Francisco, California, 94111, dwells[drosidi][ryoungs]@geomatrix.com

A new probabilistic seismic source model has been developed to assess ground motion hazard in Alaska. The model includes four types of earthquake sources: plate interface sources, subducted plate (intraslab) sources, crustal faults, and crustal source zones. Interface sources include three east-northeast to northwest-dipping segments of Pacific-North American plate boundary extending from Cape Yakataga to south of Kodiak Island. Intraslab sources include an east-northeast dipping segment and a northwest-dipping segment of the subducted Pacific Plate. Ten crustal faults and fourteen crustal source zones within the North American Plate in central and south-central Alaska also are characterized in the source model, including several alternative models for neotectonic deformation in Cook Inlet and along the Alaska Range. Source characteristics include probability of activity, fault geometry, maximum magnitude, and earthquake recurrence (from geologic slip rates and historic seismicity data). A conditional probability was assigned to the 1964 rupture segment on the interface source.

Site-specific ground motions have been calculated from the source model for two sites, one near Anchorage, and one north of Denali National Park. Ground motions are presently being calculated for a third site near Fairbanks. Attenuation relationships were selected based on consideration of the tectonic environment, earthquake source mechanisms, and site conditions. The results are expressed as equal hazard response spectra for probabilities of exceedence of 5 percent in 50 years and 50 percent in 50 years, for periods ranging from 0.03 to 4.0 seconds. Preliminary analysis of the total hazard shows that for sites near Anchorage and Denali National Park, the peak ground acceleration and 5-percent damped spectral acceleration (at a period of 1.0 second) hazard results generally are dominated by the contribution from the intraslab source. For spectral accelerations of 0.5g or higher at a period of 1.0 second, the hazard is dominated by the plate interface source.

Non-Characteristic Behavior and Complex Recurrence of Large Subduction Zone Earthquakes

SCHWARTZ, S.Y., Earth Sciences Department and Institute of Tectonics, University of California, Santa Cruz, CA, 95064, USA, sschwartz@earthsci.ucsc.edu

The last three years have been remarkable with respect to the number of large underthrusting earthquakes in subduction zones that re-ruptured plate boundary segments that failed in previous great events. Availability of modern seismic data for two consecutive large earthquakes rupturing the same portion of the plate interface provides the opportunity to compare the spatial distribution of moment release for both events. Such comparisons have been made for the plate boundary segments that failed in: 1) the 1957 (Mw=8.6), 1986 (Mw=8.2) and 1996 (Mw=7.9) Aleutian Islands; 2) the 1963 (Mw=8.5) and 1995 (Mw=7.9) Kurile Islands; 3) the 1971 (Mw=8.0) and 1995 (Mw=7.8) Solomon Islands; and 4) the 1968 (Mw=8.2) and 1994 (Mw=7.7) northern Honshu earthquakes. Comparisons of the spatial distribution of moment release for sequential earthquake ruptures reveal considerable differences in the pattern of recurrent fault slip. The 1994 northern Honshu and 1995 Solomon Islands earthquakes primarily fill in areas of slip deficit left by their preceding events rather than re-rupture identical asperities. The 1995 Kurile Islands and the 1996 Aleutian Islands earthquakes both re-rupture portions of an asperity distribution defined by preceding events, but with variable amounts of slip. Although variability in the rupture process of large recurrent circum-Pacific plate boundary events has been suggested based on their timing, size, and spatial extent, this study provides the first direct evidence for their non-characteristic recurrent behavior. Recurrent fault slip for the four plate boundary segments studied does not support characteristic slip models where either failure on an entire fault segment occurs repeatedly in events with nearly identical rupture lengths, locations, and slip magnitudes, or where failure of individual asperities occurs with identical slip functions through consecutive earthquake cycles. These sequential slip patterns are not consistent with physical models of earthquake rutpure where slip complexity is exclusively controlled by invariant geometric and/or material heterogeneity but suggest that dynamic considerations are also important.

The Relationship of Seismicity in the Prince William Sound Region (1964–1996) to the Asperities of the 1964 Great Alaskan Earthquake

VELASQUEZ, M., DOSER, D.I., and VEILLEUX, A.M., Department of Geological Sciences, University of Texas at El Paso, El Paso, TX 79968, monique@geo.utep.edu

Body waveform modeling has been used to determine the focal mechanisms and depths of 18 mb ≥ 5.4 earthquakes occurring within the Prince William Sound (PWS) region between 1964 and 1983, following the Great Alaskan earthquake (Mw=9.2). Our source parameter information is supplemented by Harvard CMT solutions for 17 mb ≥ 4.8 events occurring in the same region between 1977 and 1996. The earthquakes have been relocated using a master event technique. The locations and source parameter information suggest these earthquakes fall into three groups. The first group consists of shallow (depth < 20 km) events with reverse and thrust mechanisms that are located above or on the portion of the megathrust that slipped 5 to 20 m during the mainshock. A second group consists of events with normal fault mechanisms occurring at depths of 30 to 60 km near the base of the Pacific plate. These events are below and immediately to the east of the portion of the megathrust that slipped 20 to 25 m during the mainshock. A third group occurs well downdip of the 1964 PWS asperity at depths of 60 to 100 km within the subducting Pacific plate. The three earthquake groups show temporal differences as well, with 90% of events in the third group occurring after 1974, whereas only 35% of the events in the first two groups occurred after 1974.

Variability of Local Tsunami Runup Relative to M_w

GEIST, E.L., U.S. Geological Survey, Menlo Park, CA 94025, geist@octopus.wr.usgs.gov

Although moment magnitude (M_w) is a good measure of far-field tsunami amplitude, there is substantial variation in local runup with respect to M_w. This variation can be ascribed to differences in rupture width, source depth, and location of slip maxima among events. To demonstrate the effect of these source parameters on the local tsunami, several tsunamigenic, subduction zone earthquakes are examined that have both broadside runup measurements and calculated slip distributions. Those earthquakes for which slip is localized near the updip edge of the rupture zone are more likely to result in higher local tsunami runup than events with broad regions of slip toward the down-dip edge of the rupture zone. Analysis of local runup measurements from subduction zone earthquakes indicates that local runup is consistently higher relative to M_w for tsunami earthquakes in comparison to other tsunamigenic events. Several characteristics of tsunami earthquakes explain the local runup anomaly with respect to M_w. First, tsunami earthquakes rupture the shallow part of the interplate thrust in relatively deep water, resulting in greater amplification due to shoaling than typical subduction zone earthquakes. Second, tsunami earthquakes are associated with higher amounts of slip with respect to M_w than other tsunamigenic earthquakes, possibly relating to rupture of the seafloor. Third, the rupture width of tsunami earthquakes is generally shorter than typical subduction zone events, corresponding to higher leading wave steepness and higher runup. Therefore, the unique source parameters of tsunami earthquakes, including deep water depth in the source region, higher slip, shallow source depth, and smaller rupture width are indicative of higher local runup with respect to M_w in comparison to other tsunamigenic earthquakes.

Investigation of Regional and Site Attenuation Characteristics in the Bursa City, Northwestern Anatolia, Using the Acceleration Records of Micro-Earthquakes

AKINCI, A., University of Saint Louis, Earth and Atm. Sci. Dept. 3507 Laclede Ave. St. Louis, MO, 63103, USA, akinci@eas.slu.edu. EYIDOGAN, H., Istanbul Technical University, Faculty of Mining, Dept. of Geophysics, Maslak, Istanbul, 80626, TURKEY, eyidogan@sariyer.cc.itu.edu.tr

The ancient part of Bursa city was located on the foothills of the Uludag mountain, but in recent years city has being grown in Bursa basin, which is filled with Quaternary deposits. Istanbul Technical University and ETH of Zurich installed 5 acceleographs in the vicinity of Bursa city on different type of geological sites and operated them during 1992–1997. 77 earthquake records that had a high S/N ratio were used for this study. The hypocentral distances of studied earthquakes range between 1 and 20 km and the magnitudes range between 1.5–3.5. Only S wave acceleration spectra of micro-earthquakes were analysed to investigate characteristics of the regional, near surface (site effect) attenuation and source parameters.

The avarage frequency dependent coda Q was obtained as $Qc(f)=40f^{0.84}$ for a shortxh lapse times by using Single Scattering Model (Aki&Chouet, 75). Assuming the Qc is proportional to Qs (Aki, 80) and presents frequency dependent regional attenuation, the observed S wave acceleration spectra of the local earthquakes were corrected for this value. Fall-off rates of corrected spectra were still found high at some stations than those that have been estimated for Brune and Aki source models (*e.g.,* W^{-2}, W^{-3}. In comparison to the observations at SIGD station, located on hard-rock site, the high fall-off rates can be explained by the attenuation mechanism generated at the shallow structure under some particular station sites (*e.g.,* SHMT, SHMK, SDEM).

We determined kappa which represents the site attenuation from the slope of the asymptotic spectral decay for each spectrum in the frequency interval between corner frequency and 30Hz. The calculated kappa values vary in the range of 0.0062–0.022 s for all stations and increase from rock sites to soil sites. The avarage acceleration spectrum obtained for the SIGD station which locates on the thick Permian limestone, did not show any important site attenuation effect and the best fitting to observed spectra is found for (W^{-2}).

We have also calculated the amplification ratios for all the stations using Nakamura (1989)'s method that does not require a reference station. It is found that the spectral ratio of H/V S waves recorded on the rock site (*e.g.,* SKAY, SIGD) approaches to unity while the sedimentary sites (SHMT, SDEM, SHMK) showed considerable amplification for particular frequencies.

An Energy-Based Motion Parameter for Probabilistic Determination of Scenario Earthquakes

CHAPMAN M.C., Department of Geological Sciences, Virginia Tech, Blacksburg, VA, 24061 chapman@vtso.geol.vt.edu

Amplitude and duration of strong motion are important considerations for engineering analysis. However, duration is not modeled routinely in seismic hazard assessments. Probabilistic assessment based on elastic input-energy may prove useful in the identification of scenario events, because input-energy depends on duration and amplitude. To investigate this application, regression models are derived for the elastic input-energy spectrum using data from western U.S. earthquakes. Those results are compared with PSV response spectra derived from the same data set, in terms of effect on de-aggregated seismic hazard for generalized cases.

Similar regression models are used for PSV spectra and equivalent velocity spectra derived from the absolute and relative input-energy spectra. Variances of the regressions systematically decrease with increasing oscillator frequency in the range 0.5 to 5 Hz. In that frequency range, variance associated with the energy parameter is slightly smaller than for PSV. Response differences due to NEHRP site class are largest at the lowest frequencies, for both energy and PSV models. The energy models are almost independent of site class for frequencies greater than approximately 4 Hz. The energy models show stronger dependence upon earthquake magnitude, compared to PSV: the ratio of the equivalent velocity spectral amplitudes to the PSV amplitudes increases with magnitude. Also, that ratio increases with distance for frequencies in the range 0.5 to 7 Hz. These results are attributable to duration of shaking. The effect upon hazard is such that larger, more distant earthquakes typically contribute significantly more to the total hazard, for any given return period, when the hazard model is based upon the energy parameter, rather than PSV. This effect is most pronounced at the higher oscillator frequencies, in the range 3 to 10 Hz.

Geologic Hazards Evaluation of the U.S. Military Academy, West Point, New York

ROSIDI, D., WELLS, D.L., and EGAN, J.A., Geomatrix Consultants, Inc., 100 Pine Street, 10th Floor, San Francisco, California 94111, drosidi[dwells][jegan]@geomatrix.com

Potential earthquake-related geologic hazards, including surface-fault rupture, liquefaction, differential compaction, landsliding, and flooding, were evaluated for the habitation area of the U.S. Military Academy (USMA) using conservative screening and simplified evaluation procedures. The study was conducted using only existing data, including boring logs, groundwater data, geologic maps, and aerial photographs, in conjunction with brief site reconnaissance. This study assessed whether 1) significant (life-threatening) hazards do not exist; 2) significant hazards may exist but additional data are required to evaluate them; or 3) significant hazards exist and hazard mitigation should be considered. Geologic hazards were evaluated on the basis of ground motions developed from a site-specific probabilistic seismic hazard analysis.

No evidence of Quaternary displacement was identified for any faults near the USMA. Subsurface materials in the habitation area typically comprise rock, dense soils, or clayey soils that are not susceptible to liquefaction. Where soils susceptible to liquefaction are present, a liquefaction potential analysis indicates that surficial soil deposits generally are not expected to liquefy under the ground motion levels considered. While localized liquefaction may occur at some sites, it is not expected to result in a significant hazard to any structures. Analysis of the settlement potential of soils indicates that there is no significant differential compaction hazard. No significant flooding hazard resulting from tectonic movements, seiches, landslides, or dam failure was identified.

Four types of potential landslide hazards were identified for the habitation area: toppling failures on rock slopes steeper than 1:1.5 (horizontal:vertical), landsliding of boulders or rock masses on slopes steeper than 1.5:1, rotational soil slides on slopes steeper than 1.5:1, and subsidence of filled areas along the Hudson River. Based on these criteria, a potential landslide hazard exists for several structures located at the base of the bluffs along the Hudson River.

Probabilistic Ground Motion Hazard Analysis for the State of Oklahoma

LAFORGE, R., Seismotectonics and Geophysics Group, U.S. Bureau of Reclamation, Denver, Colorado, 80225

Probabilistic ground motions for the state of Oklahoma were developed as part of risk assessments for seven federal dams. The seismic hazard was modeled as three zones of random seismicity and the Meers fault. The zones of random seismicity were defined solely on the basis of historic seismicity patterns, and bear little relation to known geologic structures. Eastern and western zones consist of

large areas of relatively low-level, spatially homogeneous activity. A narrow zone in the mid-to-south central part of the state contains three clusters of activity, the northernmost of which is the location of the mb 5.0 1952 El Reno event. Maximum magnitudes of mb 6.0 were estimated for the eastern and western zones, and mb 6.5 for the central zone.

The Meers fault is the only North American surface fault east of the Rocky Mountain front known to have experienced Holocene rupture. Its occurrence behavior was modeled as Poissonian, at a rate of two Mw 7 events per 10,000 years. Considering its pre-Holocene quiescence of several hundred thousand years, the fault was assigned a 70% probability of being active for the life of the dams.

A probabilistic seismic hazard analysis was performed for each dam based on earthquake recurrence statistics developed for the three zones and the Meers fault, incorporating uncertainties in seismicity rates and ground motion attenuation. The attenuation relations of EPRI (1993) and Atkinson and Boore (1995) for rock sites were used. Results consist of hazard curves for peak acceleration and response spectra for various return periods.

Wednesday, 8:30 AM–5:00 PM
Glenn Miller Ballroom
Posters
Intraplate Seismotectonics

Determination of *RMS Lg* values and seismic energy for regional earthquakes in northeastern United States

Jinghua Shi, Won-Young Kim, and Paul G. Richards, Lamont-Doherty Earth Observatory of Columbia University, Palisades, NY 10964

We analyzed the property of *Lg* waves in terms of *RMS Lg* (root mean square value of *Lg* wave amplitude within a certain group velocity range), especially the stability of *RMS Lg* values for natural earthquakes, in order to develop a physically-based magnitude scale that improves upon current procedures. From 52 regional earthquakes, we measured *RMS Lg* values from the observed vertical-component *Lg* signals across a wide frequency range that well covers most of the seismic energy radiated into *Lg* waves. The *RMS Lg* values for the events with epicentral distances (Δ) up to 900 kilometers decrease with Δ like $\Delta^{-1.18}$ after correcting for anelastic frequency-dependent attenuation. The correlation between single station's distance-corrected *RMS Lg* yields very low standard deviation, with orthogonal regression slope near 1, indicating excellent consistency and stability. For the events we analyzed, the network averaged Log_{10}(*RMS Lg*) values have better correlation with Log_{10}(seismic moment) than with body wave or coda wave magnitudes. Hence, *RMS Lg* can be used to develop a magnitude scale which is a good complement to seismic moment magnitude.

Seismic energy is a physical concept related to the broadband information of the earthquake source. Improved estimates of seismic energy can improve the scientific framework for interpreting observed seismicity in terms of physical source processes. *RMS Lg* amplitude is proportional to the square-root of *Lg* wave radiated energy flux, a good quantity in estimating the energy release of regional earthquakes. From both observational and synthetic seismograms, we obtained the absolute scaling of the total seismic energy with the measured *Lg* wave energy in terms of *RMS Lg*. By interpreting synthetic seismograms from different source types and velocity models, it is found that different velocity structure has an effect on the efficiency of *Lg* wave radiation. The radiation of *Lg* wave energy varies if the source moves in different layers, but has no significant dependence on the source depth for events located in the same layer. The vertical strike-slip source tends to radiate less *Lg* wave energy than other source types.

Paleoseismicity: Seismicity Evidence for Past Large Earthquakes

EBEL, J.E., Weston Observatory, Department of Geology and Geophysics, Boston College, Weston, Massachusetts, 02193, ebel@bc.edu, BONJER, K.-P. and ONCESCU, M.C., Geophysical Institute, University of Karlsruhe, 76187 Karlsruhe, Germany

Clusters of earthquakes in continental intraplate regions are used to estimate the times and magnitudes of past earthquakes in a model we call "paleoseismicity." The time of a past earthquake is estimated from an Omori-law decay of aftershocks with time, while the magnitude of the earthquake is inferred from the length of the current zone of seismic activity. The aftershock decay rates of a number of recent continental, intraplate earthquakes from North America and Europe were determined. While some of the events had relatively active aftershock sequences and others had few aftershocks, the range of aftershock decay rates are similar to those reported from California. Using parameters derived for average aftershock decays, we find that the earthquake activity in the main New Madrid seismic zone and in the Charleston, SC areas could be regarded as aftershocks of the major events in 1811–1812 and 1886, respectively. We have applied the paleoseismicity model several localities in northeastern North America and in western Europe to estimate the possible dates and magnitudes of past strong events.

Seismograms Recorded by New England PEPP Stations

KAFKA, A.L., HONKONEN, A., RUSZCZYK, E., STROTHER, P.K., and COCHRANE, L., Weston Observatory, Dept. of Geology and Geophysics, Boston College, Weston, MA 02193, kafka@bcvms.bc.edu; Lincoln-Sudbury Regional High School, Sudbury, MA 01776, anita_honkonen@lsrhs.net; New Canaan High School, New Canaan, CT 06840, eruz@aol.com; Weston Observatory, Dept. of Geology and Geophysics, Boston College, Chestnut Hill, MA 02193, strother@bc.edu; Public Seismic Network, Redwood City, CA 94002, cochrane@webtronics.com.

Four Princeton Earth Physics Project (PEPP) seismic stations have been installed in New England, and one more installation is planned. The instrument response is flat to velocity from 0.033 Hz to either 10 Hz or 50 Hz (depending on the site). To date, two of the four stations have been routinely recording earthquakes. The other two are experiencing technical difficulties, but are expected to be recording earthquakes soon.

The two stations that have recorded earthquakes are PPLSR (located at Lincoln-Sudbury High School in Sudbury, MA) and PPNCA (located in New Canaan High School, in New Canaan, CT). Some examples of earthquakes that we have recorded are:

Date	*Magnitude*	*Location*
11/08/97	7.9 (M_S)	Xizang, Tibet
11/09/97	5.5 (m_b)	El Salvador
11/29/97	5.2 (M_S)	Near coast of Nicaragua
12/05/97	7.7 (M_S)	Near coast of Kamchatka
12/22/97	5.1 (m_b)	Guerrero, Mexico

We have focused our efforts on getting the stations up and running, rather than on optimal siting of the sensors (which we plan to begin working on in the spring). Thus, the sensors that recorded these earthquakes are located on the floor inside the buildings, PPLSR on a first floor and PPNCA on a second floor. In spite of the high frequency noise generated in and around the building, we have been able to obtain rather high quality waveforms of the earthquakes by band-pass filtering the seismograms between about 0.01 Hz and 1.3 Hz. Both the raw data and the filtered records provide opportunities for teachers to demonstrate many of the principles of seismology to their students. We have also downloaded waveforms from nearby USNSN stations in MA (station HRV) and in NH (station LBNH), and we compare and contrast the signals recorded at our New England PEPP stations with signals recorded by the USNSN stations.

Focal Mechanism and Source Parameters of the 1997 November 6, Quebec Earthquake

KIM, Won-Young, Lamont-Doherty Earth Observatory of Columbia University, Palisades, NY 10964, USA, wykim@ldeo.columbia.edu

On November 06, 1997 (02:34 GMT), an earthquake of magnitude M_L = 4.7 occurred near Quebec City, Quebec, Canada. The earthquake was felt around Quebec City and Saguenay region in southern Quebec. Even though the event was a moderate sized one, seismic signals from the event are well recorded by numerous seismographic stations in North America and as far away as some quiet stations in northern Kazakstan (distance about 75°). This underscores an important opportunity that will arise from the recent deployment of about 50 primary and over 100 auxiliary network stations of the International Seismic Monitoring System for CTBT, and their possible contributions to earthquake researches, in particular, to study small to medium sized events occurring in intraplate regions worldwide.

We analyzed teleseismic *P* waves from the Quebec earthquake and determined focal depth and source mechanism by using teleseismic body-wave waveform inversion. The best fit waveforms constrain the focal depth at 22 km for a point source with a simple triangular source time function. The best double couple solution shows a predominantly thrust motion with a substantial right-lateral strike-slip component along a nodal plan with strike = 321°, dip = 53°, and rake = 135°. The scalar seismic moment is 6.61E+22 dyne-cm, which yields a moment magnitude, $\mathbf{M}$ = 4.5.

The earthquake is also very well recorded by 57 regional broadband stations of the United States National Seismographic Network (USNSN) and the Canadian National Seismographic Network (CNSN) in North America. The displacement amplitude spectra of the transverse component *Lg* waves at 10 stations in the distance range 100 to 1000 km are used to determine source spectrum corner frequency and seismic moment. The spectral analysis of *Lg* waves yields the corner frequency=3.1 Hz and the seismic moment=5.4E+22 dyne-cm, and hence, corresponding stress-drop is about 300 bar.

Source Studies of Seismic Events in North America using Broadband Data Recorded by the United States and Canadian National Networks

THIO, H.K., SAIKIA, C.K., Woodward-Clyde Federal Services, Pasadena, Ca 91101, hkthiox0@wcc.com

We are studying the source parameters of seismic events in North America using broadband data recorded by the United States and Canadian National Seismic Networks. Recent moderatre sized earthquakes that occurred within the stable continental interior of North America, i.e Alabama (97/10/24) and Quebec (97/11/06), have emphasized the importance of the National Networks for real-time earthquake analysis as well as the potential for significant earthquakes in parts of North America that are not considered to be seismically active.

Intermediate and short-period surface wave inversion has proven to be a very effective tool for analyzing source parameters at regional distances in many parts of the world. We have studied some recent earthquakes in North America using this method, including the 1995 Texas earthquake, and the aforementioned Alabama and Quebec events. Our preliminary results are consistent with other observations, and demonstrates the usefulness of this approach for events in Eastern North America. We are currently refining this method for routine use by including laterally varying phase velocity models for propogation corrections and by regionalizing the excitation functions.

A Noteworthy Earthquake in an Unlikely Place

GOMBERG, J., U.S. Geological Survey, Campus Box 526590, Memphis, TN 38152, gomberg@usgs.gov; WOLF, L., Auburn University, Auburn, AL 36849; RAYMOND, D., Geological Survey of Alabama, P.O. Box O, University Station, Tuscaloosa, AL 35486; RAYMOND, R., State Oil and Gas Board of Alabama, P.O. Box O, Tuscaloosa, AL 35486-9780; BARNES, A., Auburn University, Auburn, AL 36849; CARVER, D., BICE, T., CRANSWICK, E., MEREMONTE, M., FRANKEL, A., OVERTURF, D., HOPPER, M., RHEA, S., U.S. Geological Survey, MS 966, Box 25046, Denver Federal Center, Denver, CO 80225; ECKHOFF, O., 701 Williams Ave., B-4, P.O. Box 277, Picayune, MI 39466

On October 24, 1997 a M4.9 earthquake occurred in the Coastal Plain of southwest Alabama. A rapid response to the event was executed by the USGS, IRIS, Auburn University, the Geological Survey of Alabama, the Alabama State Oil and Gas Board, and the Escambia County Emergency Management Agency. The October 24 earthquake was preceded by one felt foreshock in May and followed by more than ten smaller aftershocks, two of which were felt. Although not damaging, this earthquake sequence was noteworthy because earthquakes of this magnitude are unprecedented in the southeastern U.S.. Only two modern earthquakes (M3.0–3.5 in 1974 and May, 1997) are documented within ~100 km of the epicentral area. Historical records report an earthquake near Pensacola in 1789 with MMI 6, although a concurrent hurricane makes reporting uncertainties significant. Aftershocks were recorded within a few km of their epicenters by a temporary network deployed following the mainshock. These recordings provide the first in situ ground motion data in this part of the southeastern U.S. and now make it possible to evaluate ground motion and source models. A thorough intensity survey provides complementary data for mainshock characterization and for site response studies. Preliminary epicentral locations, based on instrumental and intensity data, show that the earthquakes most likely occurred on a segment of the Pollard fault system which provides structural control for hydrocarbon reservoirs. The Pollard fault system occurs at the updip limit of the Jurassic Louann Salt; movement and removal of Louann Salt resulted in formation of the Pollard fault zone and down-to-the-Gulf basement faults. The epicentral region includes the Big Escambia Creek, Sizemore Creek and Little Rock production fields where gas is extracted from depths as great as 4.6 km, just above basement. Two injection wells (depths of 2.1 km) located within ~5 km of the epicenters have been operated since the 1970s. Any relationship between oil and gas production and the earthquake is thus far indeterminate and is the subject of further investigation.

AFTERSHOCK INVESTIGATION OF THE OCTOBER 24, 1997, EARTHQUAKE NEAR ATMORE, ALABAMA

CARVER, D., BICE, T., CRANSWICK, E., MEREMONTE, M., GOMBERG, J., FRANKEL, A., RHEA, S. and OVERTURF, D.
U.S. Geological Survey, Geologic Hazards Team, MS966, Box 25046, DFC, Denver, CO 80225, carver@usgs.gov

Starting 22 hours after the mainshock, we deployed an array of portable seismographs to record aftershocks of the October 24, 1997, Atmore earthquake (mb 4.9) in southern Alabama where there are no local and few regional permanent seismograph stations. Initially we installed two RefTek seismographs operating in continuous record mode, four Kinemetrics K2 accelerographs operating in triggered mode, and two MEQ-800 continuous analog seismographs running at 72 dB to monitor the activity. No aftershocks occurred for 62 hours after the mainshock, so the first six recording sites were chosen using intensity information from interviews of residents in an area near the NEIC preliminary location of the mainshock. That array configuration later proved to only cover azimuths northwest clockwise through southeast from the aftershocks. After we had recorded and located the first aftershocks, we installed four more RefTek seismographs sent by IRIS to cover the southeast through northwest quadrants. The digital array detected a total of 15 aftershocks at two or more sites and recorded five aftershocks with four stations or more. The largest aftershock, a mb 3.7 event on October 26,1997, was recorded at 0.03g peak-to-peak. We operated an eleven-station array for 42 days following the mainshock and a four station array continued to monitor the epicentral area for about 100 days. We are currently locating the earthquakes and will present the hypocenters and focal mechanisms at the meeting.

ANALYSIS OF LOCAL AND REGIONAL SEISMOGRAMS OF THE 1997 SOUTHERN ALABAMA EARTHQUAKE SEQUENCE: SOURCE PARAMETERS, SITE RESPONSE, AND CRUSTAL PROPAGATION

FRANKEL, A. , CARVER, D., CRANSWICK, E., MEREMONTE, M., GOMBERG, J., BICE, T., RHEA, S., and OVERTURF, D.
U.S. Geological Survey, Geologic Hazards Team, MS 966, Box 25046, DFC, Denver, CO 80225, afrankel@usgs.gov

We are analyzing local and regional seismograms of the October/November 1997 southern Alabama earthquake sequence (mainshock m_b 4.9). We use spectral ratios from regional seismograms (R > 300 km) to determine the source corner frequencies and stress drops of the mainshock, pre-shock, and larger aftershocks. Spectral ratios and empirical Green's function deconvolution of the locally-recorded (R < 20 km) seismograms are used to ascertain the corner frequencies, pulse widths, and stress drops of the aftershocks. Local recordings of the two largest aftershocks (m_{bLg} 3.7 and 3.0) show azimuthally-dependent spectral amplitudes and corner frequencies that are likely caused by source directivity. Our preliminary estimate of the stress drop of the mainshock is about 60 bars. The largest aftershocks appear to have lower stress drops than the mainshock. We invert spectra from the locally-recorded seismograms to determine site response for these sites on the Gulf coastal plain. Comparison of regional and local recordings reveals how the frequency content of L_g waves relates to the source spectra of the earthquakes. This is useful for determining the transfer function of L_g wave propagation and the Q of the crust in the southeast U.S.

Faulting Parameters of the October 24, 1997 Southern Alabama Earthquake

CHANG, T.M., AMMON, C.J., and HERRMANN, R.B., Department of Earth and Atmospheric Science, Saint Louis University, St. Louis, MO 63103, changt@mnw.eas.slu.edu

The October 24, 1997 Alabama earthquake (31.2N, 87.3W, 08:35:16.7UT) occurred in a region of historically low seismicity. In this study, we estimate the faulting parameters (strike, dip, slip, depth, and seismic moment) using surface-wave radiation pattern grid searches, regional-waveform moment-tensor inversion, and teleseismic P-waveform modeling. Modeling Rayleigh- and Love-wave fundamental mode spectral amplitudes observed at about 40 seismic stations using a grid search algorithm, we identified faulting parameters that generate consistent Rayleigh and Love-wave spectral amplitudes in the period range from 5 to 60 seconds. Specifically, we used a two-stage search (a 5 degree crude search followed by a 2 degree fine search) and repeated the procedure for a range of trial source depths. To complement the surface-wave spectral amplitude search, which nicely constrains the event depth but allows some ambiguity in the faulting mechanism, we inverted complete, three-component regional waveforms using observations from the 10 nearest broadband seismometers. These observations span a range of 120 degrees in azimuth, and prior to inversion, were low-pass filtered to include periods longer than 20 seconds to minimize the effects of unkown earth structure on the results. We then used teleseismic P waveform observations from 17 vertical, short-period seismometers of the Yellowknife Array in northwest Canada to confirm the results of the spectral amplitude and regional waveform inversions. Our preferred solution is strike, dip, rake angles of 94, 62, and –90 degrees, respectively with Mw = 4.9 at 4.5 km depth, indicative of shallow north-south extension.

Three Dimensional P-Wave Velocity Structure for the New Madrid Seismic Zone

VLAHOVIC, G., POWELL, C., Department of Geology, UNC Chapel Hill, Chapel Hill, NC 27599-3315, vlahovic@geosci.unc.edu, cap@geosci.unc.edu, and CHIU J.-M., Center for Earthquake Research and Information, University of Memphis, Memphis, TN 38152, chiu@ceri.memphis.edu.

A new 3-D P-wave velocity model for the New Madrid seismic zone was determined using an iterative, tomographic inversion code developed by Benz et al. (1996). In each iteration, the P-wave velocity model was determined then hypocenters were computed using P and S wave arrival times. The S wave velocity model was determined from the P-wave velocity model and specified Vp/Vs ratios. The initial data set consisted of 925 regional earthquakes providing 8,661 P-wave and 8,887 S-wave arrivals recorded by PANDA stations between 1989 and 1992. Results were compared with known potential field anomalies.

The resolving power of our data was tested by inversion of a synthetic data set. The synthetic velocity model consisted of blocks with 6% velocity anomalies arranged in a chess board pattern and embedded in the 1-D model determined for the region by Chiu (1992). The synthetic tests allowed smoothing parameters to be chosen that resolved the amplitude of the synthetic anomalies and minimized vertical smearing.

The inversion results, using the chosen smoothing parameters, imaged velocity anomalies of less than 10%. Maximum rms improvement was about 25%. Strongest velocity anomalies occur below shallow sediments. The upper few km are characterized by lower than average velocities along the trend of seismicity and isolated high velocity anomalies that correlate with gravity highs. Most earthquakes occur between 5 and 15 km depth and are associated with the boundaries between low and high velocity anomalies. A cross section along the major NW - SE trend of seismicity indicates that seismicity dips beneath imaged high velocity bodies.

The robustness of the 3-D solution was tested using different 1D velocity models. The choice of Vp/Vs ratios proved to be critical for resolution in the top few kilometers of the model. A very high Vp/Vs ratio of 3 for the top layer (representing unconsolidated sediments) produced a strong positive anomaly in the poorly resolved SW part of the model that does not correspond to observed gravity anomalies. Inversion with a Vp/Vs ratio less than 2.5 for the top layer and a constant Vp/Vs ratio of 1.73 for lower layers produces results in better agreement with those obtained using only P-wave arrival times.

APPLICATIONS OF MODERN, GIS-BASED, SEISMOTECTONIC MAPS

WHEELER, Russell L., RHEA, Susan, and DIEHL, Sharon F., USGS, Box 25046, MS 966, Federal Center, Denver, CO 80225, wheeler@gldvxa.cr.usgs.gov.

Seismotectonic (ST) maps are tools for generating ideas about seismogenesis by showing compilations of previously scattered data that, when examined together, can reveal spatial associations that lead to testable hypotheses about geologic controls on seismicity. GIS technology allows modern ST map folios and their equally valuable digital databases to include an order of magnitude more data than could be shown on hand-drafted, single-sheet ST maps. While making ST map folios of the New Madrid and Wabash seismic zones in the central U.S., we and others made the following observations that illustrate the value of the maps. (1) Magnetotelluric and aeromagnetic analyses led to two different estimates of the locations of graben margins in the Reelfoot Rift. An ST map shows that the two methods detected tops and bottoms, respectively, of the same step-faulted margins, thereby resolving the discrepancy. (2) Fault traces mapped at the surface and on a deep unconformity allowed us to estimate the shapes and locations of large faults at hypocentral depths. (3) Scattered seismicity near the NNE-trending Wabash Valley Fault System (WVFS) was attributed to the WVFS as a possible northward extension of the NE-trending Reelfoot Rift. However, an ST map shows that the deep, sparsely seismic Rough Creek Graben trends E between the rift and the WVFS, and that the faults of the WVFS do not intersect the large northern border fault of the Rough Creek Graben. Thus, the WVFS is probably decoupled from the Reelfoot Rift. See the poster for more examples. We suggest that ST maps are most useful in seismically active areas that have few or no surface ruptures to indicate which faults might be active. Thus, future ST maps are most likely to benefit work in Cascadia, New England, the Illinois Basin, the Western Quebec seismic zone, eastern Tennessee, Charleston, SC, and Charlevoix, Quebec.

Wednesday, 8:30 AM–5:00 PM
Glenn Miller Ballroom
Posters
Explosion and Impact Event Analyses and Monitoring

MONITORING MINE EXPLOSIONS IN THE CONTERMINOUS U.S.

Dewey, J. W., U. S. Geological Survey, MS 966, Federal Center, Denver, CO 80225, dewey@usgs.gov.

We have begun applying routine USGS/NEIC earthquake detection and location methodologies to monitor mine explosions in the conterminous U.S. Explosions from mines and quarries in the conterminous U.S. are frequently detected by seismographs of the U.S. National Seismograph Network (USNSN) and other cooperating networks, and are recorded in near real-time at the USGS/National Earthquake Information Center (USGS/NEIC). The USGS/NEIC has historically dealt with mine explosions by identifying them at an early stage of analysis and not analyzing them further, but beginning in late 1998 the USGS/NEIC will routinely catalog large U.S. mine-blasts as a confidence-building measure in the context of the Comprehensive Test Ban Treaty.

Suspected U.S. mine explosions occurring in May-October, 1997, have been located and assigned magnitudes. During the half-year study period, 453 presumed mine explosions having $M \geq 2.0$ were located; half of these had $M \geq 2.5$. Catalogs of the located explosions and maps of their locations are available on the World-Wide Web (http://earthquake.usgs.gov/neis/mineblast/).

Most of the located explosions occurred in the central Appalachians of West Virginia and adjacent states and in the Rocky Mountain West from Wyoming southward. The location procedure used in this study did not detect explosions from some important surface-mining districts, such as the northern Great Lakes iron-mining districts, Texas coal-mining districts, and southern Appalachian coal mining districts. Our failure to detect explosions from these active mining districts is probably a consequence of the low sensitivity of the USNSN for events in these areas. On the basis of USGS/NEIC experience with small earthquakes, explosions in these regions that have magnitude 3.0 or slightly larger could have escaped detection by the network of seismographs that recorded at the USGS/NEIC during the time-period of the study. The resolution of the location process, as estimated by the semi-axes of 90 percent confidence ellipses on the epicenters, also varied dramatically for different mining districts within the conterminous U.S., again reflecting the configuration of recording seismographs. We will report on special studies to understand the nature of mine-explosion activity in districts from which events are poorly detected or located by the routine USGS/NEIC procedures.

THE SEISMIC SIGNAL STRENGTH OF CHEMICAL EXPLOSIONS, AND MAGNITUDE DISTRIBUTIONS OF MINE BLASTING ACTIVITY IN DIFFERENT REGIONS

Vitaly I. Khalturin, Tatyana G. Rautian and Paul G. Richards[1]
Lamont-Doherty Earth Observatory of Columbia University
Palisades, NY 10964, richards@LDEO.columbia.edu
([1]also, Dept. of Earth and Environmental Sciences, Columbia Univ.)

We have compared the seismic magnitude of a wide variety of chemical explosions to the magnitude expected for explosions set off in hard rock under conditions most favorable for generating strong seismic signals. We define the deficit of an explosion, as this largest magnitude, minus the actual magnitude. In practice, the deficit is found to be around 1.5 to 2 magnitude units, for the great majority of explosions.

We have also obtained data on regional magnitude for several thousands of chemical explosions in more than 30 mining regions worldwide, and have used these data to provide summaries of the numbers of chemical explosions likely to be of interest in monitoring compliance with the Comprehensive Test Ban Treaty. We find that few mining regions carry out blasting associated with seismic signals above magnitude 3.5. In the United States, there are about 10 mining blasts per year with magnitude greater than 3.5. In Russia, there are about 100 blasts per year with magnitude greater than 3.5. Most of them, are associated with the Kuzbass and Abakan mining regions in Western Siberia.

The 16 August 1997 Novaya Zemlya Seismic Event as Viewed from GSN Stations KEV and KBS

HARTSE, H.E., Geophysics Group, Earth and Environmental Sciences Division, MS C335, Los Alamos National Lab, Los Alamos, NM 87545, hartse@lanl.gov.

Using current and historic seismic records from Global Seismic Network stations KEV and KBS, I find that S-minus-P time comparisons between nuclear explosions and the 16 August 1997 seismic event (mb near 3.6) from near Novaya Zemlya clearly indicate that (relative to KEV) the 16 August event occurred at least 80 km east of the Russian test site. Including S-minus-P arrival times from KBS constrains the location to beneath the Kara Sea and in good agreement with previously reported locations, over 100 km southeast of the test site. From an analysis of Pn/Sn waveform ratios at frequencies above 4 Hz, I

find that the 16 August event falls within the population of regional earthquakes and is distinctly separated from Novaya Zemlya and other northern Eurasian nuclear explosion populations. Thus, given its location and waveform characteristics, I conclude the 16 August event was an earthquake. The 16 August event was not detected at teleseismic distances, and thus, this event provides a good example of the regional detection, location, and identification efforts that will be required to monitor the Comprehensive Test Ban Treaty below about mb 4.0.

Regional recordings of the 1997 Kazakhstan Depth of Burial Experiment

Stephen C. Myers, William Walter, Kevin Mayeda, and Lewis Glenn.
Geophysics and Global Security Division, Lawrence Livermore National Laboratory
L-206, Livermore, CA 94550, myers@s42.es.llnl.gov

In August and September of 1997 three, 25-ton, chemical explosions were detonated at nominal depths of 550 m, 300 m and 50 m in boreholes at the former Soviet test site in Balapan, Kazakhstan. Detonation of these explosions was a joint effort between the U.S. Department of Energy (DOE), the U.S. Defense Special Weapons Agency (DSWA) and the National Nuclear Center of the Republic of Kazakhstan (NNC). The explosions were recorded on broadband and short period seismic stations at regional distances (between ~100 and ~1000 km from the explosions). All three explosions were well recorded out to about 700 km.

One objective of this experiment was to evaluate the effect of differing source depth on the regional wavefield. Two observations are presented here: 1) at frequencies near Hz, overall seismic amplitudes of the shallowest shot are several times the amplitude of the deeper shots; 2) P/S amplitude ratios near 1 Hz suggest increased S-wave excitation for the shallow shot. The trend of both decreasing overall amplitude of regional phases and relative decrease in S-wave excitation with depth are also observed for the 300 m and 550 m shots; however, the differences between the deeper shots are not as dramatic as they are between the 50 m and the deeper shots. At frequencies greater than about 6 hz the differences in the P- and S-wave amplitudes are not as evident for the three shots, suggesting a frequency dependence. These observations have particular importance for both the estimation of magnitude (yield) and the application of P/S amplitude ratios as a discriminant for source type. If a non-depth-dependent source is assumed, the greater amplitude of the shallow shot would falsely predict greater explosive yield. Additionally, these observations predict increased variance for P/S ratios when very shallow and deep shots are mixed.

Field observations at the time of shot detonation document that a ~30 m diameter crater was created by shallow shot, whereas the deeper shots did not produce such dramatic surface expressions. A possible explanation for the disparity between the seismic recordings of the 50 m and deeper shots is that the reduced overburden pressure of the shallow shot allowed considerably greater particle displacement. Additionally, the asymmetric displacement documented by the crater may cause increased S-wave excitation.

Work performed under the auspices of the U.S. Department of Energy by Lawrence Livermore National Laboratory under contract W-7405-ENG-48.

Analysis of Seismograms from the Atmospheric Impact of the El Paso Bolide (October 9, 1997)

DOSER, D.I., Dept. Geol. Sciences, Univ. Texas at El Paso, El Paso, TX 79968, doser@geo.utep.edu; CHAEL, E.P., Sandia Laboratories MS 0655, PO Box 5800, Albuquerque, NM 87185, epchael@sandia.gov; BAKER, M.R., Geomedia Res. and Devel., 6040 S. Strahan, El Paso, TX 79932, mbaker7@compuserve.com

On October 9, 1997 at 18:47:15 a bolide impacted the atmosphere at an altitude of ~36 km near the city of El Paso. The shock wave from the impact was heard throughout the border region and a fireball large enough to cast discernable shadows was observed. Over 10 seismograph stations operating in west Texas and southern New Mexico recorded the atmospheric impact. Unfiltered, digital broadband and analog recordings at El Paso (EPT, the station nearest the impact) show two distinct pulses of energy release. Using altitude and origin time constraints from DoD satellites and a constant sonic velocity of 295 m/s we obtain a location of 31.75N, 105.93W, but with large residuals (up to 40 sec). Fixing only the origin time, gives smaller residuals (<10 sec), a lower altitude (25–30 km) and a location of 31.80N, 106.06W. We are currently attempting to locate the impact using a model that allows for velocity anisotropy within the atmosphere, to account for wind effects. We also plan to analyze the broadband records showing multiple pulses of energy release and to examine the amplitude decay of the shock wave with distance. These studies will give us insight into how seismograph recordings can be better utilized to study atmospheric impact and explosion phenomena.

A Comparison of Seismic Signals from Several Bolide Events

CHAEL, E.P., Sandia National Laboratories, Albuquerque, NM 87185, epchael@sandia.gov

At least 15 examples of bright meteors or bolides producing seismic signals have been documented. Unusual events such as these are likely to attract increased attention in coming years, as the international community begins monitoring atmospheric explosions for CTBT verification. Because the planned infrasound network is relatively sparse, with only 60 stations worldwide, data from the far more numerous seismic stations could contribute to the analysis of events in the atmosphere. Three distinct types of seismic signals from meteors can be identified. In the majority of cases, the observed arrival corresponds to the air wave produced by the terminal explosion of the meteor, typically at altitudes of 20 to 40 km. Such signals may be detected to distances of several hundred kilometers, and arrival time patterns are consistent with a point source. A second category of signals has been attributed to the sonic boom resulting from a meteor's supersonic flight. Sonic booms can be recognized by their non-circular arrival time isochrons, and they tend to have high frequency waveforms of short duration. Finally, a few meteors have generated P and S waves in the ground from the source region, presumably resulting from impacts with the earth's surface. Amplitudes of seismic or acoustic signals from a bolide should provide information on its kinetic energy. The mass of the object could then be estimated if a velocity were available from other evidence, such as eyewitness reports.

Modelling of Oceanic and On-Land Propagation of (T-) Waves from an Underwater Explosion.

PISERCHIA, P.-F., RODRIGUES, D., Laboratoire de Détection et de Géophysique, 91680 Bruyères-Le-Châtel, France, piserchi@ldg.bruyeres.cea.fr; VIRIEUX, J., GAFFET, S., rue A. Einstein U.M.R. Géosciences Azur, 06560 Valbonne, viri@faille.unice.fr.

The channelling efficiency of the deep ocean sound channel allows long range propagation of acoustic waves over a few thousand kilometers. Consequently, strong signals are commonly observed on both underwater and coastal receivers, when an oceanic earthquake or an underwater explosion occurs, even for small events. However, improvement of identification capabilities of coastal seismic stations, which are much more cost-effective than hydrophones, is needed because of complex wave diffraction phenomena on sea shores. To analyse these signals, we propose a new hybrid numerical scheme, combining in a single approach two powerful techniques, a ray tracing method completed by the Maslov summation and a finite difference scheme, which allows us to model T-wave underwater propagation and on-land conversion, including complex interactions with obstacles. In our modelling, before the T-waves arrive in front of an obstacle such as a continental shelf, an island shore or a sea-mount, the propagation is resumed on a vertical artificial boundary and the hydroacoustic wave field is considered as the input for a finite difference method. The (1989) Midplate experiment released in the South Pacific and its modelling have illustrated the key role played on the envelope shape of T-waves by the source depth, the SOFAR channel propagation, the bathymetry of the continental slope and the distance of the receiver from the source and to the top of the continental slope. Our approach gives a straightforward interpretation of a SOFAR channel propagation and may provide a phase identification, as well as a source characterisation capability. Therefore, this technique is particularly relevant for monitoring the Comprehensive Test Ban Treaty in oceans.

SSA '98
Abstracts of the 93rd Annual Meeting

Author Index

CAMPUS MAP

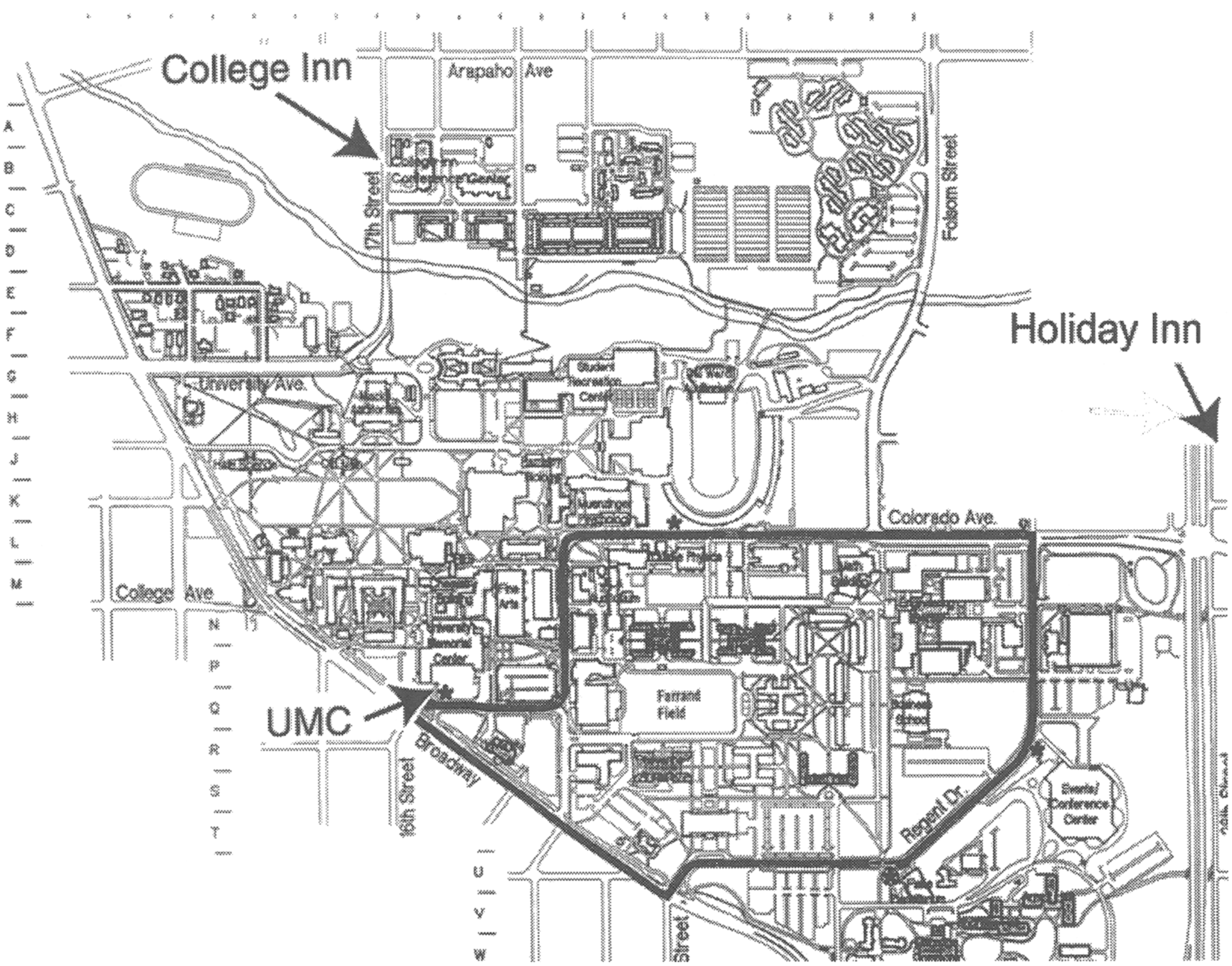
College Inn
Arapaho Ave
17th Street
Folsom Street
Holiday Inn
University Ave.
Colorado Ave.
College Ave
Fine Arts
Farrand Field
UMC
Broadway
16th Street
Regent Dr.
Events/ Conference Center
A
B
C
D
E
F
G
H
J
K
L
M
N
P
Q
R
S
T
U
V
W